Alma Mater Studiorum – Università di Bologna
in cotutela con Université de Bordeaux

DOTTORATO DI RICERCA IN

SCIENZE BIOMEDICHE E NEUROMOTORIE

Ciclo XXXIV

Settore Concorsuale: 05/E1 – Biochimica generale e biochimica clinica

Settore Scientifico Disciplinare: BIO/10 – Biochimica

Macrophage respiratory supercomplexes and metabolic reprogramming upon anti-bacterial immunity

Presentata da: Gaia Tioli

Coordinatore Dottorato

Prof.ssa Matilde Yung Follo

Supervisore

Prof.ssa Maria Luisa Genova

Supervisore

Dott. Johan Garaude

Esame finale anno 2021

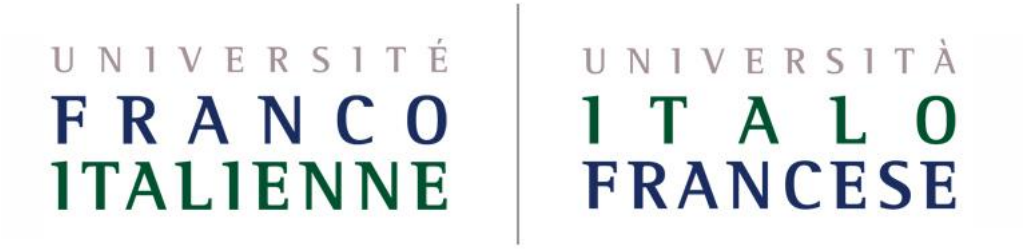

We would like to acknowledge the Université Franco Italienne / Italo-French University (https://www.universite-franco-italienne.org/) for the financial support that allowed the development of this three-year doctoral thesis (Bando Vinci – cap. III) in co-tutorship between the University of Bologna (Italy) and the University of Bordeaux (France).

Index

Abbreviations

3NPA	3-nitropropionic acid
α-KG	α-ketoglutarate
AA	Antimycin A
AAC	ADP/ATP translocase
ADP	adenosine 5'-diphosphate
ALRs	AIM-like receptors
ANT	adenine nucleotide translocator
AOX	alternative oxidase
APCs	antigen-presenting cells
ATP	adenosine 5′-triphosphate
BCA	bicinchoninic acid
BHM	bovine heart mitochondria
BMDMs	bone marrow derived macrophages
BN-PAGE	blue native polyacrylamide gel electrophoresis
BRR	basal respiration rate
BSA	bovine serum albumin
CCCP	carbonyl cyanide m-chlorophenylhydrazone
CI	Complex I
CII	Complex II
CIII	Complex III
CIV	Complex IV
CDP-DAG	CDP-acylglycerol
CL	cardiolipin
CLRs	C-type lectin receptors
Cyt c	cytochrome c
DB	decylubiquinone
DCs	dendritic cells
DCPIP	2,6- dichlorophenolindophenol
DMA	N,N dimetilacrilamide
DNA	deoxyribonucleic acid
DDM	n-dodecyl-β-D-maltoside
DMF	dimethyl fumarate
DMM	dimethyl malonate
DOC	deoxycholate

ELISA	enzyme-linked immunosorbent assay
ETS	electron transport system
FAD^+	flavin adenine dinucleotide, oxidized form
$FADH_2$	flavin adenine dinucleotide, reduced form
FAO	fatty acids oxidation
FMN	flavin mononucleotide
HRP	horseradish peroxidase
HSCs	hematopoietic stem cells
IDH	isocitrate dehydrogenase
IL-6	interleukin-6
IL-10	interleukin-10
IL-1β	interleukin-1β
IMM	inner mitochondrial membrane
IMS	intermembrane space
Ig	immunoglobulin
KCN	potassium cyanide
LB	lysogeny broth
LPS	lipopolysaccharide
MHC	major histocompatibility complex
MOI	multiplicity of infection
MPTP	mitochondrial permeability transition pore
MRR	maximal respiration rate
NAD^+	nicotinamide adenine dinucleotide, oxidized form
NADH	nicotinamide adenine dinucleotide, reduced form
NADH-cyt c	NADH-cytochrome c oxidoreductase activity
NADH-DB	NADH-ubiquinone oxidoreductase activity
$NADH\text{-}O_2$	NADH-oxidase activity
NADPH	nicotinamide dinucleotide phosphate
NK	natural killer
NLRs	NOD-like receptors
OCR	oxygen-consumption rate
ODG	n-octil-β-D-glucopyranoside
OMM	outer mitochondrial membrane
OXPHOS	oxidative phosphorylation

PA	phosphatidic acid
PAMPs	pathogen-associated molecular patterns
PBS	phosphate-buffered saline
PGP	phosphatidylglycerol phosphate
PL	phospholipid
PRRs	pattern recognition receptors
PVDF	polyvinylidene difluoride
Q	coenzyme Q, ubiquinone
QH_2	ubiquinol, reduced form ubiquinone
RET	reverse electron transfer
RLRs	RIG-1 like receptors
ROS	reactive oxygen species
SDH	succinate dehydrogenase
SDS	sodium dodecyl sulfate
SDS-PAGE	Sodium Dodecyl Sulphate-PolyAcrylamide Gel Electrophoresis
SOD	superoxide dismutase
Succ-cyt c	succinate:cytochrome c oxidoreductase
Succ-DCPIP	succinate:DCPIP oxidoreductase
TCA cycle	tricarboxylic acids cycle
TLRs	Toll-like receptors
TMB	5,5'- tetramethylbenzidine
TNFα	tumor necrosis factor
$UQ^{\bullet-}$	ubisemiquinone

Abstract

Macrophages are specialized innate immune cells that can recognize pathogens and induce an immune response best suited to eradicate the threat. Metabolic reprogramming has recently emerged as a major feature of innate immune cells following microbial infection. At the core of this physiological process are mitochondria, key organelles for energy production that also serve as immune signaling platforms [1]. The dynamic supramolecular organization of the mitochondrial electron transport system complexes forming the respiratory supercomplexes (SCs) may confer functional advantages to mitochondria [2]. However, the precise role of SCs in metabolic adaptations in immune host defense remains to be determined. Recent evidence nevertheless indicates that organizational and functional adaptations occur in the ETS of macrophages to allow metabolic plasticity during engulfment of live *E. coli* [3] and upon engagement of innate immune receptors [4]. Furthermore, several groups have demonstrated that the tricarboxylic acid (TCA) cycle (or Krebs cycle) of macrophages stimulated with the Toll-like receptor 4 (TLR4) ligand lipopolysaccharides (LPS) – the main component of Gram-negative cell wall – shows two breakpoints at the isocitrate dehydrogenase (IDH) and at the succinate dehydrogenase (SDH, or Complex II) [5]. Importantly, previous experiments conducted in Garaude's laboratory suggested the involvement of Complex II/SDH in macrophages metabolic reprogramming, depending on the microbial stimulus [3].

In my thesis work, I have investigated whether mitochondrial reprogramming depends on the nature of the bacteria encountered and how this in turn modulates innate immune outcomes.

Our data show that the sensing of Gram-negative bacteria and Gram-positive bacteria by macrophages differentially regulates mitochondrial oxygen consumption rate (OCR), mitochondrial ATP synthesis and respiratory CII activity throughout the time of infection. Metabolomics analysis of bacteria-treated macrophages and plasma samples from patients with sepsis show distinct reprogramming of the TCA cycle induced by Gram-negative and Gram-positive bacteria. While Gram-negative-treated macrophages accumulate fumarate, macrophages stimulated with Gram-positive bacteria accumulate α-ketoglutarate. Those two metabolites are known modulators of histone- and DNA-methyl transferase [6], suggesting that the metabolic reprogramming at the level of mitochondria may also lead to epigenetics control of gene expression in macrophages upon bacterial infection. We thus investigated whether the pharmacological manipulation of fumarate/α-ketoglutarate ratio and SDH/CII

activity modulate pro- and anti-inflammatory cytokines production *in vitro* and *in vivo*. Our preliminary results indicate that there is no significant difference in mitochondrial respiration capacity and ATP production induced by CII inhibitors, which suggest possible compensatory effects mediated by SCs and the other dehydrogenases composing the mitochondrial electron transport system. Further studies are still ongoing to elucidate the effect of CII inhibition on cytokine production since we observed discrepant results on cytokine levels *in vitro* and *in vivo*.

Résumé de la thèse

Les macrophages sont des cellules spécialisées de l'immunité innée capables de reconnaître les agents pathogènes et d'induire une réponse immunitaire pour éradiquer la menace. La reprogrammation métabolique est récemment émergée comme une composante majeure des cellules de l'immunité innée après une infection microbienne. Au cœur de ce processus physiologique se trouvent les mitochondries, des organelles clés pour la production d'énergie qui servent également de plateformes de signalisation immunitaire [1]. L'organisation supramoléculaire dynamique des complexes de la chaîne de transport d'électrons (CTE) des mitochondries en supercomplexes (SCs) peut conférer certains avantages fonctionnels aux mitochondries [2]. Néanmoins, le rôle précis de ces SCs dans les adaptations métaboliques liées à la réponse immunitaire de l'hôte reste à déterminer. Une étude récente indique que suite l'ingestion de bactéries Gram-négatives *E. coli* vivantes et après engagement des récepteurs de reconnaissance de l'immunité innée, des adaptations structurelles et fonctionnelles du métabolisme mitochondrial sont mise en place dans les macrophages contribuant ainsi à la réponse anti-microbienne [3].

Dans mon travail de thèse, j'ai voulu déterminé si la reprogrammation mitochondriale dépend de la nature des bactéries rencontrées et comment cela module l'immunité innée.

Nos résultats montrent que la détection des bactéries Gram-négatives et des bactéries Gram-positives par les macrophages régule différemment le taux de consommation d'oxygène mitochondrial (OCR), la synthèse d'ATP mitochondrial et l'activité respiratoire du CII de la chaîne respiratoire mitochondrial. L'analyse métabolomique des macrophages et d'échantillons de plasma de patients atteints de sepsis montre une reprogrammation distincte du cycle du TCA induite par les bactéries Gram-négatives et Gram-positives. Alors que les macrophages traités avec des bactéries Gram-négatives accumulent du fumarate, les macrophages stimulés par des bactéries Gram-positives accumulent du α-cétoglutarate. Ces deux métabolites sont des modulateurs connus de méthyltransférases [4], suggérant que la reprogrammation métabolique des mitochondries peut conduire à un contrôle épigénétique de l'expression des gènes dans les macrophages après une infection bactérienne. Nous avons donc étudié si la manipulation pharmacologique du rapport fumarate/α-cétoglutarate et de l'activité SDH/CII module la production de cytokines pro- et anti-inflammatoires *in vitro* et *in vivo*. Nos résultats préliminaires indiquent qu'il n'y a pas de différence significative dans la

capacité respiratoire mitochondriale et la production d'ATP induite par les inhibiteurs de CII, ce qui suggère des effets compensatoires possibles médiés par les SC et les autres déshydrogénases composant le système de transport d'électrons mitochondrial. D'autres études sont toujours en cours pour élucider l'effet de l'inhibition du CII sur la production de cytokines puisque nous avons observé des niveaux de cytokines opposés *in vitro* et *in vivo*.

Riassunto della tesi

I macrofagi sono cellule specializzate dell'immunità innata in grado di riconoscere agenti patogeni e indurre una risposta immunitaria allo scopo di eliminare la minaccia di infezione. Recentemente la riprogrammazione metabolica è emersa come una delle principali caratteristiche delle cellule dell'immunità innata a seguito di infezione microbica. Al centro di questo processo fisiologico si trova il mitocondrio, elemento chiave per la produzione di energia della cellula, che funge anche da sistema integrato per la biosegnalazione nella risposta immunitaria [1]. L'organizzazione dinamica supramolecolare dei complessi della catena respiratoria mitocondriale (ETS), che forma i supercomplessi respiratori (SCs), può conferire vantaggi funzionali ai mitocondri [2]. Tuttavia, il ruolo specifico dei SCs negli adattamenti metabolici alla base delle difese immunitarie dell'ospite rimane da definire. Uno studio recente ha dimostrato che nell'ETS dei macrofagi si verificano adattamenti strutturali e funzionali per consentire le necessarie modificazioni metaboliche durante la fagocitosi di batteri *E. coli* vivi [3] o dopo stimolazione di recettori di riconoscimento dell'immunità innata [4]. Inoltre, diversi autori hanno dimostrato che il ciclo degli acidi tricarbossilici (TCA, o ciclo di Krebs) dei macrofagi attivati dal lipopolisaccaride (LPS), principale determinante patogenico della parete cellulare dei batteri Gram-negativi, per effetto del legame con il recettore di riconoscimento Toll-like 4 (TLR4), presenta due interruzioni a livello dell'isocitrato deidrogenasi (IDH) e della succinato deidrogenasi (SDH, o Complesso II) [5]. È importante inoltre sottolineare che precedenti esperimenti condotti nel laboratorio di Garaude suggeriscono il coinvolgimento del Complesso II/SDH nella riprogrammazione metabolica dei macrofagi, in funzione del tipo di stimolazione microbica [3].

Il lavoro sperimentale descritto nella mia tesi è finalizzato a verificare se la riprogrammazione mitocondriale nella cellula ospite dipenda dalla natura dei batteri infettanti e come questo fenomeno possa a sua volta modulare gli effetti dell'immunità innata.

I nostri dati mostrano che il riconoscimento di batteri Gram-negativi e Gram-positivi da parte dei macrofagi regola in modo differente la velocità di consumo di ossigeno mitocondriale (OCR), la sintesi di ATP mitocondriale e l'attività respiratoria del CII durante l'infezione. L'analisi metabolomica di macrofagi trattati con diversi ceppi batterici e di campioni di plasma di pazienti con sepsi mostra una distinta riprogrammazione del

ciclo di Krebs indotta da batteri Gram-negativi e Gram-positivi. In particolare, mentre i macrofagi trattati con Gram-negativi accumulano fumarato, i macrofagi stimolati con batteri Gram-positivi accumulano α-chetoglutarato. Questi due metaboliti sono noti modulatori degli enzimi appartenenti alla famiglia delle istone- e delle DNA-metiltransferasi [6], suggerendo che la riprogrammazione metabolica a livello dei mitocondri può anche portare al controllo epigenetico dell'espressione genica nei macrofagi in seguito ad infezione batterica. Abbiamo quindi studiato se la manipolazione farmacologica del rapporto fumarato/α-chetoglutarato e dell'attività del CII/SDH sia in grado di modulare la produzione di citochine pro- e anti-infiammatorie *in vitro* e *in vivo*. I nostri risultati preliminari non evidenziano differenze nella capacità respiratoria mitocondriale e nella produzione di ATP indotta dagli inibitori del CII, il che suggerisce possibili effetti compensatori mediati dai SCs e da altre deidrogenasi che compongono il sistema mitocondriale di trasporto degli elettroni. Tuttavia, ulteriori studi sono ancora in corso per chiarire l'effetto dell'inibizione del CII sulla produzione di citochine poiché finora abbiamo raccolto risultati discordanti in cellule *in vitro* e in modelli murini *in vivo*.

Introduction

2.1 The immune system – a brief overview

The homeostasis of an organism maintains the stability of biological processes in a normal physiological state as a result of external or internal perturbations. Inflammation is induced when homeostasis is no longer sufficient the system could develop a pathological state [7]. Several triggers can activate sensors and effectors which promote the inflammation and if they are not well regulated that leads to a different pathological outcomes [8].

The immune system is a complex network of specialized cell types, tissues and organs responsible of protecting the host from invading pathogens and therefore plays a crucial role in fighting infection and tissue damage by discriminating what is "non-self" (foreign) or "altered-self" (degenerated) from what is part of the host "self".

The most rapid immune response is the innate immunity and it is occurs in the first phase (0-4h) of the pathogen invasion in the body. The activation of sensors recruits nonspecific effectors which produce an immune response in order to clear the microorganism. If the microorganism is able to bypass this step, the innate immune induced response takes places (4h-4days). Effector cells produce a signal to activate and recruit more specific effector cells aimed at eliminating the pathogens. A more long-lasting response, adaptive response, can be trigger by the body in the case the first two mechanisms are not sufficient to eradicate the infection. This adaptive immunity is induced by the transport of an antigen to lymphoid organs which drives the activation of naïve B and T cells. These cells have the capacity to proliferate and differentiate into specific and potent effectors cells that drive either the antibody response in the case of the B cells or the cytotoxic in the case of T cells (Figure 1).

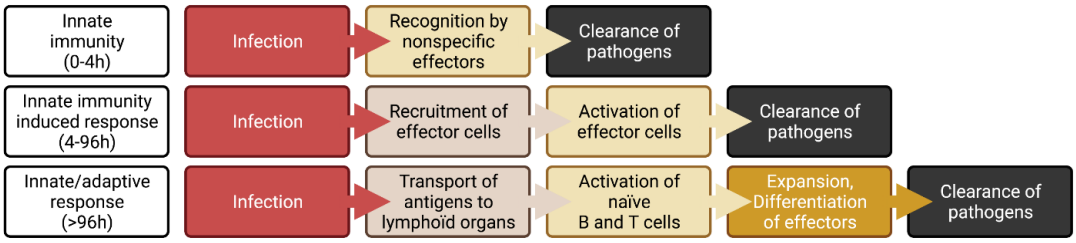

Figure 1. Schematic representation of the different immune responses trigger during the pathogen infection (created with BioRender.com).

Conventionally in mammals, immunity lays on two branches: the innate immune system and the adaptive immune system.

The **innate** immunity forms the first line of host defence during the infection and the response is more nonspecific and general. In fact, the main role of the innate immune system is to recognize and limit the pathogen early during infection, thus including physical and chemical barriers such as in the skin, ciliated respiratory epithelium, vascular endothelium and mucosal surfaces. The innate immune system is based on the recognition of specific types of molecules present into many pathogens but not in the host (self).

The **adaptive** immune system sets the acquired immunity. It is more specific and takes place in the late phase of the infection. To induce an adaptive response, antigen-presenting cells (APCs) present small fragments of pathogens (antigens) to B and T lymphocytes, which detect the foreign peptides with their antigen receptors expressed on the cell surface.

In particular, there are two different adaptive immune responses: antibody response and cell-mediated immune response.

In **antibody response**, B cells receptors bind a protein antigen which stimulates the maturation and proliferation of the effector cells (mature B cells), so that mature B cells subsequently produce and secrete specific antibodies that expose two antigen-binding sites. In mammals, there are five classes of antibodies or immunoglobulins (Igs: IgA, IgD, IgE, IgG and IgM) with distinct biological properties and function. Once the

immunoglobulins are secreted by mature B cells in the bloodstream, they can reach the site of infection and act away from their initial production site.

In the **cell-mediated immune response**, like for the antibody response, the binding of a foreign antigen by T cell receptors at the cell surface induces the proliferation and the maturation of naïve T cell into effector cells but only when the antigen is presented by antigen-presenting cells (APCs). APCs degrade the protein antigen into small peptide fragments that T cells recognize. APCs present the antigen fragments to T cells by expressing on the cell surface of major histocompatibility complex (MHC) proteins. There are two classes of MHC proteins: Class I MHC proteins, which are expressed by all cells and mostly present intracellular/cytoplasmatic peptides, and Class II MHC proteins, which are expressed only by professional APCs specialized in presenting exogenous fragment antigens [9].

Importantly, adaptive immunity provides lifelong immunological memory, the capacity of the immune cells to remember previous infection and leads to a faster and enhanced response to future encounters with similar invading pathogens.

2.2 The innate immunity

All immune cells develop from multipotent hematopoietic stem cells (HSCs) in the bone marrow, which gives rise to lymphoid and myeloid progenitors. Each of these progenitors differentiate into a range of innate and adaptive immune cell types (Figure 2).

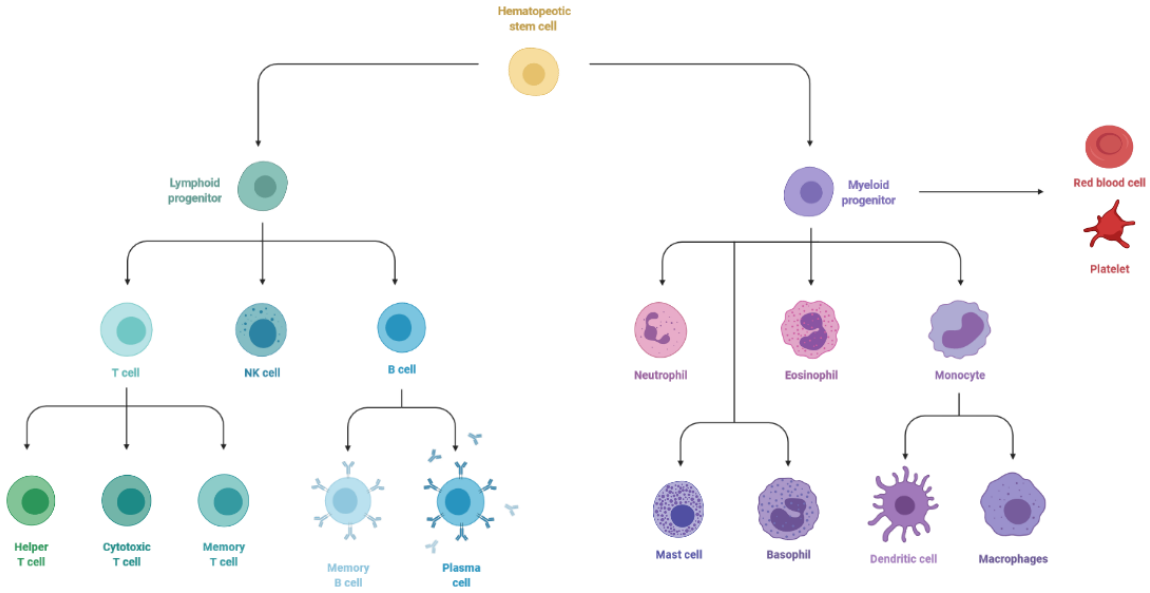

Figure 2. Representation of the cells of the immune system. Lymphoid (left) and myeloid (right) progenitors originate derived from hematopoietic stem cells (HSCs). They differentiate into more specific cell types of innate and adaptive immunity (created with BioRender.com).

Lymphoid progenitor differentiates into three cell classes: B cells, Natural Killer (NK) cells and T cells. Once activated, B cells differentiate into memory B cells or plasma cells that circulate in the bloodstream. They are responsible for storing information on different antigens encountered in previous infections and for speeding up the immune response by secreting antibodies.

NK cells are cytotoxic cells which detects virus-infected cells, cancer cells as well, etc and induce the infected cells to kill themselves by apoptosis. Once activated, T cells differentiate into memory T cells, cytotoxic T cells and helper T cells. Memory T cells, like memory B cells, memorize characteristics of pathogen antigens and generate a faster immune response. Cytotoxic T cells recognize infected cells or cancer cells, similar to NK cells, and cause the programmed cell death of the target cells by releasing granules which contain cytotoxins.

Helper T cells are important cells of the immune system secrete cytokines that boost the adaptive immune response. They help activate B cells to produce and secrete antibodies,

sustain and drive macrophages activation and differentiation and support them to phagocyte foreign pathogens and activate cytotoxic T cells to kill infected cells.

Myeloid progenitor also gives rise to neutrophils, eosinophils and monocytes, which further differentiate into dendritic cells (DCs) and macrophages.

Neutrophils are phagocytic cells present in the bloodstream that, upon infection, are able to migrate to the site of inflammation to destroy the pathogen.

Eosinophils are a type of granulocyte mainly involved in allergic inflammatory responses by releasing cytokines to fight against pathogens.

Dendritic cells (DCs) are a specialized phagocytic cell, they are potent APCs.

Macrophages are tissue resident phagocytic cells, which engulf invading pathogens releasing cytokines and chemokines to trigger an immune response (see Chapter 2.2.1).

There are two additional types of cells derive from the myeloid progenitor: mast cells, another type of granulocytes also involved in allergy, and basophils, which are engaged in the immune response to parasites.

Myeloid progenitors also give rise to red blood cells and platelets. The red blood cells, or erythrocytes, remain within the blood vessels and transport O_2/CO_2 bound to haemoglobin. Platelets are small cell fragments involved in blood clotting and reparation of breaches.

2.2.1 Macrophages

Macrophages are phagocytic cells, present in almost every tissue of mammalian body. They are important cells for the maintaining of the homeostasis functions of many different tissues, but they are also important immune player regarding the inflammatory

response. Together with dendritic cells, they are at the forefront of initiating an innate immune response by phagocytosis and cytokine release.

One important feature of macrophages is to express a huge variety of phagocytic receptors (mannose receptors, β-glucan receptors, lipid receptors, scavenger receptors and complement receptors). These receptors, activated by binding to their ligand, drive a signalling pathway that leads to the expression of genes responsible for the phagocytic program, several well-defined steps for engulfment a pathogen. For example, a bacteria can be recognized by receptors and induce the formation of phagosome, which is composed of plasma membrane and contains the microbe. Through an actin-dependent movement can move in the cytosol and the phagosome is fused with a lysosome which is a specific type of endosome, forming the phagolysosome. Inside the phagolysosome are present all the elements to degrade/digest of the engulfed microbe.

Macrophages have two roles: to respond immediately to infection (bacteria, fungi and virus) and to help repair the tissue damage (apoptotic and necrotic cells) that arises as a consequence of the response. To perform these two functions, macrophages acquire a pro-inflammatory phenotype in the first phase of the infection, and then later, acquire an anti-inflammatory phenotype to promote tissue repair. They can have a different phenotype depending on the signal received and the surrounding microenvironment. Between these two types of macrophages exists a broad spectrum of macrophage differentiation leading to completely different cellular and tissue functions (Figure 3).

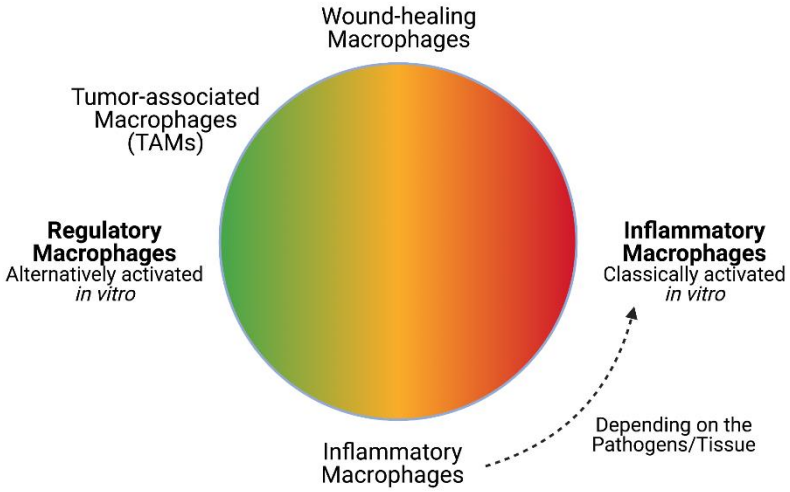

Figure 3. Schematic representation of activated macrophages in vitro (created with BioRender.com).

Activated macrophages are often divided into two subgroups according to cytokines they produce, cellular features and their function in the immune response: M1 macrophages (or inflammatory macrophages) and M2 macrophages (or regulatory macrophages). This phenomenon of the two different M1/M2 phenotypes is referred to term 'macrophage polarization" [10].

To differentiate M0 macrophages (or resting macrophages) *in vitro*, it is necessary to culture monocyte using M-CSF (macrophage colony stimulating factor) or GM-CSF (granulocyte–macrophage colony stimulating factor) (Figure 4).

The classical inflammatory macrophages, or M1, are associated with inflammatory responses. They are *in vitro* generated by stimulating resting macrophages with inflammatory signal such as LPS in combination or not with interferon gamma (IFN-γ). M1 macrophages exhibited a high level of phagocytic activity and produce inflammatory molecules: reactive oxygen species (ROS), nitric oxide (NO), pro-inflammatory cytokines interleukin-1β (IL-1β), tumor necrosis factor (TNFα) and interleukin-6 (IL-6), and several chemokines.

The alternative "anti-inflammatory" macrophages, or M2, are associated with tissue repair, regulation of inflammation and anti-inflammatory responses. *In vitro* they are generated by stimulating resting macrophages with interleukin-4 (IL-4) and interleukin-

13 (IL-13), anti-inflammatory stimulus, and they secrete growth factors, such as TGF-β, to help in tissue renovation and anti-inflammatory cytokine.

However, the M1/M2 phenotype does not reflect all the different phenotypic subsets of macrophages [11]. M2 macrophages can be further divided into M2b and M2c macrophages. M2b macrophages are induced by stimulation with immune complex (IC) + LPS and interleukin-1 receptor (IL-1R) while M2c macrophages are generated by treatment with interleukin-10 (IL-10) and transforming growth factor (TGF-β).

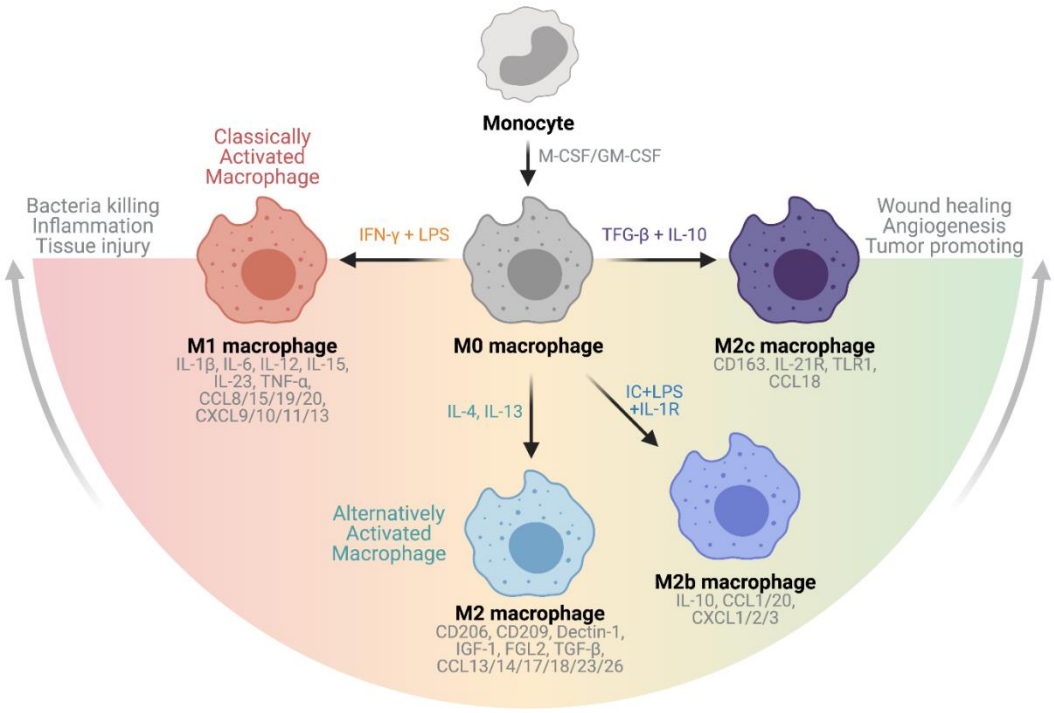

Figure 4. Schematic representation of macrophage differentiation (created with BioRender.com).

The characterization of all these types of macrophages led to the identification of the different cellular functions performed by each subgroup. M1 macrophages are dedicated to bacterial killing, generate inflammation and produce tissue injury while M2 macrophages are specialized to induce wound healing, angiogenesis and tumor promoting [12].

In general, macrophages are able to recognize different threats and to generate specific immune responses depending on the nature of the threat.

The transition between M1 macrophages and M2 macrophages is a dynamic process which requires metabolic adjustments. An increasing number of studies nevertheless collocates mitochondria at the centre of these physiological metabolic events during innate immune activation. The metabolism of M1 and M2 macrophages are completely different (Figure 5). M1 macrophages are characterized by antimicrobial properties, with low fatty acids oxidation (FAO) and high glycolytic flux that feeds the pentose phosphate pathway (PPP) instead of providing pyruvate to TCA cycle thereby decreasing oxidative phosphorylation (OXPHOS). Moreover, M1 macrophages show a broken Krebs cycle resulting in the accumulation of several intermediates, such as succinate, citrate and its itaconic acid derivate (see Chapter 2.3.3.2). M2 macrophages drives the tissue repair producing anti-inflammatory cytokines. Metabolism of M2 macrophages also increases glycolysis but the Krebs cycle is intact with high levels of fatty acid oxidation (FAO) and oxidative phosphorylation (OXPHOS) [13].

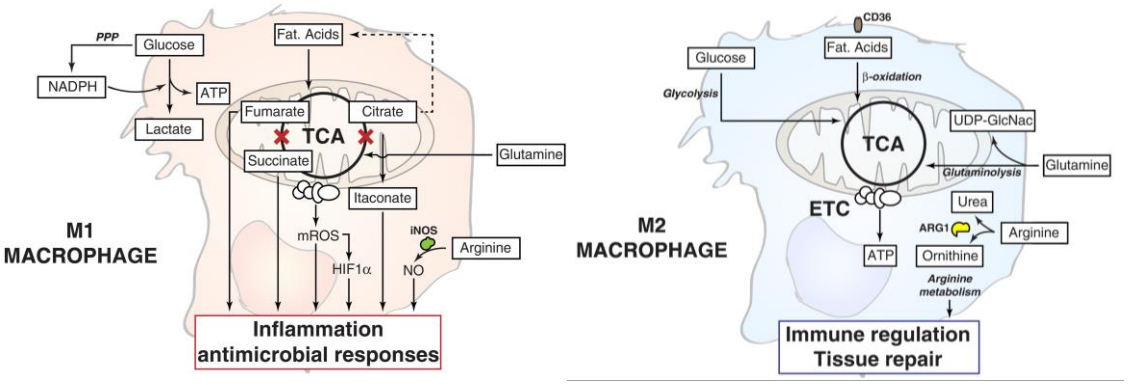

Figure 5. Schematic representation of metabolic pathways of activated M1 and M2 macrophages [14].

Macrophages are very rapid to switch from a resting to an activated state. As described in the following sections, there is evidence in the literature showing that alterations in mitochondrial structure and function, ROS production and various metabolic pathways occur during this switch, but although the factors driving this change are not yet fully understood.

2.2.2 Pattern recognition receptors (PRRs) and pathogen-associated molecular patterns (PAMPs)

An old theory of pathogen recognition by immune cells predicted that a pathogen could trigger the innate immunity but also activate adaptive immunity, through the antigen, and lead to the pathogen removal. In this view, innate and adaptive immunity are completely separated and not linked each other. C. Janeway provided a new vision of the pathogen recognition by immune cells, called the pattern recognition theory. He proposed that the sensing of the infection is mediated by receptors of the innate immunity system, which not only detect the presence of a pathogen but also determines the nature of the antigen recognized by the adaptative cells. He suggested that the innate immune system relies on germ-line encoded receptors that recognize conserved molecular patterns found only in pathogen agents [15,16].

Cells of the innate immune system express a family of innate receptors known as pattern recognition receptors (PRRs) at their surface. PRRs are evolutionarily conserved germ-line-encoded receptors capable to recognize conserved structures on pathogens, called pathogen-associated molecular pattern (PAMPs). PAMPs are small molecules well conserved within a class of pathogens, important for the pathogenicity but also are essential for the survival of the pathogen. Sensing of PAMPs by PRRs rapidly activates a cascade of intracellular signalling pathways that result in the induction of inflammatory responses with the activation of gene expression and synthesis of pro-inflammatory molecules, such as cytokines and chemokines [17].

The PRRs are divided into five families: Toll-like receptors (TLRs), NOD-like receptors (NLRs), C-type lectin receptors (CLRs) and RIG-1 like receptors (RLRs), AIM-like receptors (ALRs) (Figure 6).

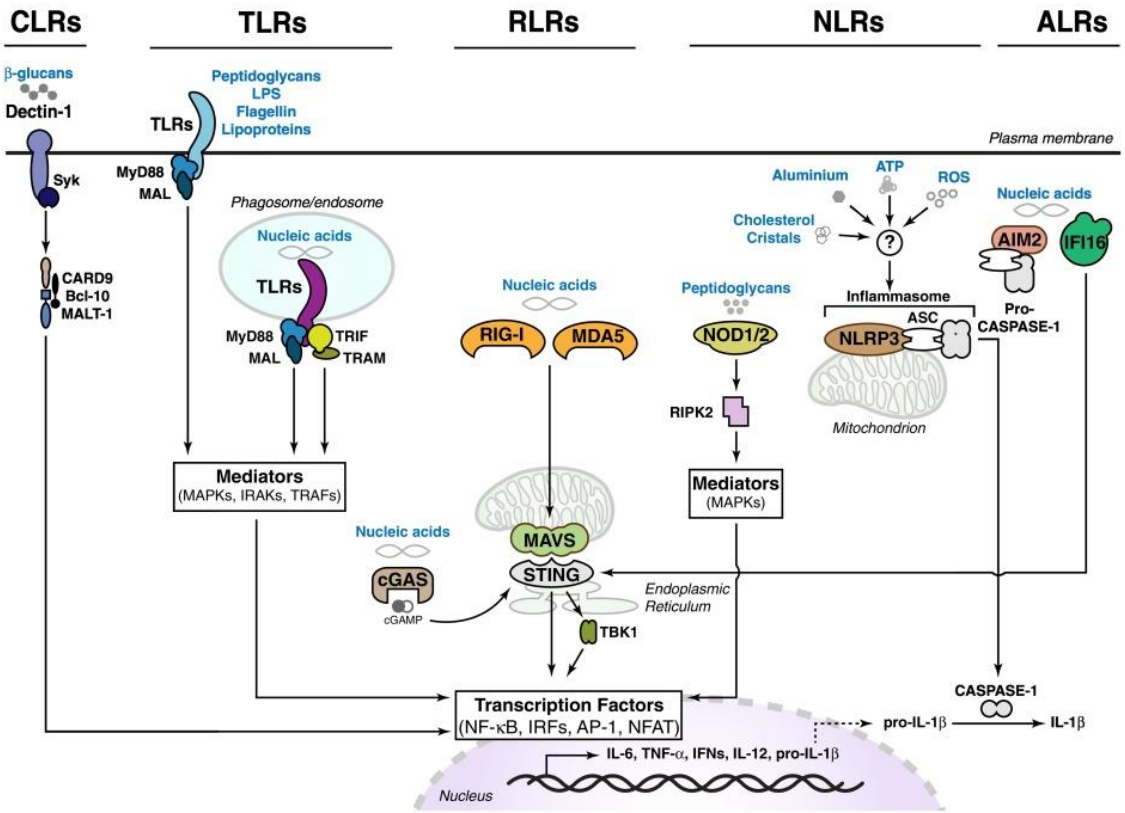

Figure 6. Schematic representation of the main signalling pathway activated by several PRRs expressed in macrophages [14].

Toll-like receptors

Toll-like receptors (TLRs) are the first PRRs identified by Jules Hoffman and Bruce Beutler (Nobel Prize winners in 2011), with the contribution of Charles Janeway and Ruslan Medzhitov, and it is the best characterized class of PRRs involved in the recognition of pathogen pattern [18].

TLRs are type I transmembrane integral glycoproteins with a large extracellular domain containing an amino-terminal leucine-rich repeats (LRRs), a transmembrane domain and a carboxy-terminal cytosolic Toll/interleukin-1 (IL-1) receptor (TIR) domain. The extracellular domain is important for PAMPs recognition, and the intracellular portion activate downstream signalling pathways.

In human, 10 TLR family members have been identified and each TLR detects different PAMPs derived from various pathogens, such as viruses, bacteria, fungi and parasites.

TLRs can be divided into subfamilies according to the specific PAMP recognized; TLR1, TLR2, TLR4 and TLR6 detect lipids, whereas TLR3, TLR7, TLR8 and TLR9 recognize nucleic acids.

Another TLRs classification is based on the cellular localization. TLR1, TLR2, TLR4, TLR5 and TLR6 are expressed on the plasma membrane, whereas TLR3, TLR7, TLR8 and TLR9 are predominately located in intracellular compartments, like endosome or lysosome.

TLRs are expressed in epithelial and immune cells, in particular in B lymphocytes, dendritic cells and macrophages.

Upon PAMPs recognition, the interaction between the ligand and the receptor induces receptor oligomerization. This conformational change is required for the recruitment of a specific family of cytosolic TIR domain-containing adaptor molecules (e.g. MyD88, TRIF, TIRAP or TRAM) [19].

MyD88 (Myeloid differentiation primary response 88) is recruited by all the TLRs (except for TLR3) and a MyD88-dependent signalling is activated downstream of all receptors. This signalling relies to the activation of NF-κB and MAP kinases with the induction of pro-inflammatory cytokines.

Upon TLR stimulation, MyD88 associates with the cytoplasmatic portion of the receptor and recruits members of the IL-1 receptor-associated kinase (IRAK) family (IRAK4, IRAK2 and IRAK1). After the association with MyD88, all IRAK members are phosphorylated, resulting in activation of the kinases. Activated IRAKs form a complex with tumor necrosis factor (TNF) receptor-associated factor 6 (TRAF6) which leads to activation of transcription factors through activation of MAP kinases that regulate the expression of pro- and anti-inflammatory genes as well as pro- and anti-inflammatory, IFNs, etc [20].

C-type lectin receptors

C-type lectin receptors (CLRs) comprised a large family of transmembrane and soluble receptors containing at least one carbohydrate recognition domain, a C-type lectin-like domain (CTLD). These receptors bind carbohydrate moieties in a Ca^{2+}-dependent manner [21].

A CLRs classification is based on their signalling potential, activation or inhibition. CLRs can be subdivided into 1) activation of spleen tyrosine kinase (Syk) -coupled CLRs with immunoreceptor tyrosine-based activation motif (ITAM) domains, 2) inhibitory CLRs with immunoreceptor tyrosine-based inhibition motif (ITIM) domains or 3) CLRs without clear ITAM or ITIM domains. This categorization is not exhaustive because it was demonstrated that the same CLR can combine positive and negative signals and modulate the immune response.

CLRs play an important role in recognizing fungi, bacteria, helminths and protozoa, but more and more studies demonstrate a key role in autoimmunity, allergy and in maintaining cellular homeostasis [22,23].

RIG-1 like receptors

Retinoic acid-inducible gene 1 (RIG-1)-like receptors (RLRs) are a family of cytosolic helicase that sense immunostimulatory viral RNA. All RLRs have a central helicase domain and a carboxy- terminal domain (CTD).

To date, three RLRs have been identified: RIG-I (retinoic acid-inducible gene I), MDA5 (melanoma differentiation associated factor 5), and LGP2 (laboratory of genetics and physiology 2) [24].

RIG- I and MDA5 additionally have two amino- terminal caspase activation and recruitment domains (CARDs), which mediate downstream signal transduction. LGP2 do not have the CARDs then it was supposed to regulate RIG- I and MDA5 activation.

Once RIG- I and MDA5 detect an immunostimulatory RNA, they undergo conformational changes that expose their CARDs which lead to CARD–CARD interactions with mitochondrial antiviral signaling (MAVS) protein. MAVS relays the signal to TANK- binding kinase 1 (TBK1) which activates interferon regulatory factors and induces the expression of type I interferons and other antiviral genes [25].

NOD-like receptors

NOD-like receptors (NLRs) are a family of intracellular receptors and they have a central nucleotide-binding oligomerization (NOD) domain, and a C-terminal leucine-rich repeat (LRR) domain [26].

NOD1 and NOD2 are the well characterized cytosolic NLRs and both recognize peptidoglycans, heterogeneous polymers present in the cell walls of bacteria. Activation of these receptors triggers intracellular signalling cascades by recruitment of Rip2 (receptor-interacting serine–threonine kinase 2) kinase, which activates downstream signalling, including nuclear factor-κB (NF-κB) and mitogen-activated protein kinases (MAPKs) and subsequent expression of pro-inflammatory cytokines [27].

NOD-like receptor protein 3 (NLRP3) inflammasome is composed of NOD-like receptor 3, procaspase 1, and the adaptor protein apoptosis-associated speck-like protein comprising a caspase recruitment domain (ASC). The NLRP3 inflammasome in turn triggers the cleavage of pro-interleukin 1β (pro-IL-1β) into mature IL-1β [28].

AIM-like receptors

Absent in melanoma 2 (AIM2)-like receptors (ALRs) are a family of cytosolic receptors able to detect bacterial and viral double stranded DNA. All ALRs have a pyrin signaling domain (PYD) and the DNA-binding HIN domain.

Activated AIM2 recruits apoptosis-associated speck-like protein containing a CARD (ASC) forming of AIM2 inflammasome. ASC binds caspase-1 then leads to the induction of the proteolytically cleavage of proinflammatory cytokines IL-1β into IL-1β [29].

Based on the discover of all these immune receptors and the pattern recognition theory, in 1994 P. Matzinger proposed a complementary theory, called danger recognition theory. Parallel to what happen with a foreign pathogen, also stressed cell or dying cells can provide different type of molecules, defined damage-associated molecular patterns (DAMPs), like ATP, mitochondrial DNA, etc. The release of these molecules by altered cells activate the innate immune receptors, so tissue damage can trigger innate immunity and inflammation through a similar mechanism that is driven by microbial infection [30].

2.2.3 Immune response to Gram-negative and Gram-positive bacteria

Bacteria are microscopical prokaryotic single-celled organisms that can proliferate and survive also in extreme conditions. These organisms lack intracellular organelles such as nucleus and mitochondria and all the activities normally performed by those organelles take place also in the cytoplasm of bacteria. Genetic information is encoded in bacteria by a single long circular DNA filament, called bacterial chromosome, which forms an irregular structure (nucleoid) in association with numerous proteins and RNA molecules in the cytoplasm.

On the basis of the cell wall composition, bacteria are classified as Gram-negative and Gram-positive (Figure 7). The Gram stain is a technique developed by Hans Christian Gram in 1884 [31] which allows to distinguish between the two bacterial groups by staining their different cell wall constituents with a red or violet colour. After the staining, Gram-positive bacteria stain violet whereas Gram-negative bacteria stain red and this different colour is due to the thickness of the peptidoglycan layer in the cell wall.

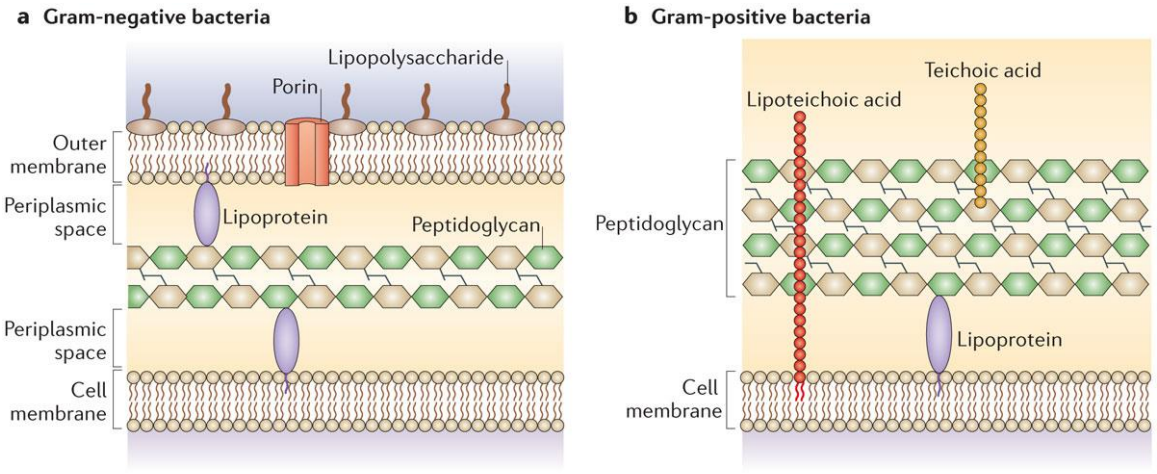

Figure 7. The cell wall organization of Gram-negative bacteria (a) and Gram-positive bacteria (b) [32].

Gram-positive bacteria have a single membrane formed by a phospholipid bilayer which comprises numerous membrane proteins. Externally, it is present a thick layer of peptidoglycans, a long linear chain polymer composed of two repeating sugars (n-acetylglucosamine and n-acetylmuramic acid). Several peptidoglycan chain can be cross-linked by peptide bridges to form a rigid structure around the inner membrane. Anchored at the cell membrane there are several copies of teichoic acid, lipoteichoic acid and lipoprotein.

Gram-negative bacteria have two membranes, outer and cytoplasmic membrane, separated by a periplasmic space which includes a thin layer of peptidoglycan. The inner membrane is a regular phospholipid bilayer and contains several membrane proteins, whereas the outer membrane is internally composed of a phospholipid layer and externally an exclusive glycosylated lipid called lipopolysaccharide (LPS) (Figure 8) [33]. LPS, also called endotoxin, in composed of three parts: O antigen, core polysaccharide and lipid A. The lipid A moiety is the most conserved portion of LPS and it is crucial for the toxicity of the bacteria. It is composed of two phosphorylated glucosamine molecules and numerous acyl chains attached that allow anchoring in the phospholipid bilayer of the cell membrane. The core polysaccharide is the link between the lipid A and the O antigen and it consists in a hydrophilic chain of 8-12 sugars. The O antigen is a long polymer of repeating oligosaccharide units up to 40 times in the most external portion of LPS. Its

composition is extremely different among bacterial strains, this feature increases the variety of antigenic types between species.

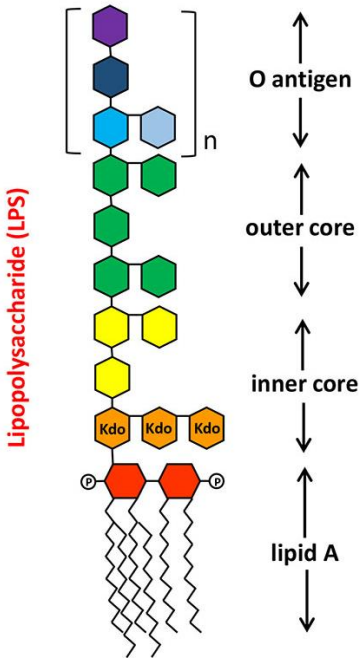

Figure 8. Schematic structure of lipopolysaccharide (LPS) of Gram-negative bacteria [34].

Gram-negative bacteria and Gram-positive bacteria can activate different TLRs trough the presence of PAMPs in the cytosol or at cell membrane or cell wall [35].

TLR2 is involved in cell wall PAMPs recognition of Gram-positive and Gram-negative bacteria. In particular, for Gram-positive bacteria detects peptidoglycan, lipoteichoic acid and lipoproteins, while for Gram-negative bacteria senses peptidoglycan and porin.

LPS is a powerful PAMP and a strong virulent factor of Gram-negative bacteria and is sensed specifically by TLR4. Moreover, flagellin, a structural protein of the flagellum, an organ dedicated to bacterial motility, strongly activates TLR5.

Bacterial DNA is recognized by TLR9 either for Gram-positive or Gram-negative bacteria.

Each pathogen express different PAMPs (DNA, RNA, structural protein of the cell wall, etc) that can be recognize by different type of pathogen recognition receptors. All the signals are integrated to trigger the more specific innate immune response and eradicate the inflammation (Figure 9).

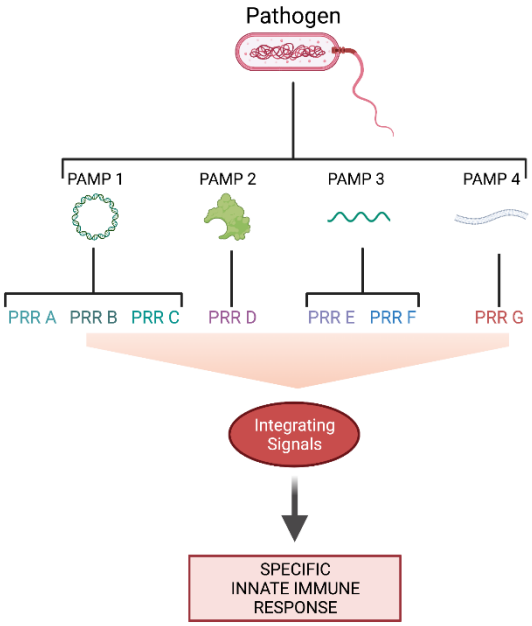

Figure 9. Schematic representation of the integration of signals given by the recognition of several PAMPs.

2.3 Mitochondria

Mitochondria are cytoplasmic organelles present in almost all eukaryotic cells, known as the powerhouse of the cell, producing adenosine triphosphate (ATP) [36]. However, their cellular contribution does not only include energy production, but also programmed cell death, reactive species of oxygen (ROS) production and homeostasis.

Mitochondria possess their own genome, the mitochondrial DNA (mtDNA), but most of the proteins of the mitochondrial proteome are encoded by the nucleus.

Each mitochondrion is made up of two highly specialized membranes, the outer mitochondrial membrane (OMM) and the inner mitochondrial membrane (IMM). These two membranes have completely different functions. The OMM is permeable to ions and

small cytoplasmic molecules, while the IMM, characterized by numerous invaginations which are called mitochondrial cristae, is highly selective and only with specific carriers is possible to cross it. The phospholipid bilayer of the inner mitochondrial membrane has additional unique characteristics, such as the total absence of cholesterol and the presence of a particular acid phospholipid, cardiolipin (CL). The two membranes identify two distinct compartments: the intermembrane space (IMS), which separates the outer mitochondrial membrane from the inner membrane, and the mitochondrial matrix, the space within the inner mitochondrial membrane (figure 10).

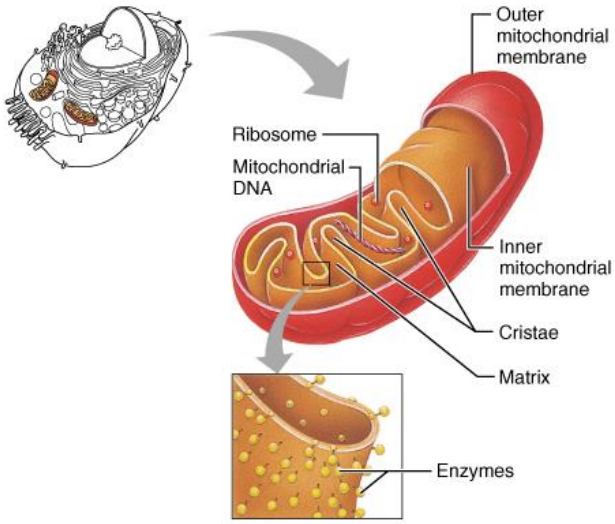

Figure 10. Schematic representation of mitochondrial ultrastructure of a mitochondrion showing the spatial compartmentalization (Copyright 2001 Benjamin Cummings).

Several metabolic processes take place in mitochondria, as such the Krebs cycle (section 2.3.1) and the electron transfer pathways of energy metabolism focused on catalysing the entry of electrons into the respiratory Q-junction to allow oxidative phosphorylation (OXPHOS) coupling (section 2.3.2).

Compartmentalization is a concept of spatial segregation of macromolecules, metabolites and biochemical pathways that bridges mitochondrial structure and function. Three protein complexes influence the cristae morphology: the mitochondrial contact site and cristae-organizing system (MICOS) complex, assemblies of the mitochondrial genome maintenance (Mgm1)/optic atrophy (OPA1) and the F_1F_O-ATP synthase.

MICOS complex is a multisubunits assembly composed of six-seven subunits that establishes multiple contacts with proteins of the OMM and forms cristae junctions. The two compartments resulted are functionally distinct. Mgm1/OPA1 are GTPases, involved in the fusion of the IMM, which can assemble into dimers, trimers, and tetramers through homotypic interactions that stabilize and tighten cristae walls. The F_1F_O-ATP synthase, enzyme responsible of the ATP production, shape cristae structure by assembling into dimers along the crest of lamellar cristae. The positive or negative membrane curvature is also affected by the different lipid composition of the mitochondrial membrane. Depletion of these complexes lead to an alteration of the ultrastructure of the mitochondria, which results in development of disease associated to a mitochondrial dysfunction [37].

2.3.1 The Krebs cycle

In aerobic organisms (pro- and eukaryotes), the Krebs cycle, also called the tricarboxylic acid (TCA) or citric acid cycle, is a series of chemical reactions in a metabolic loop used to generate energy via the oxidation of acetyl-coenzyme A (CoA) derived from carbohydrates, fatty acids and proteins. In eukaryotes, the TCA cycle takes place in the mitochondrial matrix. In prokaryotes, these steps occur within the cytosol. The cycle begins with the irreversible condensation of oxalacetate and acetyl-CoA to form citrate (Figure 11).

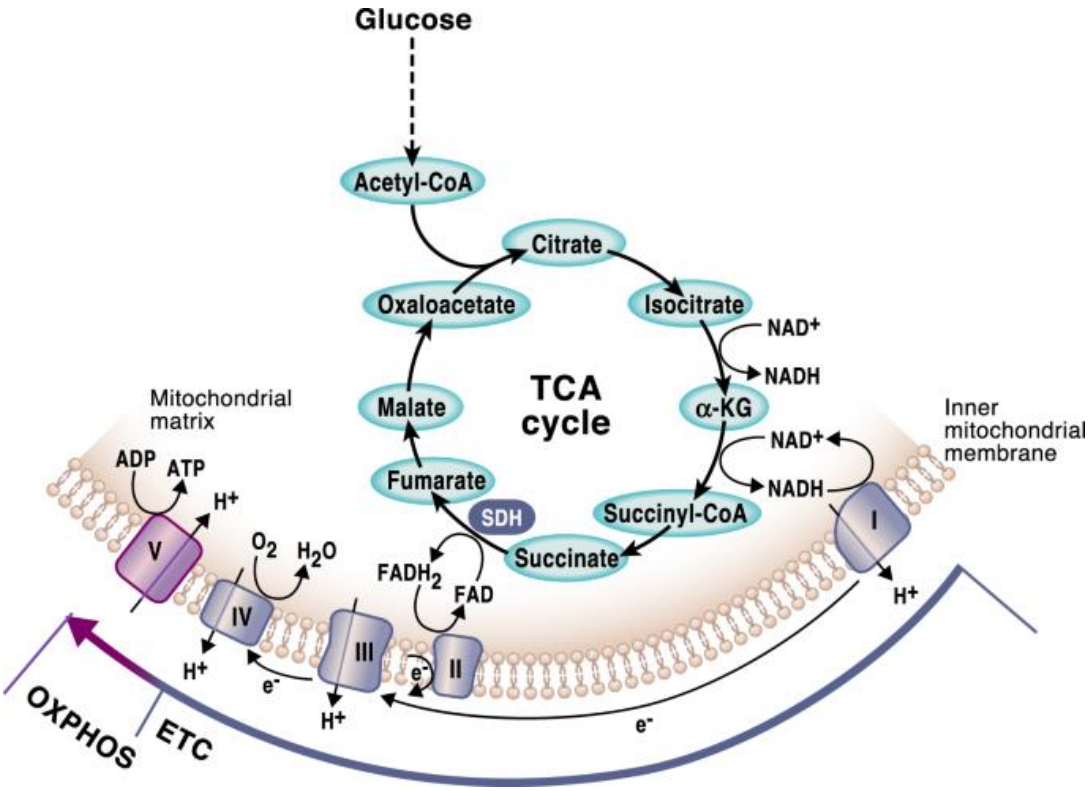

Figure 11. The TCA cycle and oxidative phosphorylation. Abbreviation: I-V, Complex I-V; ETC, Electron Transfer Chain; OXPHOS, oxidative phosphorylation; SDH, succinate dehydrogenase; α-KG, α-ketoglutarate [6].

This first reaction is catalysed by citrate synthase through the formation of a transient enzyme-bound intermediate, citroyl-CoA. In the following reaction, citrate is converted by the enzyme aconitase into its isomer, isocitrate. This reversible isomerization is a two-step process; the dehydration of citrate to form *cis*-aconitate and the rehydration of *cis*-aconitate to isocitrate. In the third step, the isocitrate dehydrogenase (IDH) catalyses the irreversible oxidation of isocitrate to a five-carbon molecule, α-ketoglutarate. The oxidative decarboxylation yields the release of a molecule of carbon dioxide and two electrons, which reduce NAD+ to form the first molecule of NADH of the cycle. IDH is allosterically regulated: activated by the substrates (isocitrate and NAD+) or inhibited by ATP and the products (α-ketoglutarate and NADH). The next step is similar to the previous reaction because it is another oxidative decarboxylation. In the case, the α-ketoglutarate dehydrogenase converts α-ketoglutarate to succinyl-CoA with the loss of another molecule of CO_2 and the formation of a second molecule of NADH. The enzyme is inhibited by ATP and the products (succinyl-CoA and NADH). In the next

reversible step, the succinyl-CoA synthetase catalyses the cleavage of CoA from the substrate forming succinate. The release of CoA is coupled with the phosphorylation of guanosine diphosphate (GDP) and therefore produces GTP. The following reaction involves the oxidation of the succinate to fumarate by succinate dehydrogenase (SDH), also known as Complex II of the mitochondrial respiratory chain (see section 2.3.2). This conversion also produces the reduction of one molecule of $FADH_2$, which can feed its electrons directly into the electron transport chain. In the continuation of the Krebs cycle, one molecule of water is added to fumarate by fumarate hydratase, converting it into another four-carbon molecule called malate. Finally, the malate dehydrogenase catalyses the oxidation of malate to oxaloacetate with the reduction of NAD+ to form the third molecule of the NADH.

In conclusion, one turn of the cycle produces three molecules of NADH, one molecule of GTP and one molecule of $FADH_2$ with the release of two molecules of CO_2.

The TCA cycle and OXPHOS (see Chapter 2.3.2) are tightly interconnected since the TCA cycle generates NADH and succinate, two metabolites required for the Complex I and the Complex II of the mitochondrial respiratory chain. Moreover, increasing evidence suggests that the TCA cycle intermediates, which can be transported into the cytosol, can play an important role in regulating cellular immunity [38].

2.3.2 The mitochondrial respiratory chain and OXPHOS system

The mitochondrial respiratory chain, or electron transport system (ETS), is formed by a series of enzymes located in the inner mitochondrial membrane that couple the transfer of electrons for the formation of ATP to the pumping of protons through the phospholipid bilayer of the IMM. The ETS is composed of four functional primary enzyme complexes: Complex I (or *NADH-ubiquinone oxidoreductase*, CI), Complex II (or *succinate-ubiquinone oxidoreductase*, CII), Complex III (or *ubiquinol-cytochrome c oxidoreductase*, CIII), Complex IV (or *cytochrome c oxidase*, CIV) [39]. In addition, flavoprotein proteins, such as glycerol-3-phosphate dehydrogenase (G3PDH), NAD(P)H

dehydrogenase (ND), ETF-ubiquinone oxidoreductase (ETF-QO) and dihydroorotate dehydrogenase (DHODH), are able to provide electrons to the respiratory chain reducing directly ubiquinone [40].

The electron transfer occurs via two small mobile electron carriers: ubiquinone (Coenzyme Q, Q), present in the phospholipid bilayer of the inner membrane, and cytochrome c (cyt c), placed on the external surface of the IMM (Figure 12).

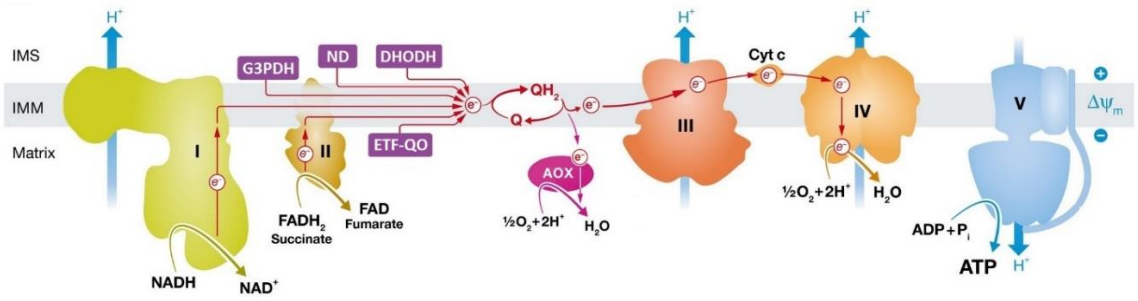

Figure 12. Schematic representation of the OXPHOS apparatus with mitochondrial respiratory complexes and their substrates. Abbreviations: I-IV, complex I-IV; V, ATP synthase; cyt c, cytochrome c; Q, coenzyme Q; QH2, reduced coenzyme Q or ubiquinol; G3PDH, glycerol-3-phosphate dehydrogenase; ND, NAD(P)H dehydrogenases; DHODH, dihydroorotate dehydrogenase; ETF-QO, electron transfer flavoprotein-ubiquinone oxidoreductase; AOX, alternative oxidase (only present in plants); IMM, inner mitochondrial membrane; IMS, intermembrane space. [Figure adapted from Fig 1. in [41]].

The ETS takes the electrons from NADH (or nicotinamide adenin dinucleotide) and from succinate. The TCA cycle generate NADH and succinate, the two substrates of the Complex I and the Complex II. $FADH_2$ is the product of Complex II, electrons from succinate reduce FAD forming $FADH_2$. Electrons of NADH are transferred to Complex I, while the electrons of the succinate, an intermediate of the Krebs cycle, are transferred to the prosthetic group of the Complex II. Both routes converge on the CoQ pool which transports the electrons to Complex III. A second mobile transporter, cytochrome c (cyt c), transfers the electrons from the Complex III to the Complex IV. The Complex IV is able to reduce molecular oxygen, converting it into H_2O through the bond of free protons from the internal matrix [42].

This flow of electrons down an electro-chemical redox potential liberates energy, which is converted by proton pumping across the IMM from the matrix to the IMS, as

achieved by Complexes I and III. The proton transport produces both a chemical gradient (ΔpH) and an electrical gradient (ΔΨ), thus generating a proton-motive force that is used to generate ATP.

In the inner mitochondrial membrane, it is also present ATP-synthase (or F_1F_0-ATPase) which catalyzes the reversible formation of adenosine triphosphate (ATP) from adenosine diphosphate (ADP) and inorganic phosphate (P_i).

As the internal membrane is impermeable to ions, protons pass through the transmembrane channel of the F_0 portion of ATP synthase to re-enter in the mitochondrial matrix. The proton-motive force drives protons towards the matrix and allows the synthesis of ATP, catalyzed by the F_1 portion of the ATP synthase. Part of the ATP produced by oxidative phosphorylation process is used by the mitochondrion, but most of it is carried outside by the adenine-nucleotide translocase (ANT) and used in other metabolic processes of the cell. Protons can also return to the matrix through the UCPs (uncoupling proteins), transmembrane proteins that increase the permeability of the inner mitochondrial membrane.

2.3.2.1 Complex I

Complex I (or *NADH-ubiquinone oxidoreductase,* EC 7.1.1.2) is a large integral membrane protein embedded in the IMM.

The enzyme has a typical "L" structure, with a hydrophobic arm (membrane arm, P-module) inserted into the IMM and a hydrophilic arm mitochondrial (peripheral or matrix arm, N- and Q- modules) that protrudes into the mitochondrial matrix. In prokaryotes, each arm consists of 7 subunits (core); the membrane arm contains 4 domains that promote translocation of protons, while the peripheral arm comprises a flavoprotein (FMN), 8 Fe-S centres and the binding sites for the two substrates, ubiquinone and NADH (Figure 13) [43].

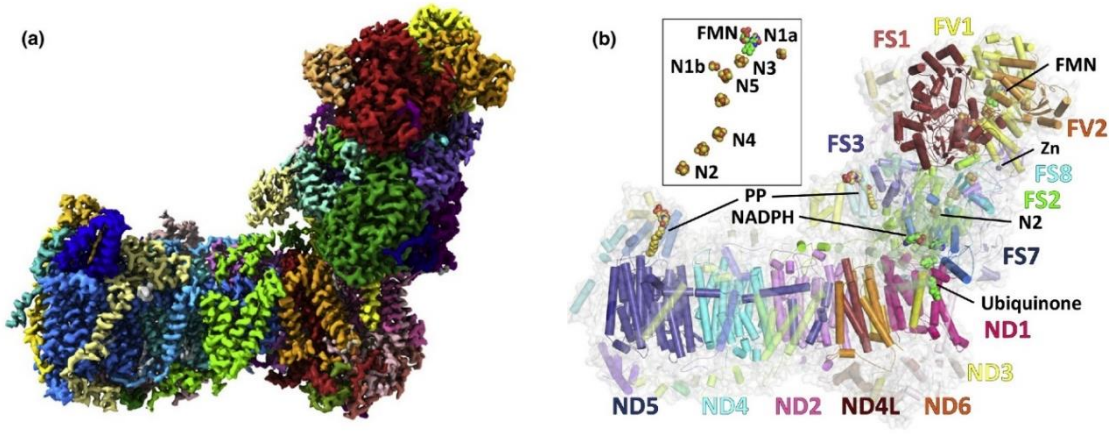

Figure 13. Structure of the Complex I (NADH:ubiquinone oxidoreductase) [44].

While the prokaryotic enzyme is made up of only 14 subunits and its mass is about 550 kDa, in eukaryotes the enzyme is made up of 44/45 subunits and the molecular weight is about 1000 kDa. High-resolution structures have enabled molecular modelling and molecular dynamics simulation approaches, providing a structural basis for unravelling both the evolutionary relationships and the mechanism of redox-linked proton translocation in the Complex I family [44].

The 14 subunits of the so-called "catalytic core" of Complex I are highly conserved from bacteria to humans and are assigned to three functional modules: the N module for NADH oxidation and the Q module for ubiquinone reduction are located in the matrix arm (central subunits NDUFS1, NDUFV1, NDUFV2 and NDUFS2, NDUFS3, NDUFS7, NDUFS8, respectively), while the P module for proton translocation is in the membrane arm (central subunits ND1 to ND6 and ND4L). During evolution, the eukaryotes accumulated the remaining 30 subunits that are defined as "accessory subunits", as their function is not yet fully known although it is generally accepted that they are involved in regulation, stability, assembly and protection against oxidative stress [44].

In eukaryotes, the genes for the seven central subunits of the membrane arm represent a substantial part of the mitochondrial genome. All other subunits, mostly hydrophilic, and all assembly factors of Complex I are encoded by nuclear DNA and subsequently imported inside the mitochondria [45,46].

Complex I catalyses the oxidation of NADH to NAD^+ within the mitochondrial matrix. The initial electron acceptor is the flavin mononucleotide (FMN) in subunit NDUFV1, which is completely reduced to form $FMNH_2$. Then, a chain of seven Fe-S clusters in the matrix arm of Complex I connects the NADH binding site with the CoQ reduction site. Cluster N1a, which is located on the distal side of FMN in NDUFV2, is thought to have a special function in controlling access of NADH and protecting against overreduction of Complex I. The last Fe-S cluster is N2, the immediate reductant for CoQ, buried in the peripheral arm above the membrane surface [44]. Hydrophobic CoQ has to move in a tunnel from the lipid bilayer to the CoQ reduction site in Complex I. The long isoprenoid tail is thought to be important for guiding and facilitating movement of CoQ in the extended access pathway [47].

This electron transfer in complex I is coupled, for each pair of electrons donated by NADH, at the translocation of 4 protons, from the inner mitochondrial membrane to the intermembrane space, contributing to the proton motive force [48]. Complex I provides approximately 40% of the proton flow which is necessary for the production of ATP in the cell.

The activity of Complex I is the limiting step of the mitochondrial respiratory chain and is therefore a very important factor in the regulation of oxidative phosphorylation.

Complex I is also the major source of reactive oxygen species (ROS). Recent studies [49] show that this enzyme can transfer one electron to oxygen, thus producing superoxide anion in mitochondria. Superoxide can spontaneously convert into hydrogen peroxide or via superoxide dismutase (SOD). Various possible sites exist for superoxide production within Complex I: FMN, Fe-S N2 and the Q binding site.

Complex I can generate ROS either during forward electron transfer (NADH to Q, as in normal respiration) or reverse electron transfer (RET, QH_2 to NAD^+), the latter occurring in particular conditions such as high protonmotive force, high ATP/ADP ratio and coenzyme Q pool over-reduced by Complex II/SDH or other dehydrogenases present in the inner mitochondrial membrane [50].

2.3.2.2 Complex II/SDH

Complex II (CII, *succinate-ubiquinone oxidoreductase*, or SDH, *succinate dehydrogenase*, EC 1.3.5.1) is the smallest mitochondrial respiratory complex. CII is a component of both the electron transport chain and the TCA cycle (see section 2.3.1) and completely encoded by the nuclear DNA (Figure 14).

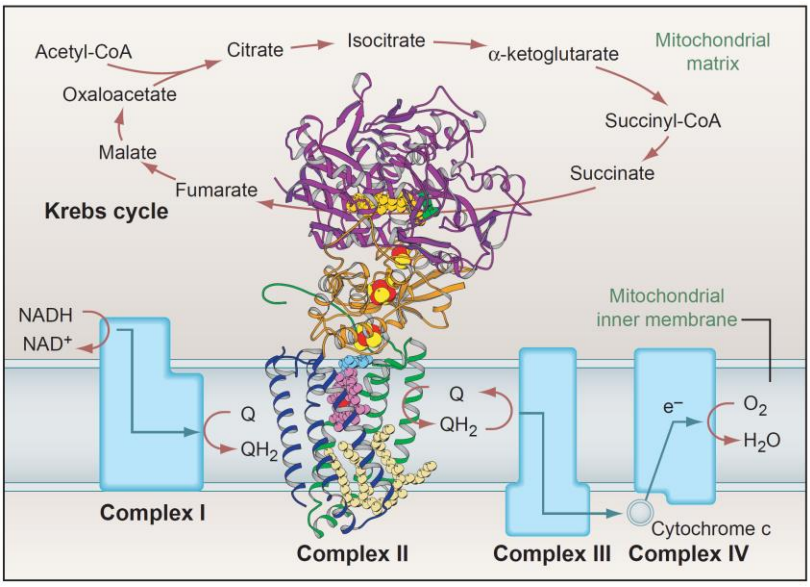

Figure 14. Complex II connects the respiratory chain of the inner mitochondrial membrane with the Krebs cycle enzymes in the mitochondrial matrix [50].

Notably, the CII is not involved in the formation of respiratory supercomplexes (see sections 2.3.2.6 and 2.3.2.7).

CII catalyses the oxidation of succinate to fumarate in the mitochondrial matrix by transferring two electrons to ubiquinone, as the electron acceptor. At difference from other respiratory complexes, the electron transfer mediated by CII is not coupled to proton pumping across the IMM. Subsequently ubiquinone is reduced to ubiquinol, which fuels the Complex III and the Complex IV. The CII is allosterically regulated by oxaloacetate, one of its products, and is activated by ATP in the process.

In eukaryotes, CII is composed by four subunits, SDHA-B-C-D and five prosthetic groups FAD, three 2Fe-2S centres and heme b (Figure 15).

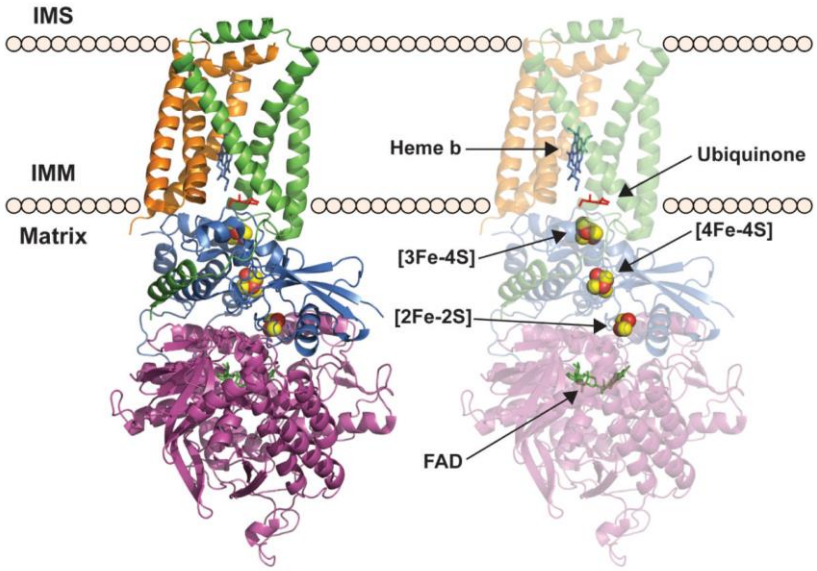

Figure 15. Structure of Complex II (succinate dehydrogenase). Abbreviations: IMS, intermembrane space; IMM, inner mitochondrial membrane; FAD, flavine adenine dinucleotide [51].

SDHA, the largest subunit, is a flavoprotein that contains the binding site for succinate and one FAD (flavine adenine dinucleotide) molecule as a redox centre, which receives two electrons from succinate. SDHB is an iron-sulfur (Fe-S) subunit that includes three aligned Fe-S clusters, also important for the electron transfer. SDHA and SDHB extend into the matrix, while SDHC and SDHD are two small integral membrane proteins, each formed by three transmembrane helices, that anchor the CII to the inner mitochondrial membrane. SDHC and SDHD bind heme-*b* to form *b*-type cytochromes and include the binding site for CoQ [52].

In the past, several groups have identified numerous mutations in human CII that induce increased production of ROS, resulting in tissue damage and disease. In particular, deletions, missense or nonsense mutations in the genes encoding CII and its assembly factors are associated with several diseases [53]. Mutations in SDHA, SDHB, SDHC, SDHD and SDHAF2, encoding for succinate dehydrogenase (SDH) complex assembly factor 2, cause rare neuroendocrine tumours, hereditary pheochromocytomas and paragangliomas (PPGL) [54]. SDHx mutations lead to the decrease or loss of SDH/CII enzymatic activity and therefore as a consequence an accumulation of succinate occurs due to the truncated TCA cycle (see Chapter 2.3.3.2). Moreover, SDHx mutations induce cell metabolic reprogramming and redox imbalance.

The ROS production by CII is somewhat controversial and not entirely clear. When high concentrations of succinate are present in the matrix, electrons from succinate reduce the ubiquinone pool. The over reduction of the Q pool, electrons are forced to come back from ubiquinone towards CI (reverse electron transfer, RET) [55]. When the succinate concentration is low, the electrons of the succinate reach FAD in SDHA and can react with free oxygen molecules present in the active site.
Moreover, inhibitors of CII can affect ROS production in mitochondria. It has been demonstrated that several inhibitors can block either the binding site of succinate (e.g. oxalacetate or malonate) or the binding site of CoQ (e.g. thenoyltrifluoroacetone-TTFA). In the former case, ROS production decreases whereas, in the latter ROS generation increases [56].

2.3.2.3 Complex III

Complex III (CIII, *cytochrome bc_1 complex* or *ubiquinol-cytochrome c oxidoreductase*, EC 7.1.1.8) is composed by two identical monomer units, each consisting of 11 different protein subunits. The dimeric structure is essential for the correct functioning of the enzyme and each monomer contains 3 subunits with redox prosthetic groups: cytochrome b with 2 heme groups (b_H and b_L), Rieske iron-sulfur protein with its 2Fe-2S centre, and cytochrome c_1 with its heme group. Cytochrome c_1 and Rieske protein protrude towards the IMS and they can interact with cytochrome c, which is a small soluble protein located on the outer surface of the same IMM. Each CIII monomer possesses two binding sites for ubiquinone: Q_N (or Q_i, "negative centre" or "centre in", facing the side of matrix) and Q_P (or Q_o, "positive centre" or "centre out", facing the IMS) (Figure 16).

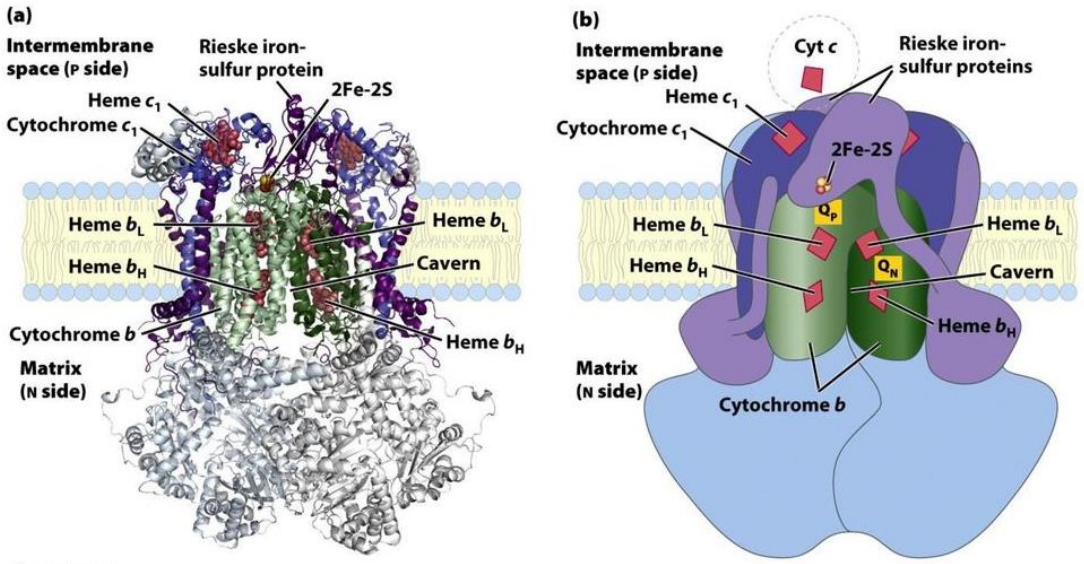

Figure 16. Structure of Complex III (cytochrome bc1 complex) [40].

Complex III can transfer electrons from ubiquinol (QH_2), the fully reduced form of ubiquinone present located in the IMS, to cytochrome c. This reaction is also coupled with the transport of protons from the matrix to the intermembrane space [57].

To explain the flow of electrons and proton transportation through Complex III, in 1975 Mitchell [58] proposed a model called the Q cycle (Figure 17).

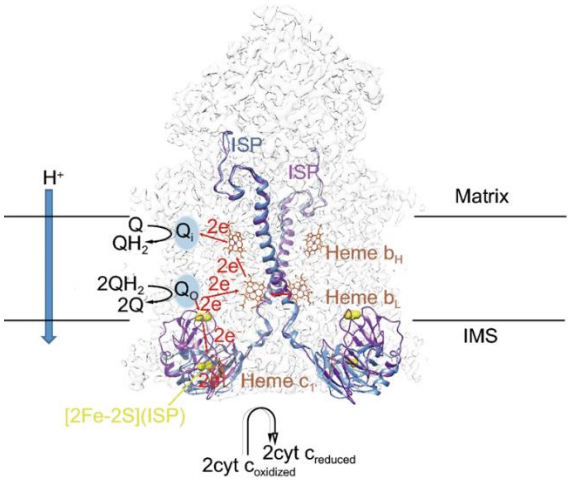

Figure 17. Schematic representation of the Q cycle of the Complex III [59].

The model predicts the involvement of both CoQ-binding sites, Q_P and Q_N respectively. In brief, the Q_P is the site for ubiquinol oxidation, while Q_N is the site where quinone reduction occurs. In fact, the cycle can be divided in two stages: A) ubiquinol binds the Q_P site and gives a first electron to the Fe-S center of the Rieske protein which, through cytochrome c_1, reaches cytochrome c. In this way, at the level of the Q_P site, a molecule of ubisemiquinone ($UQ^{\cdot}$-) and two protons are generated and released into the IMS. The semiquinone immediately oxidizes to ubiquinone (Q), releasing the second electron, which is first transferred to the low potential heme (b_L) and then to the high potential (b_H). At this point the electron reaches the site Q_N, where there is a ubiquinone molecule, that is immediately converted to deprotonated ubisemiquinone ($UQ^{\cdot}$-). B) The second half of the cycle is similar to the first and also begins with a ubiquinol molecule oxidized at the Q_P site, releasing two more protons into the intermembrane space. The first electron is transferred to one molecule of cytochrome c as in the A-stage, while the second, again passing through the two hemes, b_L and b_H, reacts with the ubisemiquinone molecule that formed earlier at the Q_N site, reducing it completely to ubiquinol. For this last step, two protons are captured from the mitochondrial matrix. Ubiquinol frees itself from the Q_N site and becomes part of the pool of CoQ in the lipid membrane, thus completing the cycle [60].

The mitochondrial CIII is a symmetrical dimer, but it was shown that the dimer behaves as a functional monomer. Covian et al. [61] demonstrated that the Fe-S centre of the Rieske protein is anchored in one monomer and the peripherical domain of the subunit is placed in the second monomer, crossing the dimeric structure. Remarkable evidence exists suggesting that the hydrophilic domain of the Rieske protein moves from a position near heme b_L to a position near the heme centre of cytochrome c_1, facilitating electron transfer within the enzyme [41].

Complex III is considered one of the important producers of superoxide in living organisms. To date the exact mechanism of superoxide production by CIII and the remain poorly understood but a possible mechanism was suggested from the analysis of the ROS production by CIII in the presence of antimycin A, specific inhibitor of Q_N/Q_i site of the CIII. At the level of Q_P/Q_o site is possible to have two reactions: oxidation of ubiquinol

and reduction of ubiquinone. The first reaction leads to ubisemiquinone (UB) production which is an unstable molecule that can easily react with molecular oxygen to form a superoxide anion radical ($O2^{\bullet-}$) [62,63].

2.3.2.4 Complex IV

Complex IV (CIV, or *cytochrome c oxidase*, EC 7.1.1.9) is the last redox complex of the respiratory chain, which transfers electron from cytochrome c to molecular oxygen, reducing it to H_2O. Cytochrome c is a small soluble protein located on the outer side of the IMM and represents the second mobile electron carrier of the respiratory chain between C III and CIV.

Eukaryotic Complex IV comprised 3-4 subunits, while the mammalian enzyme consists of 13 subunits in each monomer of its dimeric structure, 3 catalytic subunits (subunit I, II and III, MTCO1-3), encoded by mitochondrial DNA, essential for the electron flow and the other 10, encoded by nuclear DNA, contribute to the assembly and stability of the complex (Figure 18) [64].

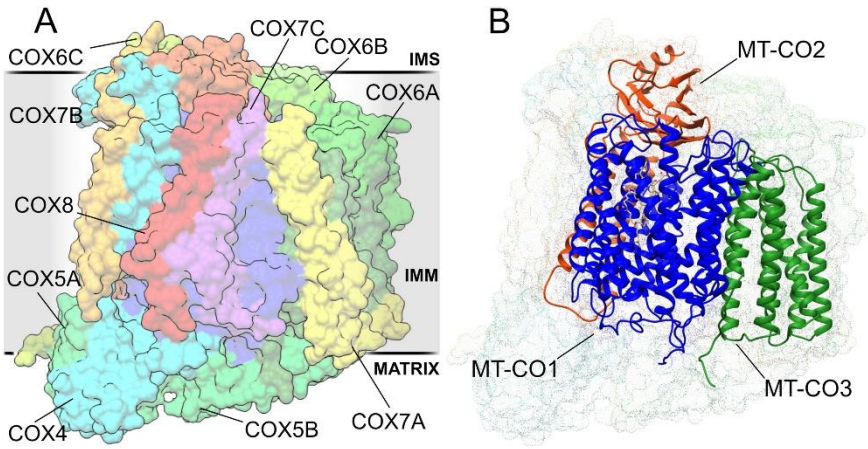

Figure 18. Structure of the CIV (cytochrome c oxidase). Structural organization of the a) 10 "accessory" subunits and the b) three catalytic subunits of CIV. Abbreviations: COX, cytochrome c oxidase; IMS, intermembrane space; MT-CO1-3, mitochondrially encoded cytochrome c oxidase 1-3 [65].

Subunit I has a tubular shape and consists of 12 transmembrane helices which form the channel for the passage of protons. It contains a heme *a* group and the heme a_3-Cu_B binuclear centre, responsible for reducing oxygen to H_2O.

Subunits II and III are on opposite sides of subunit I and they are not in contact with each other. Subunit II has a transmembrane domain on the outer side of the IMM and contains the cytochrome c binding site and two Cu atoms complexed with the thiol groups (-SH) of 2 cysteine residues (Cu_A binuclear centre) which resembles the 2Fe-2S centres of iron sulfur proteins. The Cu_A centre represents the primary electron acceptor with reduced cytochrome c. Subunit III consists of 7 transmembrane helices and does not contain reactive centres. The functional role is not still clear, but its presence stabilizes the proton pumping.

Electron transfer through CIV begins with two molecules of reduced cytochrome c, where each donate an electron to the Cu_A binuclear centre of the subunit II. Electrons pass through heme *a* to the heme a_3-Cu_B binuclear centre. Oxygen is reduced to its peroxy derivate by the two electrons from Cu_B center. Other two electrons from another molecule of cytochrome c completely convert peroxy intermediate into two molecules of water, consuming four “substrate” protons from the mitochondrial matrix. At the same time, two protons are pumped from the mitochondrial matrix to the IMS for each pair of electrons crossing the CIV. Three different hydrophilic channels, called H-, D- and K-channels, are suggested in the subunit I of the CIV to drive protons from the mitochondrial matrix to the IMS, through the redox enzyme, but it is not fully understood the precise mechanism (Figure 19) [66].

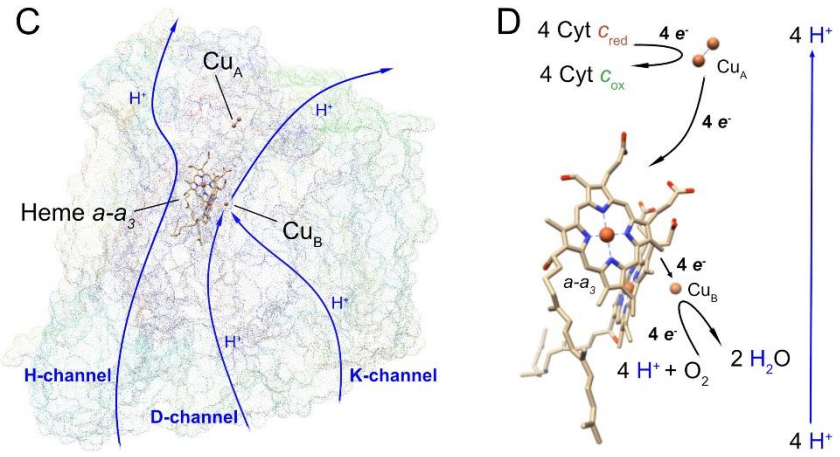

Figure 19. c) Schematic representation of the three different hydrophilic channels for proton translocation (H-, D- and K-channels) and d) electron transfer from cytochrome c to oxygen through the redox centres of CIV [66].

2.3.2.5 ATP synthase

ATP-synthase (or *F_1F_O-ATPase*, EC 7.1.2.2) is a multiunit transmembrane enzyme found in membranes of bacteria, chloroplasts and mitochondria.

Mitochondrial ATP-synthase is a functionally reversible F-type of ATPase, which produce ATP from adenosine diphosphate (ADP) and inorganic phosphate (P_i), using the proton motive force generated by the ETS across the IMM and can also hydrolyse ATP to pump protons against the electrochemical gradient [67].

The enzyme is composed of two structural and functional domains: an integral F_O domain ("o" refer to oligomycin-sensitive) crossing the IMM and a peripherical F_1 domain that protrudes into the mitochondrial matrix. The two domains are linked by a central and a peripheral stalk (Figure 20) [68].

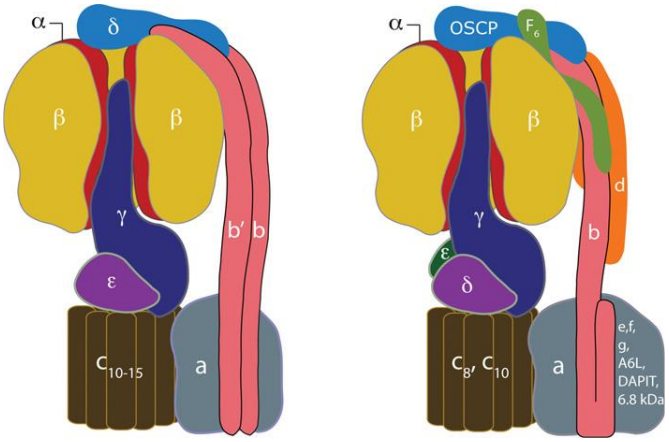

Figure 20. Organization of protein subunits in the bacterial and chloroplast ATP synthases on the left and the mitochondrial ATP synthase on the right [69].

The F_1 portion five different types of subunits (α, β, γ, δ, ε) with the stoichiometry of 3α:3β:γ:δ:ε. The three α and the three β subunits are alternately arranged to form a hexamer around the γ subunit. Each of the three β subunits contain a catalytic site for ATP synthesis/hydrolysis. The γ subunit, together with the δ and the ε subunits, constitutes the central stalk of the complex, which attach the catalytic portion of F_1 domain to the structure of F_O portion [69].

The F_O domain consists of three subunits (a, b, and c) with the stoichiometry of a:2b:9–12c. The proton channel is a ring of 9-12 c subunits placed in the IMM and tightly attached to the a subunit and two b subunits. The c subunits in the ring rotate together as a single entity around a perpendicular axis respect to the membrane. From the centre of the c ring, the γ and ε subunits of F_1 domain protrude into the mitochondrial matrix and bound, through the δ subunit, the two b subunits of F_O portion.

In mitochondria, the F_1 component is attached to F_O domain by the peripheral stalk or stator, which consists of single copies of subunits OSCP (oligomycin sensitivity conferral protein, the homologue of the bacterial *δ*-subunit), b, d and F6 [70].

ATP synthase is fully active as a monomer, but several studies demonstrated that is more efficient in dimeric or oligomeric forms (Figure 21) [71]. The ATP dimers are associated together in back-to-front rows along the edges of the cristae.

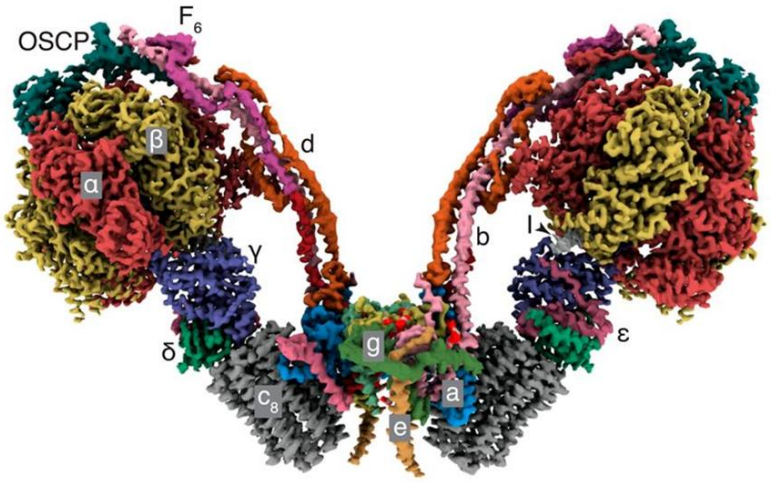

Figure 21. Structure of dimeric bovine ATP synthase [72].

2.3.2.6 Different models of organization of the respiratory complexes

The first hypothesis on the organization of the mitochondrial complexes, the so-called *solid-state model*, was proposed in 1956 by Chance and Williams [72]. In this model the different electron carriers of the respiratory chain are arranged in an ordered sequence along the inner mitochondrial membrane. The various protein components were supposed to be physically anchored to the phospholipid bilayer (Figure 22).

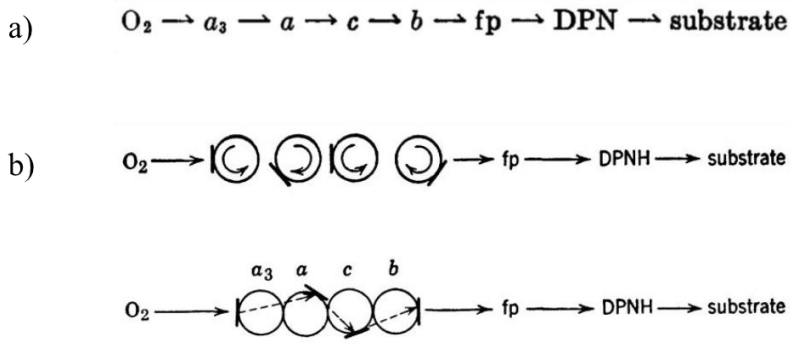

Figure 22. Solid-model of Chance and Williams (1955). a) Sequence of respiratory components in solid-array determined spectrophotometrically and b) two different models of electron transfer mechanisms along the fixed electron carriers in the respiratory chain. Abbreviations: *a3*, *a*, *c*, *b*, cytochromes *a3*, *a*, *c*, and *b*; *fp*, flavoprotein; DPN /DPNH, diphosphopyridine nucleotide (NADH) [73].

In another theory, the *liquid-state model*, suggested in 1966 by Green and Tzagoloff [73], the four respiratory complexes are randomly distributed at the level of the inner mitochondrial membrane and are interconnected by diffusible elements: coenzyme Q and cytochrome c.

The last model proposed was the *random collision model* by Hackenbrock in 1986 [74]. In this model all components of the respiratory chain, both enzymatic complexes and mobile elements, are randomly distributed in the inner membrane and can freely spread by lateral diffusion. The transport of electrons depends on the ability of all these components to collide randomly along the phospholipid bilayer, so the diffusion rate of these elements could act as a limiting stage for the transport of electrons (Figure 23).

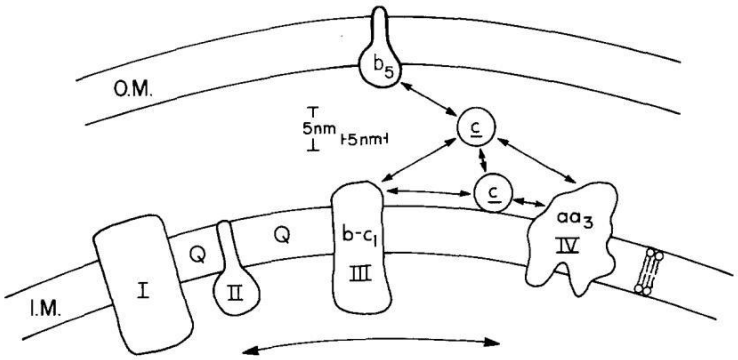

Figure 23. Random collision model of Hackenbrock (1986). Abbreviations: O.M, outer membrane, I.M., inner membrane, b5, cytochrome *b5;* c, cytochrome *c*; Q, ubiquinone; I, II, III, IV, complexes I, II, III, and IV [75].

Contrary to the long-established concept of mitochondrial respiratory chain organization, much evidence supports the new view according to which some complexes of the respiratory chain aggregate to form macromolecules, called respiratory supercomplexes (SCs). The complexes involved in these aggregates are Complex I, Complex III and Complex IV, with different stochiometric ratios.

In 2000 H. Schägger [75] demonstrated the existence of functional aggregates among two or more enzymes, called supercomplexes (SCs), at the level of the inner mitochondrial membrane (see Chapter 2.4.1.2). He applied the technique blue native

polyacrylamide gel electrophoresis (BN-PAGE) on high molecular weight protein fractions purified from bovine heart mitochondria using a bland non-ionic detergent, digitonin, which preserve free complexes and protein aggregates during extraction from the mitochondrial membrane.

A further vision of the organization of mitochondrial complexes has been recently proposed. In 2008 R. Acín-Pérez and J.A. Enriquez suggested an integrated model defined as *plasticity model* [76]. They confirmed the existence of supercomplexes in mammalian cells suggesting that, under physiological conditions, respiratory aggregates coexist in a dynamic equilibrium with the single free forms of Complex I, III and IV along the inner mitochondrial membrane.

2.4.1.2 Respiratory supercomplexes

Numerous experimental findings demonstrated the existence of respiratory supercomplexes (SCs) in many different species, also including plants, fungi and bacteria.

The supercomplex $I_1III_2IV_n$ is formed by a monomer of Complex I, a dimer of Complex III and by n copies of Complex IV. The entire supramolecular assembly has a molecular weight of around 1700 kDa. It is worth nothing that the supercomplex $I_1III_2IV_n$ contains all the enzyme complexes required to accomplish the autonomous complete oxidation of NADH and full reduction of molecular oxygen, for this reason it is called respirasome (Figure 24) [60].

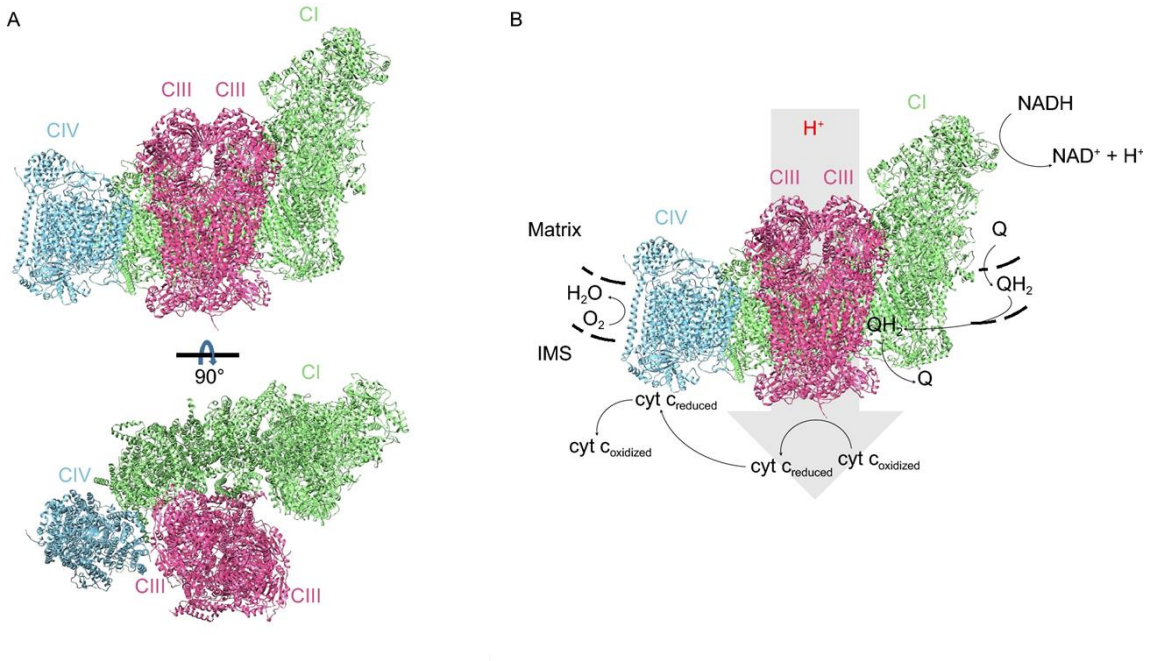

Figure 24. Structure of Mammalian SC $I_1III_2IV_1$. A) Cryo-EM structure of human SC $I_1III_2IV_1$ in two different orientations and B) substrate translocation in SC $I_1III_2IV_1$ [60].

The respirasome is the high-order assembly of the mitochondrial electron transport chain but other types of supercomplexes, containing fewer enzyme components, are physiological present in large amounts in mitochondria, such as the SC I_1III_2 or the SC III_1IV. Only Complex II tends to exist in a non-associated form in plant and mammalian mitochondria.

In 2005 Dudkina et al. [77] were able to isolate the SC I_1III_2 from digitonin-solubilized *Arabidopsis thaliana* mitochondria and were able to reconstruct a 3D model of the aggregate based on electron microscopy results. In their 3D reconstruction, the dimer of Complex III is laterally associated with the hydrophobic membrane arm of Complex I, in correspondence with the central portion of the arm. Moreover, they isolated the SC $I_1III_2IV_n$ from purified bovine heart mitochondria and, by BN-PAGE and cryo-EM analysis, they concluded that the individual respiratory complexes, within the aggregate, are spaced from each other with only few protein-protein contact. Furthermore, they showed how Complex IV is associated with the dimer III_2 and also interacts with the membrane arm tip of Complex I [78].

Since then, stable and functional assemblies composed of complexes I, III and IV, were isolated and studied by various authors [60,79,80]. Althoff et al. [81], by using a polymer of ampholytes which binds the hydrophobic surfaces of the SC and stabilizes it in an active form in solution, first revealed important molecular details about the connection between Complex III and the membrane domain of Complex I. They showed that only one of the two monomers of $CIII_2$ takes contact with CI and demonstrated the presence of ubiquinone inside the isolated SC. They also suggested the presence of residual amounts of cytochrome c. Furthermore, Althoff et al. analysed the distance between Complex I and Complex III, which they found to be 13 nm, suggesting that electrons within the SC are channelled into a precise route. It is possible that Coenzyme Q could cover this distance, probably filled with lipid molecules, remaining within the SC as bound CoQ without spreading into the membrane pool as free CoQ molecules.

To date, all mitochondrial complexes isolated have been purified as lipoprotein complexes, and the lipid component appears to play a decisive role in the formation and stability of those SCs. The most discussed phospholipids include phosphatidylcholine (PC), phosphatidylethanolamine (PE), and cardiolipin (CL), the hallmark phospholipid of mitochondria [82]. The overall lipid composition of a cell contributes to control the mitochondria dynamics (shape and function) via alterations of membrane structure and curvature and regulation of protein interactions. An alteration of the lipid composition can lead to the disassembly of SCs which induces the development of several diseases such as Alzheimer's disease, Parkinson's disease, Huntington's disease, Barth syndrome, etc [83,84].

In vitro studies conducted on proteoliposomes have shown that a high lipid:protein ratio precludes the formation of supercomplexes. On the contrary, the addition of cardiolipin molecules preserves the supramolecular organization of the supercomplex and therefore increases the efficiency of electronic transport between the respiratory complexes in samples even with a high lipid content [50].

Maranzana et al. [85] showed that, in the bovine heart mitochondria, only 14-16% of the total amount of Complex I is in free form, while the rest is found associated with

Complex III in SCs. The stoichiometric ratio between the two complexes is 1:2 in favor of Complex III, then it is possible to suppose that around 30% of Complex III is still not bound to Complex I. Moreover, only 15% of Complex IV is associated with other respiratory enzymes, to form the supercomplexes $I_1III_2IV_n$. This data suggest a dynamic equilibrium of the respiratory complexes between individual complexes and the supramolecular assemblies [50,60].

While the supramolecular architecture of the respiratory chain is quite well established, the functional role of SCs is not yet fully clarify and much more evidence are still needed to dispel the doubt. SCs have been proposed to confer functional advantages to the cells and several hypotheses have been suggested to clarify their biological role.

One of the most interesting advantages is represented by the channelling of electrons between Complex I and Complex III. When Complex I and Complex III aggregate, the two binding sites for the Coenzyme Q are really close to each other so it's not possible for the ubiquinone diffuses through the phospholipid bilayer randomly, but directly transfer electrons from complex I to complex III by microdiffusion process in the small gap that separates the two complexes within the supercomplex.

As demonstrated in isolated bovine heart mitochondria, the organization in supercomplexes increases the efficiency of electron transport between Complex I and Complex III and, at the same time, decreases the ROS production by NADH dehydrogenase. *In vitro* studies also confirmed the effect of disaggregation of the SCs by using a strong detergent, dodecyl maltoside (DDM), which promotes the complete dissociation of the supercomplex into its individual components. The separation between Complex I and Complex III leads to a decrease in integrated NADH-cytochrome c oxidoreductase activity and an increase in ROS production [87].

The role of supercomplexes in the inner membrane of mitochondria is an argument for great interest, as an alteration of these aggregates seems to be related to particular pathologies (e.g. heart failure, Parkinson's, schizophrenia, ischemia, aging, etc).

2.3.3 Mitochondrial ETS adaptations upon infection in macrophages

As mentioned above, profound metabolic changes occur during macrophages activation. Reprogramming of catabolic pathways is therefore closely related to macrophage differentiation and function. Since most catabolic processes converge on the mitochondrial electron transport chain, it is possible to consider mitochondria, in particular the respiratory chain, at the centre of this physiological switch.

Moreover, mitochondria are important source of free radicals in the cells (see previous sections 2.3.2.1-2.3.2.3) and under normal condition ROS production contribute to the cellular function, but when the system is dysregulated oxidative stress could lead to pathological consequences. J.A. Enriquez et al. [86] have recently demonstrated that Complex I produces ROS in the forward or reverse direction depending on the substrates available (glucose or fatty acids).

Recent evidence indicates that organizational and functional adaptations occur in the ETS of macrophages to allow metabolic plasticity upon sensing of live *E. coli* [14] (Figure 25).

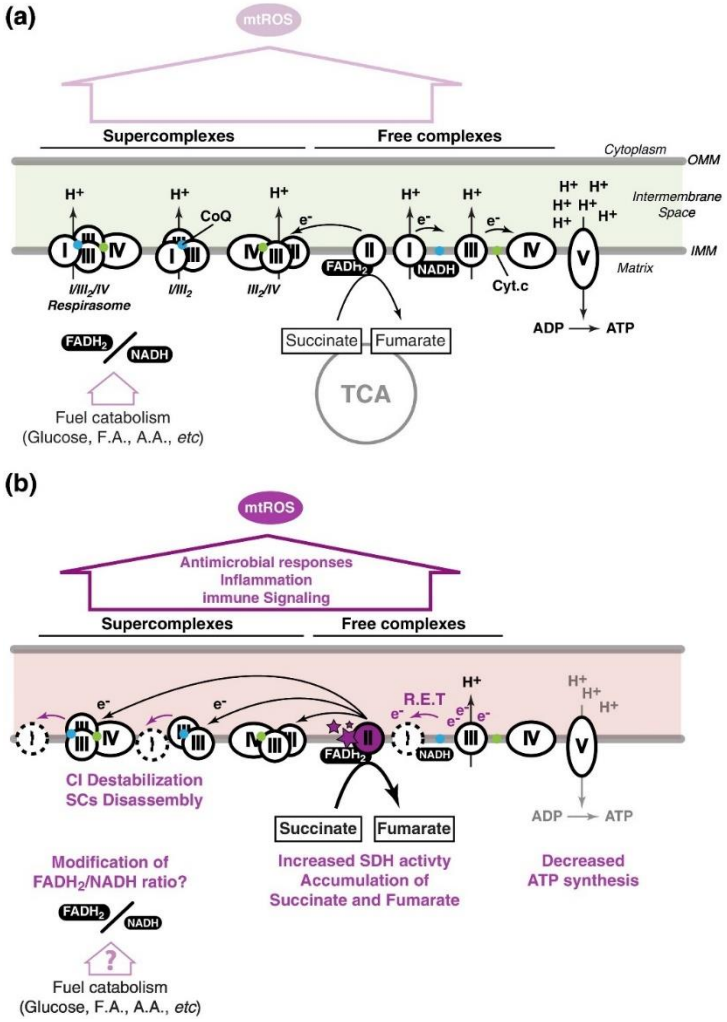

Figure 25. Schematic representation of mitochondrial respiratory chain rearrangements in (a) resting macrophages and in (b) activated macrophages [14].

In resting macrophages (i.e. prior to activation due to infection, see sections 2.2.1), the oxidation of glucose produces NADH and $FADH_2$, which feed the mitochondrial respiratory chain with low mitochondrial ROS production.

On the contrary, in activated macrophages the oxidation of fatty acids changes NADH/FADH2 ratio which leads to an over-reduction of CoQ pool and increases the ROS production via reverse electron transfer (RET). Activated macrophages block the ATP production via oxidative phosphorylation and enhance the succinate oxidation by Complex II/SDH. The CI activity decreases and leads to the disassembly of CI-containing SCs, CII activity increases and transfers electrons to coenzyme Q. This induces an over-

reduction of the CoQ pool, electrons are pumped back to Complex I by RET and ROS production increases at the level of the Complex I. These rearrangements are necessary to induce an inflammatory response characterized by production of pro-inflammatory cytokines upon TLR4 engagement [14].

Mitochondrial ROS production can be also augment upon TLR1, TLR 2 and TLR4 stimulation by bacteria [87]. TLRs activation promotes the translocation of TNF receptor-associated factor 6 (TRAF6) to mitochondria, where it recruits ECSIT (evolutionary conserved signalling intermediate in Toll pathways), which is involved in the mitochondrial Complex I assembly [88]. TRAF6 has E3-ubiquitin ligase activity and the interaction between the two proteins leads to the ubiquitylation of ECSIT and an increase the mitochondrial ROS production from oxidative phosphorylation complexes [89].

2.3.3.1 A broken Krebs cycle in macrophages

It is well known [5] that drastic changes occur in the TCA cycle in activated macrophages and Krebs cycle has emerged as the central immunometabolic hub of the macrophages. In resting state, macrophages use an intact Krebs cycle and consume oxygen normally, while upon activation macrophages enhance TCA cycle increasing OXPHOS and ATP production [90].

Activated macrophages present a truncated Krebs cycle, two metabolic breakpoints occur upon activation: the first one appears at the isocitrate dehydrogenase (IDH) and the second one at the succinate dehydrogenase (SDH) [91]. These two breakpoints lead to an accumulation of citrate and succinate and a reduced production of α-ketoglutarate.

2.3.3.2 Krebs cycle metabolites as inflammatory signalling molecules

Citrate

Citrate increases the production of itaconic acid, which is the major feature of LPS stimulated macrophages. In the mitochondrial matrix, citrate can be converted in itaconate by the enzyme *cis*-aconitate decarboxylase (CAD). Itaconate can directly inhibit SDH decreasing the fumarate production, metabolite important for inflammatory responses [92]. Increased itaconate levels decreases Complex II/SDH activity and leads to a decrease oxidative phosphorylation. Additionally, recent studies [93,94] showed that itaconate regulates inflammatory genes expression dampening specific pathway through Nrf2-dependent and Nrf2-independent pathways in activated macrophages. At the same time, it is known the anti-bacterial effect of itaconate, which inhibits the bacterial growth through the regulation of the isocitrate lyase [95].

Succinate

Succinate has recently emerged as a key pro-inflammatory modulator during macrophage activation.

Inside the cell, it was discovered that in LPS-treated macrophages succinate accumulates and enhances interleukin-1β mRNA and pro-interleukin-1β protein production and inhibits the induction of anti-inflammatory cytokines (interleukin-10 and interleukin-1RA). Succinate can be exported outside from the mitochondria into the cytosol and blocks cytolytic prolyl hydroxylase (PHD) activity. The role of PHD is to stabilize hypoxia-inducible factor 1α (HIF-1α), highly conserved member of the basic helix-loop-helix (bHLH) family of transcriptional regulars in the expression of pro-inflammatory genes. HIF-1α has a critical role in the regulation of several biological processes, directing the expression of genes involved in cellular metabolism, inflammation, proliferation, etc. One of the main effects of HIF-1α activation is the involvement in the metabolic switch from OXPHOS to glycolysis (glycolytic reprogramming). When O_2 level is high, HIF-1α is tightly regulated by prolyl

hydroxylases (PHDs) which use α-ketoglutarate and O_2 to produce succinate and to hydroxylate conserved proline residues in HIF-1α. The hydroxylation of HIF-1α lead to ubiquitination of the factor by the binding of an E3 ubiquitin ligase, the tumour suppressor protein Von Hippel-Lindau (VHL). Consequently, HIF-1α is degraded via proteasome. When the O2 level is low, then during hypoxia, the degradation of HIF-1α is prevented. HIF-1α translocates to the nucleus, forms a heterodimeric complex with HIF-1β and binds target genes.

It was demonstrated that succinate can be oxidized by SDH in LPS-activated macrophages. This event indirectly inhibits PHD activity via mitochondrial ROS (mtROS) production, which stabilizes HIF-1α and induces IL-1β production. Moreover, Mills et al. [4] showed that reducing succinate oxidation in LPS-activated macrophages with dimethyl malonate (DMM), potent inhibitor of the Complex II/SDH, potently blocks mtROS production from Complex I via reverse electron transfer (RET) [96].

An extracellular role for succinate has been identified together with its receptor succinate receptor 1 (SUCNR1), which is a G protein-coupled receptor (GPCR). It was demonstrated, in dendritic cells, that succinate induces calcium mobilization and pro-inflammatory cytokines production. In macrophages, LPS induces the release of succinate by SUCNR1, which further triggers IL-1β production [97].

α-ketoglutarate

α-ketoglutarate (α-KG), also known as 2-oxoglutarate, is the co-substrate of 2-oxoglutarate-dependent dioxygenase (2-OGDD), which catalyses hydroxylation reactions with several substrates. The activity of this enzyme depends on the intracellular ratio of α-KG to succinate and it is important in response to hypoxia and chromatin modifications [98]. Glutamine can contribute to replenishment of the TCA cycle through glutaminolysis, a metabolomic processes which starts with the conversion of glutamine to glutamate, catalyzed by glutaminases (GLSs) in mitochondria. Glutamate is converted to α-KG by either glutamate dehydrogenase (GDH) or by the alanine or aspartate transaminases

(TAs) [99]. Glutamine anaplerosis is increased in M1-like proinflammatory macrophages [100].

2.3.4 Epigenetic reprogramming

As demonstrated in various models, including cancer cells, epithelial cells, etc, it is known that TCA cycle-derived metabolites can control innate immunity through epigenetics modifications. Citrate, succinate, fumarate or a-ketoglutarate were all shown to contribute to histone and DNA demethylation in innate immune cells (Figure 26) [6].

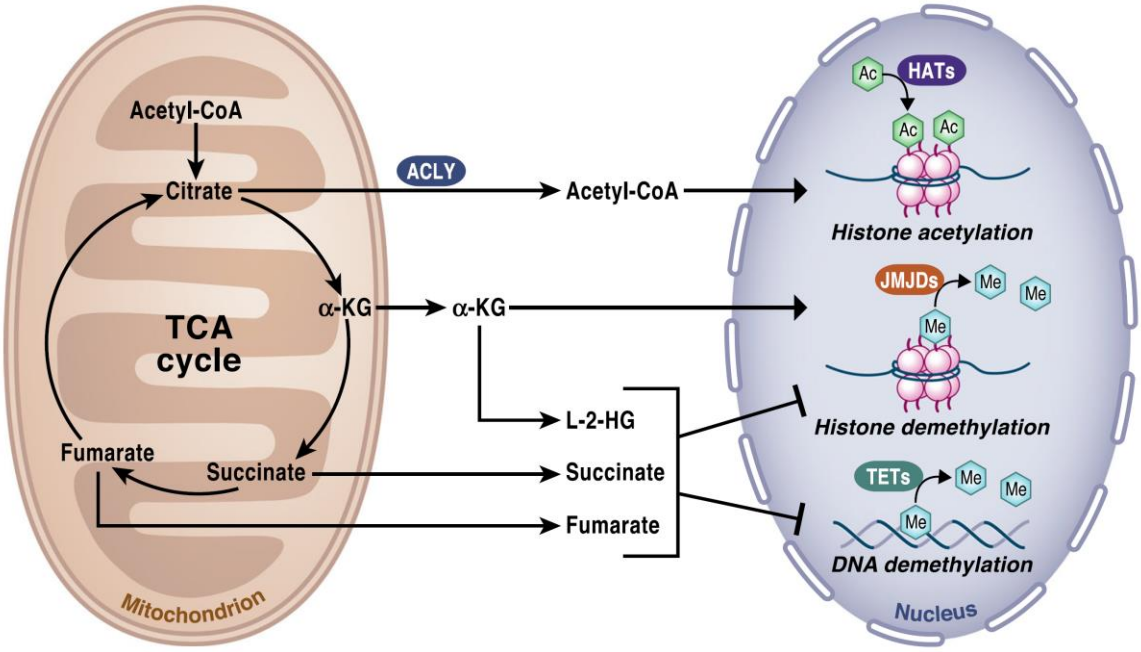

Figure 26. TCA-cycle derived metabolites control chromatin modifications and DNA methylation [6].

Citrate

Citrate can be exported from the mitochondria trough a dicarboxylate antiporter solute carrier (CIC, Slc25a1) and be converted back to aceytl-CoA and oxalacetate (OAA) by ATP citrate lyase (ACLY). One of the most important roles of acetyl-CoA in the cytosol is to serve as substrate for histone acetylation, a mechanism regulating the

dynamics of chromatin and gene expression. Inside the nucleus specific enzymes, histone acetyltransferases (HATs), are present and are able to catalyse the addition of acetyl groups on the histone. It was demonstrated that elevated histone acetylation increases the expression of genes involved in cell growth and proliferation. In cancer cells, an upregulation of ACLY occurs in the presence of high acetyl-CoA levels in the mitochondria, in order to trigger their proliferation. LPS-stimulated macrophages accumulate citrate in the mitochondria, increase cytosolic acetyl-CoA levels and upregulate ACLY to induce histone acetylation which, in turn, leads to the production of pro-inflammatory molecules [6,101].

α-ketoglutarate

α-ketoglutarate (α-KG) is an important co-factor for histone demethylases, enzymes involved in the chromatin modification. Jumonji C domain containing lysine demethylases (JMJDs) are the major histone demethylases and ten–eleven translocation (TET) hydroxylases are implicated in DNA demethylation. It was demonstrated that high α-KG levels increased activities of JMJDs and TET proteins, decreasing histone methylation and promoting the stem cells differentiation. Moreover, an important role of α-KG was established in memory T cell differentiation. In IL-4 stimulated macrophages the increase of glutaminolysis is due to increase production of α-KG that facilitates macrophages polarization and favours an anti-inflammatory profile competing with JMJDs [102].

Succinate

Succinate accumulates due to succinate dehydrogenase (SDH) mutations, and it is considered an oncometabolite. Several type of cancers present SDH mutations, such as hereditary paraganglioma (PPGL), where it was found an overall hypermethylation of DNA. Mutations in the SDH genes lead to an accumulation of succinate, which inhibits iron(II) and alpha-ketoglutarate-dependent dioxygenases therefore leading to an abnormal stabilization of HIFα. Another consequence is the inhibition of the DNA demethylase,

increasing the 5-methylcytosine/5-hydroxymethylcytosine (5-mC/5-hmC) ratio, and the histone demethylase [103].

Fumarate

Fumarate, like succinate, can accumulate due to fumarate hydratase (FH) mutations in different genetic disease and in genetic maladies, such as fumaric aciduria and hereditary leiomyomatosis. Fumarate acts as an immunomodulator by controlling chromatin modifications and regulating protein succination. Accumulation of fumarate induces hypermethylation of DNA since fumarate is a competitive inhibitor of multiple α-ketoglutarate (α-KG)-dependent dioxygenases, such as TET hydroxylases [104]. Fumarate also accumulates in LPS-stimulated macrophages by inhibiting histone demethylase, which leads to an increase of DNA methylation and boosting the gene expression of proinflammatory cytokines, TNFα and IL6 [105].

Aim of the project

The activation of macrophages drives the conversion of immune cells from metabolically quiescent stage to a highly active metabolic state. At the core of this metabolic remodelling there are mitochondria, the main metabolic organelles present in the cell that house fundamental metabolic pathways (Krebs cycle, beta-oxidation, etc). In the inner mitochondrial membrane, there is the electron transport system (ETS), composed by four major respiratory complexes (Complex I-IV) and two mobile electron carriers (coenzyme Q and cytochrome c). Physiologically, the Complex I, III and IV can aggregate to form functional assemblies called supercomplexes (SCs). The dynamic assembly of respiratory complexes into SCs has been proposed to confer functional advantages to the cells, the ETS being as central to mammalian energy metabolism as its dysfunctions are to human disease. Mitochondrial reprogramming is also tightly connected to innate immunity but the precise role of SCs in metabolic adaptations in immune host defence is still little known. Several studies have demonstrated altered metabolic pathways cause immune dysfunction and the understanding of mitochondrial reprogramming upon bacterial infection can help in understanding innate immune mechanisms in inflammatory and infectious diseases.

The first aim of this PhD project was to understand whether mitochondrial reprogramming in macrophages and in isolated mitochondria from infected mammalian tissues depends on the nature of the bacteria encountered by the host cell. To assess the contribution of the organization of the mitochondrial ETS to bacterial infection, macrophages were cultured with Gram-negative (Gram-) and Gram-positive (Gram+) bacteria and, in addition, spleen, heart and liver samples were obtained from mouse models of bacterial infection.

The second aim was to investigate the impact of the respiratory Complex II (CII, succinate dehydrogenase EC 1.3.5.1) on macrophage-mediated immune response against bacteria. To evaluate the involvement of Complex II in macrophage metabolic reprogramming, cultured macrophages were treated *in vitro* with two different CII inhibitors, 3-nitropropionic acid (3-NPA) and dimethyl malonate (DMM).

Materials and Methods

4.1 Bacteria strains

LB medium: 5 gr peptone (Condalab 1616), 5 gr yeast extract (Condalab 1702), 2.5 gr NaCl (Sigma-Aldrich 793566) in 500 ml of pure H_2O, autoclaved at 120°C for 30 minutes and stored at 4°C until use.

Gram-negative bacteria strains: *Escherichia coli DH5α* (*E. coli*), *ΔSpi1/2 Salmonella enterica* Typhimurium (SL1344) (*ΔSpi1/2 S. enterica*), *Pseudomonas aeruginosa* (*P. aeruginosa*). Gram-positive bacteria strains: *Listeria innocua* (*L. innocua*), *ΔLLO/ΔFlic Listeria monocytogenes* (*ΔLLO/ΔFlic L. monocytogenes*) and *Staphylococcus aureus* (*S. aureus*).

All bacteria strains were grown in lysogeny broth (LB) overnight at 37°C and then diluted the next day to reach logarithmic growth. Bacteria were centrifuged at 4000g for 5 minutes (Heraeus Megafuge 16R, rotor F15-6x100y, Thermo Fisher) and resuspended with Dulbecco's phosphate-buffered saline (PBS 1X, Gibco 14190) to remove LB salts. Bacterial concentrations were measured by spectrophotometer (double-beam UV-Visible spectrophotometer SAFAS UVmc2) at 600 nm before addition to cell cultures at a multiplicity of infection (MOI) of 25 (1 macrophages vs. 25 bacteria).

4.2 Cell cultures

4.2.1 Isolation of bone marrow derived macrophages (BMDMs)

BMDM medium: RPMI 1640 medium (1X) + GlutaMAX (Gibco 61870) complemented with M-CSF (30% mycoplasma-free L929 cell supernatant), 10% Fetal Bovine Serum (FBS, Gibco A4766801), 100 µg/mL Penicilin/streptomycin (Gibco 15140), 2 mM L-glutamine (Gibco 25030), 10 mM HEPES (Gibco 15630122), 1 nM sodium pyruvate (Gibco 11360), 1XMEM non-essential amino acids (Gibco 11130) and 2.5 µM β-mercaptoethanol (Gibco 21985).

Female C57BL/6N mice were sacrificed by cervical dislocation and tibia and femurs were collected in a falcon tube with PBS 1X. After cleaning from muscle tissues, the cleaned bones were collocated into a 10 cm Petri dish (Sarstedt 82.1473) with fresh PBS 1X. By keeping the tibia or femur with clean forceps, the bonne marrow was pushed out by a 20 ml syringe with a 23G needle (Terumo) into a second 10 cm Petri dish with PBS 1X. The solution was pipetted up and down with the syringe in order to make a single-cell suspension, which was filtered over a 100 μm filter and collected into a 50ml falcon tube. The suspension was centrifuged at 1500 rpm for 5 minutes (Heraeus Multifuge 1 S-R, rotor 75002010, Thermo Fisher). The supernatant was discarded and the cell pellet (dark red colour) was resuspended in 1 ml of Red Blood Cell Lysing Buffer Hybri-Max (Sigma-Aldrich R7757), in order to remove red blood cells from cell suspension. The resuspended pellet was gently mixed and incubated for 5 minutes at room temperature. 20-25ml of PBS 1X was added to the suspension and the cells were centrifugated at 1500 rpm for 5 minutes (Heraeus Multifuge 1 S-R, rotor 75002010, Thermo Fisher). The supernatant was discarded and the cell pellet (light red colour) was resuspended in 10 ml of BMDM medium.

4.2.2 Macrophage differentiation

R10 medium: RPMI 1640 medium (1X) + GlutaMAX (Gibco 61870), 10% Fetal Bovine Serum (FBS, Gibco A4766801), 100 μg/mL Penicilin/streptomycin (Gibco 15140), 2 mM L-glutamine (Gibco 25030), 10 mM HEPES (Gibco 15630122), 1nM sodium pyruvate (Gibco 11360), 1XMEM non-essential amino acids (Gibco 11130) and 2.5μM β-mercaptoethanol (Gibco 21985).

The cells were plated on a 10 cm tissue culture-treated Petri dish (Sarstedt 83.3902) and incubated overnight in a humidified incubator with 5% CO_2 at 37°C (Binder CO_2 incubator). The non-adherent progenitor cells were harvested while the adherent cells, which attached themselves to the bottom of the Petri dish during the overnight incubation, were discarded. The cells (from 2 tibia and 2 femurs) were diluted 1:1 (v:v) with BMDM medium and were splitted in 20x 10 cm Petri dishes (Sarstedt 82.1473). 8 ml of BMDM

medium was added to each Petri dish to induce macrophage differentiation. Cells were differentiated in the incubator with 5% CO_2 at 37°C for 6-7 days and every two days 2 ml of fresh BMDM medium was added to each Petri dish. After 6-7 days, macrophages were fully differentiated and adhered to the bottom of the cell dish. The medium was removed and cells were gently washed with PBS 1X. Cells were incubated few minutes with PBS 1X supplemented with 5 mM EDTA (Invitrogen AM9260G) and macrophages were harvested in a falcon tube. Cells were counted (Zeiss Microscope Primovert) and centrifugated at 1500 rpm for 5 minutes (Heraeus Multifuge 1 S-R, rotor 75002010, Thermo Fisher). The cell pellet was resuspended with R10 medium and centrifugated at 1500 rpm for 5 minutes at 4°C (Eppendorf centrifuge 5415R, rotor F45-24-11). The cell pellets were stored at -80°C until use.

4.2.3 Macrophage stimulation

Macrophages were plated in non-treated cell culture plates and left to adhere overnight before stimulation with live bacteria at MOI 25 for different time points. Bacteria were diluted in R10 medium before addition to cell cultures. After the challenge, the plate was centrifuged at 2000 rpm for 5 minutes (Heraeus Multifuge 1 S-R, rotor 75002010, Thermo Fisher) before the incubation with 5% CO_2 at 37°C (Binder CO_2 incubator). For longer times of stimulation (12-24hrs), macrophages were treated with gentamycin (Gibco 15750), added together with bacteria.

For treatment with Complex II inhibitors, 0.5 mM 3-nitropropionic acid (NPA, Sigma-Aldrich N5636) or 10 mM dimethyl malonate (DMM, Sigma-Aldrich 136441) were added to the cells respectively 1 hour or 3 hours before the bacterial challenge. For treatment with TCA cycle intermediates, 25µM or 100µM dimethyl fumarate (DMF, Sigma-Aldrich 242926) and 0.1 mM or 1mM α-ketoglutarate (α-KG, Sigma-Aldrich 349631) were separately added to the cells 4 hours before the bacterial challenge.

4.3 Cell preparation

4.3.1 Isolation of mitochondria from macrophages

Buffer A: 250 mM Sucrose (Sigma-Aldrich S7903), 2 mM HEPES (Sigma-Aldrich H0887), 0.1 mM EGTA (Sigma-Aldrich 4100), pH 7.2
Buffer B: 220 mM Mannitol (Sigma-Aldrich M4125), 70 mM Sucrose (Sigma-Aldrich S7903), 10 mM Tris (Sigma-Aldrich T8524), 1 mM EDTA (Invitrogen AM9260G), pH 7.2

For mitochondria isolation, 20 x 10^6 frozen BMDMs were suspended in 800 µl of cold buffer A and homogenized in a Potter-Elvehjem glass tube with Teflon pestle while standing on ice for 2 minutes. The sample was centrifuged at 3000 rpm x 5 min at 4°C (Eppendorf centrifuge 5415R, rotor F45-24-11) in order to remove nuclei and intact cells. The supernatant was collected and centrifuged at 9000g x 10 min at 4°C (Eppendorf centrifuge 5415R, rotor F45-24-11). The supernatant was discarded and the pellet, which contains mitochondria, was suspended with 200 µl of buffer B. Protein concentration was determined by protein assay and mitochondria aliquots were stored at -80°C until use.

4.3.2 Mitoplasts preparation

AA-buffer: 500 mM 6-aminohexanoic acid (Sigma-Aldrich 07260), 50 mM imidazole (Sigma-Aldrich I5513), 1 mM EDTA (Sigma-Aldrich E9884), pH 7
Sample buffer: 5% Blue G-250 (Sigma-Aldrich 1154440025) and 5% glycerol (Sigma-Aldrich G7893) diluted in AA -buffer

For BMDMs permeabilization and mitoplasts preparation, 3 x 10^6 frozen BMDMs were resuspended in 200 µl of cold PBS 1X. 32.5 µl digitonin (8 mg/ml, Sigma-Aldrich D5628)/200 µl sample were added to the sample and cells were incubated on ice for 10 min. 1 ml of cold PBS 1x was added and cells were centrifuged at 10,000g x 10 min at 4°C (Eppendorf centrifuge 5415R, rotor F45-24-11). The supernatants were discarded

and the pellets were suspended in 100 µl of cold AA-buffer. 10 µl of digitonin (10% solution) were added to each sample and incubated 5 min on ice. The samples were centrifuged at 18,000g x 30 min at 4°C (Eppendorf centrifuge 5415R, rotor F45-24-11) and the mitoplasts-containing supernatants were harvested. The protein content was determined by protein assay and for each 100 µl sample (i.e. protein extract sample) was added a 5 µl aliquot of sample buffer and stored at -80°C until use.

4.3.3 Isolation of mitochondria from mouse tissues

Extraction buffer: 0.22 M Mannitol (Sigma-Aldrich M4125), 0.07 M Sucrose (Sigma-Aldrich S7903), 20 mM HEPES (Sigma-Aldrich H0887), 1 mM EDTA (Sigma-Aldrich E9884), 4% BSA (Sigma-Aldrich A4503), pH 7.4
Buffer B: 220 mM Mannitol (Sigma-Aldrich M4125), 70 mM Sucrose (Sigma-Aldrich S7903), 10 mM Tris (Sigma-Aldrich T8524), 1 mM EDTA (Invitrogen AM9260G), pH 7.2

Female C57BL/6N mice were intraperitoneally injected with 1x10^9 live *E. coli* in 100 µl PBS 1X and were sacrificed 72hrs post-infection. Spleen, liver and heart tissues were collected in order to isolate mitochondria. Each organ was washed into a small becker with pure H_2O and then transferred into a 2ml Eppendorf tube. Using cleaned scissors, the organ was minced and reduced into smaller pieces in order to obtain a homogeneous compound. The minced organ was homogenized in a Potter-Elvehjem glass tube with Teflon pestle while standing on ice with 2 ml of extraction buffer. The homogenate was harvested in a falcon tube, the potter was rinced with 2 ml of extraction buffer and collected with the homogenate. The suspension was centrifuged at 2000 rpm x 10 min at 4°C (Heraeus Megafuge 16R, rotor F15-6x100y, Thermo Fisher). The supernatant was filtered over a 100 µm filter and centrifuged at 12000 rpm x 10 min at 4°C (Eppendorf centrifuge 5415R, rotor F45-24-11). The supernatant was discarded and the pellet was suspended with 2 ml of buffer B. The suspension was centrifuged at 10000 rpm x 10 min at 4°C (Eppendorf centrifuge 5415R, rotor F45-24-11). The pellet, which contains the mitochondria, was suspended with 200 µl of buffer B for spleen/heart and 400 µl for liver.

Protein concentration was determined by protein assay and the aliquots were stored at -80°C until use.

4.4 Determination of protein concentration

4.4.1 Lowry Method

Lowry reagent 1: 2% (w:v) Na_2CO_3 (Sigma-Aldrich 451614) in 0.1 N NaOH (MERCK 567530)
Lowry reagent 2: 1% (w:v) $CuSO_4 \cdot 5H_2O$ (MERCK 2790)
Lowry reagent 3: 2% (w:v) Na-K tartrate (MERCK A929287)

The Lowry method is a colorimetric technique [106] for the determination of the total protein content in purified samples, with high sensitivity (from 5 μg to 40 μg). The principle of this assay is to spectrophotometrically measure the aromatic groups present in the sample of interest through a colorimetric reaction at 750 nm wavelength.

Bovine serum albumin (BSA, Sigma-Aldrich A7030) solution was prepared at a concentration of 1 mg/ml and subsequently dosed with a double beam spectrophotometer (JASCO V-530) in quartz cuvettes at a wavelength of 278 nm (BSA absorbance is ~ 0.64). This solution was used to create the standard reference curve with serial dilutions from 0 to 40 μg of BSA solution diluted in 1 ml of pure H_2O.

The standard and protein samples were prepared in duplicate and treated with 0.1 ml of 10% (w:v) sodium deoxycholate (Na-DOC, Sigma-Aldrich D6750) and a volume of pure H_2O was added until reaching 1 ml final. Blank samples were prepared in the same way, but sample suspension buffer was used instead of the sample. A mixture of Lowry reagents was prepared immediately before use and consisted of the three Lowry reagents 1, 2 and 3 in a stoichiometric ratio of 100:1:1 (v:v:v). 2 ml of the Lowry mix was added to each sample, mixed and incubated for 10 minutes at room temperature, protected from the light. Immediately after, 0.2 ml of Folin-Ciocalteu reagent (Sigma-Aldrich F9252)

(diluted 1:1 with pure water) was quickly added to the samples, mixed and incubated for 30 minutes at room temperature, protected from the light.

After the incubation time, the absorbance of the samples was spectrophotometrically read at 750 nm. Blank absorbance values were removed to the protein absorbance values and the total protein concentrations (mg/ml) were determined on the standard calibration curve.

4.4.2 Pierce BCA Protein Assay Kit

BCA Reagent A: bicinchoninic acid, sodium carbonate, sodium bicarbonate and sodium tartrate in 0.1M sodium hydroxide (Thermo Fisher 23228)
BCA Reagent B: 4% cupric sulfate in distilled water (Thermo Fisher 23224)

Pierce BCA Protein Assay Kit (Thermo Fisher Cat. No. 23227) [107] is a rapid colorimetric protein assay for the detection and the quantification of the total protein content (from 20 μg to 2 mg). This method combines the reduction of Cu^{2+} to Cu^{1+} (cuprous cation) by proteins in an alkaline solution (the biuret reaction) with the chelation of reduced copper by bicinchoninic acid (BCA), a chromogenic compound which produces a purple-colored complex. This product presents a strong absorbance near 570 nm wavelength.

Bovine serum albumin (BSA, Sigma-Aldrich A7030) solution, already prepared at a concentration of 2 mg/ml, was used to create the standard reference curve with serial dilutions from 0 to 2 mg of BSA solution diluted in 0.5 ml of pure H_2O. The standard samples were prepared in triplicate.

10 μl of each standard or unknown sample replicate were pipetted into a microplate well (Sarstedt 82.1581). Blank samples were prepared in the same way, but sample suspension buffer was used instead of the sample. A mix of BCA reagents was prepared immediately before use and consisted of the two BCA reagents A and B in a stoichiometric ratio of

50:1 (v:v). 200 µl of the BCA mix was added to each well and the plate was gently mixed on a plate shaker for few seconds. The plate was covered from the light and incubated at 37°C for 30 minutes.

After the incubation time, the absorbance of the samples was spectrophotometrically measure at 570 nm on a microplate reader (Safas Monaco MP96). Blank absorbance values were removed to the protein absorbance values and the total protein concentrations (mg/ml) were determined on the standard calibration curve.

4.5 Enzyme activities

Buffer B: 220 mM Mannitol (Sigma-Aldrich M4125), 70 mM Sucrose (Sigma-Aldrich S7903), 10 mM Tris (Sigma-Aldrich T8524), 1 mM EDTA (Invitrogen AM9260G), pH 7.2
Kinetic buffer: 50 mM KCl (Sigma-Aldrich S9888), 10 mM Tris (Sigma-Aldrich T8524), 1 mM EDTA (Invitrogen AM9260G), *1 mM KCN (Sigma-Aldrich 60178)*, pH 7.4

For the determination of the specific activity of Complex I (NADH:ubiquinone oxidoreductase), the integrated activity by Complex I and Complex III (NADH:cytochrome c oxidoreductase), the overall respiratory activity (NADH:oxidase) and the succinate-dependent integrated activity by Complex II and Complex III (succinate:cytochrome c oxidoreductase), isolated mitochondria from spleen, heart and liver were thawed and diluted to a final concentration of 1-2 mg/ml with buffer B. The activities of respiratory complexes were spectrophotometrically measured using a dual-beam dual-wavelength spectrophotometer Jasco V-550, equipped with a mixing system in cuvette and a thermosetting apparatus (T = 30°C).

For the determination of the specific activity of Complex II (succinate dehydrogenase) in macrophages, cell pellets (3 x 10^6 BMDMs) were thawed and resuspended in 100 µl of PBS 1X. The activity of respiratory complex was spectrophotometrically measured using

a double-beam UV-Visible spectrophotometer Safas Monaco UVmc2, equipped with a thermosetting apparatus (T = 30°C).

All the catalytic activities were measured in the presence of 1 mM KCN, except for the NADH-oxidase activity and were normalized to protein content (represented as µmol substrate/min/mg protein).

4.5.1 NADH-oxidase activity

NADH-oxidase activity (NADH-O_2) was measured to assess the integrity of the respiratory chain in mitochondria isolated from spleen, liver and heart tissues. The first spectrophotometric reading on thawed mitochondria returned a low oxidation rate of NADH, confirming the integrity of the sample. The sample was then subjected to 3 sonication cycles at 150W (Labsonic U2000 sonicator, B. Braun Biotech International GmbBH) of 10 seconds each, with pauses of 50 seconds on ice and under nitrogen flow. The second spectrophotometric reading on sonicated mitochondria returned a higher oxidation rate of NADH, confirming the greater accessibility of respiratory complexes to exogenous substrates.

Mitochondria were added in kinetic buffer without 1 mM KCN and the rate of electron transfer was measured after the addition of 75 µM NADH (Sigma-Aldrich N8129). The NADH oxidation was monitored as differential absorbance (ΔA) at wavelengths of 340 minus 380 nm ($\varepsilon = 3.5\ mM^{-1} \cdot cm^{-1}$).

4.5.2 NADH:ubiquinone oxidoreductase activity

NADH-ubiquinone oxidoreductase activity (NADH-DB) was measured to assess the specific activity of Complex I. Mitochondria were added in kinetic buffer with 1 µg/ml antimycin A and 1 mM KCN in order to inhibit electron transfer towards Complex III and IV. In the presence of 60 µM decylubiquinone (DB, Sigma-Aldrich D7911) as electron

acceptor, the rate of electron transfer was measured after the addition of 75 μM NADH (Sigma-Aldrich N8129). The NADH oxidation was monitored as differential absorbance (ΔA) at wavelengths of 340 minus 380 nm ($\varepsilon = 3.5\ mM^{-1} \cdot cm^{-1}$).

4.5.3 NADH:cytochrome c oxidoreductase activity

NADH-cytochrome c oxidoreductase activity (NADH-cyt c) was measured to assess the integrated activity by Complex I and Complex III. Mitochondria were added in kinetic buffer with 1 mM KCN in order to inhibit electron transfer towards Complex IV. The rate of electron transfer was measured after the addition of 50 μM cytochrome c (Sigma-Aldrich C2037). The cytochrome c reduction was monitored as differential absorbance (ΔA) at wavelengths of 550 minus 540 nm ($\varepsilon = 19.1\ mM^{-1} \cdot cm^{-1}$).

4.5.4 Succinate:cytochrome c oxidoreductase activity

Succinate-dependent integrated activity (succ-cyt c) was measured to assess the integrated activity by Complex II and Complex III. Mitochondria were pre-incubated for 5 minutes at 37°C with succinate (Sigma-Aldrich 14160) in buffer B and then added in kinetic buffer with 1 mM KCN in order to inhibit electron transfer towards Complex IV. The rate of electron transfer was measured after the addition of 50 μM cytochrome c (Sigma-Aldrich C2037) and 26 mM succinate. The cytochrome c reduction was monitored as differential absorbance (ΔA) at wavelengths of 550 minus 540 nm ($\varepsilon = 19.1\ mM^{-1} \cdot cm^{-1}$).

4.5.5 Succinate dehydrogenase activity

Succinate dehydrogenase activity (succ-DCPIP) was measured to assess the specific activity of Complex II. Cells were pre-incubated for 5 minutes at 37°C with succinate (Sigma-Aldrich 14160) in buffer B and then added in kinetic buffer with 1 μM rotenone, 1 μg/ml antimycin A and 1 mM KCN in order to inhibit electron transfer towards

Complex I, Complex III and Complex IV. To permeabilize cells, 10 µl of Triton X100 10% were added in the cuvette. The rate of electron transfer was measured after the addition of 50 µM 2,6- dichlorophenolindophenol (DCPIP; Sigma-Aldrich, D1878) and 100 µM coenzyme Q1 (Sigma-Aldrich C7956). The DCPIP reduction was monitored at wavelength 660 nm ($\varepsilon = 19.1\ mM^{-1} \cdot cm^{-1}$).

4.6 Protein electrophoresis analysis

4.6.1 Blue native polyacrylamide gel electrophoresis (BN-PAGE)

Resuspension buffer: 50 mM NaCl (Sigma-Aldrich S9888), 5 mM 6-aminocaproic acid (Sigma-Aldrich 07260), 50 mM imidazole (Sigma-Aldrich I5513), pH 7.0
Anode buffer: Invitrogen Native-PAGE running buffer 20x (BN2001) - BisTris 50 mM, Tricina 50 mM pH 6.8
Deep blue cathode buffer: Invitrogen Native-PAGE running buffer 20x (BN2001) and Native-PAGE cathode additive 20x (BN2002) - BisTris 50 mM, Tricina 50 mM, Coomassie 0.02% pH 6.8
Light blue cathode buffer: Invitrogen Native-PAGE running buffer 20x (BN2001) and Native-PAGE cathode additive 20x (BN2002) - BisTris 50 mM, Tricina 50 mM, Coomassie 0.002% pH 6.8

Blue-native polyacrylamide gel electrophoresis (BN-PAGE) is a biochemical technique developed by Schägger [76] which allows the isolation of proteins and multimeric protein complexes with a molecular weight between 10 and 10000 kDa. It is a native electrophoresis on polyacrylamide gel that consents the separation of proteins in their native structure. Mild detergents were used to isolate supramolecular assemblies (supercomplexes), such as digitonin, or to isolate individual complexes, such as dodecyl-β-*D*-maltoside (DDM). Coomassie blue G-250 is added to the proteins prior to loading the samples onto the gel. The dye molecules, with an anionic charge, bind the surface of the proteins, cover the original charge and the proteins acquire isoelectric points extremely negative, in this way the separation of the proteins occurs in based on

molecular mass. Moreover, the negative charge on the surfaces of the individual proteins reduces the risk that the different molecules can aggregate in a non-specific way during the running.

Sample preparation

Isolated mitochondria from tissues or cells were thawed and resuspended in resuspension buffer at 1-2 mg/ml. Digitonin was added at detergent:protein ratio of 8:1 (w:w), pipetted up and down and incubated for 20 minutes on ice. The sample was centrifugated at 16000 rpm for 10 minutes at 4°C (Sorvall centrifuge R5C5, rotor F28). The pellets were discarded and the supernatants were collected and kept on ice until use.

Before loading the sample onto the gel, Coomassie blue G-250 solution, at Coomassie:digitonin ratio of 1:10 (w:w), and glycerol, at a final concentration of 10% (v:v), were added in order to increase the charge and the density of the sample. Protein extract samples were loaded (maximal volume 30 µl/well) onto precast 10-wells 3%-12% T gradient mini BN-gels (NativePAGE Novex Bis-Tris Gel, BN2011BX10, Invitrogen). 5 µl of the molecular weight marker (NativeMark^{TM} Unstained Protein Standard LC0725, Life Technologies) were loaded into a lateral well. Electrophoresis was performed at 4°C using a vertical apparatus (XCell SureLock Mini-Cell Electrophoresis System, Invitrogen) at 150V constant voltage for 1h in deep blue cathode buffer, then replaced with light blue cathode buffer for 1h and constant voltage at 250V for 1h15'. At the end of the running, the gel was extracted from the electrophoretic cell and immersed in pure water.

The first-dimension gel was immediately electroblotted onto polyvinylidene difluoride (PVDF) membrane or the strips of the first dimension gel ("lanes" 1D) were cut and stored in falcon tubes filled with pure water at 4 °C until use.

4.6.2 Sodium dodecyl sulfate polyacrylamide gel electrophoresis (SDS-PAGE)

Reducing solution: 1.25 ml Invitrogen Nu-PAGE LDS Sample Buffer 4X (NP0008), 0.5 ml Invitrogen Nu-PAGE sample reducing agent 10X (NP0009), 3.25 ml H_2O
Alkylating solution: 1.25 ml Invitrogen Nu-PAGE LDS Sample Buffer 4X (NP0008), 28 µl N, N dimethylacrylamide (DMA, Sigma-Aldrich 274135), 3.75 ml H_2O
Quenching solution: 1.25 ml Invitrogen Nu-PAGE LDS Sample Buffer 4x (NP0008), 50 µl Invitrogen Nu-PAGE Sample reducing agent 10X (NP0009), 1 ml ethanol, 2.75 ml H_2O
Anode buffer: 40 ml Invitrogen Nu-PAGE MOPS SDS running buffer 20x (NP0001), 760 ml H_2O
Cathode buffer: 200 ml of anode buffer, 0.5 ml Invitrogen Nu-PAGE Antioxidant Agent (NP0005)

The second dimension was performed by sodium dodecyl sulfate polyacrylamide gel electrophoresis (SDS-PAGE). The electrophoretic run in the second dimension (2D) allows to separate the single subunits of the native proteins previously separated by BN-PAGE.

The single 1D lanes were incubated with 3 different solutions (reducing solution, alkylating solution and quenching solution), 20 minutes each at room temperature and kept in continuous agitation by oscillation. The 1D lane was placed horizontally respect to the precast 2D gel (Nu-PAGE Novex 4-12% Bis-Tris NP0326BOX, Invitrogen) (Figure 27). 5 µl of the molecular weight marker (MagicMark^{TM} XP Western Protein Standard LC5602, Invitrogen) were loaded into a lateral well.

The 1D lane was covered with 40 µl of Nu-PAGE LDS Sample Buffer 4X (Invitrogen code NP0008) which allowed to check the level of the front in the 2D gel during the running. The gel was placed in the electrophoretic cell and around 600 ml of anode buffer were added in the external compartment, and 200 ml of buffer cathode in the external compartment. The electrophoretic separation was performed at 4°C using a vertical apparatus (XCell SureLock Mini-Cell Electrophoresis System, Invitrogen) at 110 mA for

1h15'. The running was stopped when the dye blue front of the migration came out of the gel.

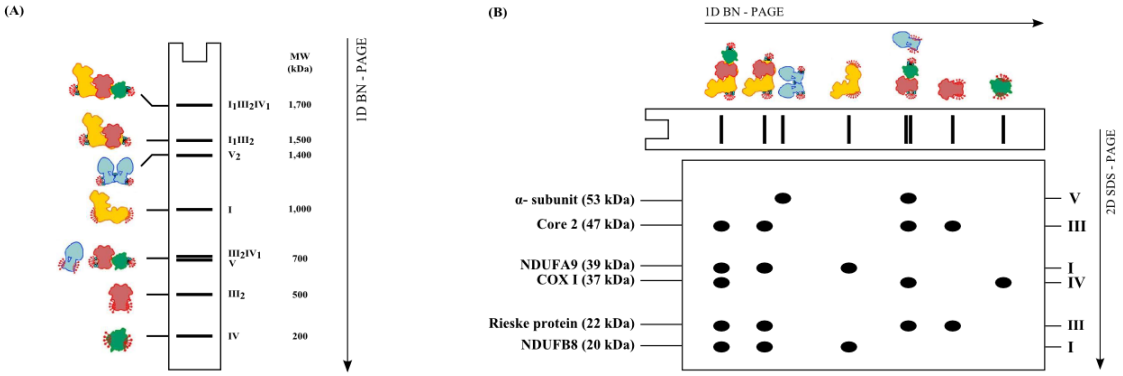

Figure 27. Schematic experimental procedure of 2D BN/SDS–PAGE. (A) Separation by 1D BN-PAGE of respiratory complexes in free and bound native forms. (B) Identification of respiratory protein subunits by 2D SDS-PAGE followed by Western blot and chemiluminescent immunodetection with specific antibodies.

4.7 Western blot protein transfer

4.7.1 Semi-dry Trans-Blot Turbo

Transfer buffer: 200 ml Trans-Blot Turbo 5x Transfer Buffer (Biorad 10026938), 200 ml ethanol, 600 ml H_2O

Following electrophoresis under non-denaturating conditions, 1D gels were immediately transferred onto polyvinylidene difluoride (PVDF) membranes. The transfer was performed using a Trans-Blot Turbo RTA Mini PVDF Transfer Kit (BioRad 1704272). The membranes (0.45 µm LF PVDF, BioRad) were pre-activated in pure ethanol for few minutes while the stacks (anode) were prewetted with transfer buffer before placing in the cassette base. The 1D gel was aligned on the membrane and a second prewetted stack was placed over on the gel. By using a blot roller, the air bubbles presented in the assembled transfer pack were removed to ensure direct contacts between the layers. The lid cassette

was placed on the base and the closed cassette was inserted in the Trans-Blot Turbo instrument. The transfer was performed at 25V, 1.3A for 7 minutes at room temperature.

4.7.2 Wet Western Blot

Transfer buffer: 20 ml Invitrogen Transfer Buffer 20X (NP0006), 1 ml Invitrogen Nu-PAGE Antioxidant Agent (NP0005), 100 ml methanol, H_2O

After 2D migration, gels were immediately transferred onto nitrocellulose membranes (Amersham^{TM} Hybond ECL RPN203D). The transfer was performed using a Mini Trans-Blot^{R} Cell (BioRad 1703930). Membranes, blotting filter papers and foam blotting pads were prewetted in transfer buffer. All the components necessary for the transfer were assembled in this sequence: a blotting pad was placed on the black side of the cassette, then a filter paper on the top of the blotting pad, the 2D gel on the filter paper, then the prewetted nitrocellulose membrane on the gel and, to complete the transfer pack, the second filter paper on the membrane. Before adding the last blotting pad, the air bubbles were removed by a blot roller to ensure direct contacts between the layers. At the end the cassette was closed and slided inside the blot tank. The transfer was performed at 100V for 90 minutes at 4°C.

4.8 Immunoblotting and immunodetection

Wash buffer: PBS 1X (Gibco 14190), 0.05% Tween-20 (Sigma-Aldrich P1379)
Blocking solution: 2% w:v BSA (Sigma-Aldrich A4503), 2% w:v non-fat milk (BioRad 1706404), 0.05% v:v Tween-20 (Sigma-Aldrich P1379) diluted in PBS 1X (Gibco 14190)

After the blotting, PVDF and nitrocellulose membranes were washed three times with wash buffer, 5 minutes each. Then, membranes were blocked with blocking solution and incubated at 4°C overnight. After washing, primary antibody diluted in blocking solution was added on the membrane and incubated for 1h at room temperature with orbital

shaking. Then, the membrane was washed twice with was buffer and a goat anti-mouse IgG (H+L) secondary antibody conjugated with horseradish peroxidase (HRP) (Molecular Probes, Invitrogen), diluted 1:1000 in blocking solution, was added on the membrane and incubated for 1h at room temperature with orbital shaking.

Monoclonal primary antibodies specific for single subunits of each respiratory complexes are purchased by Abcam: NDUFA9 subunit of Complex I (ab14713), SDHA subunit of Complex II (ab14715), Rieske protein of Complex III (ab14746) and, a cocktail of antibodies (ab110413: NDUFB8 of Complex I, subunit C-II-30 (FeS) of Complex II, Core 2 of Complex III, COX-I of Complex IV and α-subunit of Complex V), previously diluted 1:5000 in blocking solution (except for SDHA subunit of Complex II diluted 1:2000 in blocking solution).

The membrane was washed three times with wash buffer and left in PBS 1X until the immunodetection, performed using a kit of chemiluminescence detection. For PVDF membranes was used SuperSignal West Pico PLUS (ThermoFisher 34577), while for nitrocellulose membranes was used LiteAblot PLUS (EuroClone, EMP011005) according with the manufacturer's indications.

The chemiluminescence detection kit is composed by peroxide (H_2O_2) and luminol. A mix of peroxide and luminol 1: 1 ratio (v:v) was incubated to the membrane, previously drained from PBS 1X, protected from the light. The excess mixture was removed and images were acquired at different exposure times by using the ChemiDoc MP (BioRad) equipped with the Image_Lab software (BioRad).

4.9 ATP production

ATP production in BMDMs was measured by using the CellTiter-Glo® 2.0 Luminescent Cell Viability Assay (Promega, G9241). 15.000 BMDMs were plated in 96-well cell culture microplates with flat bottom black (Greiner Bio-One 655098) and incubated overnight in a humidified incubator with 5% CO_2 at 37°C (Binder CO_2 incubator). The

following day, macrophages were challenged with different strains of bacteria at a MOI 25, according to the experimental scheme, overnight. After 24hrs of stimulation, the medium was removed and half of the plate was incubated with OXPHOS inhibitors cocktail (antimycin 100 µM, rotenone 0,5 µM and oligomycin 3 µM) for 1h at 5% CO_2 at 37°C in the incubator. Standard serial dilutions of ATP solution (10 mM, Roche/Sigma-Aldrich 10519979001) were prepared immediately before use to create the standard reference curve. Standard ATP was included into the plate and CellTiter-Glo® 2.0 was then added in all the wells at equal volume of culture medium for 10 minutes at room temperature, protected from the light. The plate was read with Lumiskan Microplate Luminometer (Labsystems). Mitochondrial ATP was calculated by subtracting the ATP content obtained with inhibitors cocktail to ATP content without inhibitors (total ATP).

To normalize all the ATP values, a second microplate was seeded and treated in the same moment and in the same condition of the first one. After 24hrs post stimulation, the medium was removed and 10 µl of RIPA buffer (Sigma-Aldrich R0278) was added in each well. By using a tip, the proteins were scratched from the bottom of the wells and the samples were harvested for determining the protein content.

4.10 Oxygen consumption analysis

Seahorse medium: DMEM powder 10X (Sigma-Aldrich D5030), 1,85 gr NaCl (Sigma-Aldrich S9888), in 1L of pure H_2O, pH 7.4

Real-time oxygen-consumption rate (OCR) was measured using an XF-96 Extracellular Flux Analyzer (Seahorse Bioscience) and analysed by Wave Desktop software (Agilent Technologies). 1.5 x 10^5 BMDMs were plated in 96-wells Seahorse plate (XF-96 Cell culture microplates, Agilent) and centrifuged at 1500 rpm x 5 min (Heraeus Multifuge 1 S-R, rotor 75002010, Thermo Fisher). The plate was incubated overnight in a humidified incubator with 5% CO_2 at 37°C. A calibration plate (XFe96 sensor cartridges, Agilent), containing 200 µL/well of pure H_2O, was placed in a CO_2-free incubator at 37 °C overnight. The next day, macrophages were stimulated with different strains of bacteria at

MOI 25 for 2-24h according to the experimental scheme and the plate was centrifuged at 2000 rpm x 5 min (Heraeus Multifuge 1 S-R, rotor 75002010, Thermo Fisher). Cells were washed three times with PBS 1X and 200 µL of Seahorse medium supplemented with 2 mM Glutamine, 25 mM Glucose and 1 mM Na-Pyruvate were added in each well. The plate was incubated in a CO_2-free incubator at 37 °C for at least 30 minutes. During this incubation, the pure H_2O present in the calibration plate was replaced with 200 µL/well of calibrant solution (Agilent 100840) and the instrument calibration was performed running the plate for 20 minutes. After calibration, three consecutive measurements were performed under basal conditions and after each injection of the following inhibitors/uncouplers: 1 µM oligomycin, 1 µM carbonyl cyanide m-chlorophenylhydrazone (CCCP) and 1 µM rotenone plus 1 µM antimycin. Basal respiration rate (BRR) was defined as OCR in the absence of oligomycin and CCCP. Maximal respiration rate (MRR) was defined as OCR after adding of CCCP. Data are represented as BRR and MRR obtained after addition of rotenone and antimycin A, corresponding to specific mitochondrial respiration.

4.11 Cytokine enzyme-linked immunosorbent assay (ELISA)

ELISA wash buffer: 200 ml PBS 1X (Gibco 14190), 1 ml Tween-20 (Sigma-Aldrich P1379), 1.8 L pure H_20
Reagent diluent for IL-10, IL-6 and TNFα: 5xELISA/ELISPOT diluent (Invitrogen) diluted 1:5 with pure H_2O
Reagent diluent for IL-1β: PBS 1X (Gibco 14190), 1% BSA (Sigma-Aldrich A4503)

For the detection of cytokine profile in macrophages, 150.000 BMDMs were plated in triplicate in 24 wells tissue culture-treated plates (Sarstedt 83.3922), were centrifuged at 1500 rpm for 5 minutes (Heraeus Multifuge 1 S-R, rotor 75002010, Thermo Fisher) and incubated at 37°C, 5% CO_2 overnight. The following day, macrophages were challenged with different strains of bacteria at MOI 25, according to the experimental scheme, and supernatants were collected at 24hrs after stimulation.

Il-6, IL-10 and TNF-α ELISA kits were purchased from Invitrogen (IL-6, 88-7064-88; IL-10, 99-7105-88 and TNFα, 88-7324-88). IL-1β ELISA kit was purchased from R&D System (IL-1β, DY401).

Capture antibodies, diluted 1:250 in coating buffer (PBS 1X) were added in a 96 well plate (Nunc-Immuno MicroWell, Thermo Fisher) and incubated overnight at 4°C. The plate for the evaluation of IL-1β production was incubated overnight at room temperature according to the manufacturer's instructions. After washing the plates three times with wash buffer, 50 µl of reagent diluent was added in each well for 1h at room temperature. During this time, the samples and the standards for the standard curves were prepared and diluted in their respective reagent diluent. After washing the plates once with wash buffer, 50 µl of samples and standards were added to the appropriate wells. All the plates were incubated overnight at 4°C. All the plates were washed three times and 50 µl of the detection antibodies, biotin-conjugated anti-cytokine antibodies, were added in each well for 2hrs for IL-1β and only 1h for IL-10, IL-6 and TNFα, at room temperature. After washing the plates three times with wash buffer, 50 µl of Streptavidin-HRP/well was added and incubated for 30 minutes at room temperature, protected from the light. All the plates were washed five times with wash buffer and 50 µl of a chromogenic substrate for HRP, 5,5'- tetramethylbenzidine solution (1X TMB solution, Invitrogen)/well was added, incubated at room temperature until a blue color appears in the wells. The reaction was stopped adding TMB stop solution (Seracare 5150 or 2N H_2SO_4) and the plates were read at 450 nm using a microplate reader (Safas Monaco MP96).

4.12 Metabolomic

For metabolomic analysis, 2 × 10^6 cells were seeded in triplicate on 6 wells non-tissue culture treated plates (Falcon 351146) and left to adhere overnight in a humidified incubator with 5% CO_2 at 37°C. BMDMs were challenged with live Gram-negative and Gram-positive bacteria at a MOI 25, according to the experimental scheme. The plates were centrifugated at 2000 rpm for 5 minutes (Heraeus Multifuge 1 S-R, rotor 75002010, Thermo Fisher) and incubated for 18hrs. The medium was removed and cells were gently

washed with PBS 1X. Cells were incubated few minutes with PBS 1X supplemented with 5 mM EDTA (Invitrogen AM9260G) and macrophages were harvested in a falcon tube. Cells were counted (Zeiss Microscope Primovert) and centrifugated at 1500 rpm for 5 minutes (Heraeus Multifuge 1 S-R, rotor 75002010, Thermo Fisher). The cell pellet was resuspended with R10 medium and centrifugated at 1500 rpm for 5 minutes at 4°C (Eppendorf centrifuge 5415R, rotor F45-24-11). The cell pellets were stored at -80°C.

Metabolomic analysis was performed by MetaToul (Metabolomics & Fluxomics Facitilies, Toulouse, France, www.metatoul.fr) using a method which couples ion chromatography and mass spectrometry.

4.13 Immunoprecipitation

For immunoprecipitation assays, 36 x 10^6 BMDMs per condition were plated in 6 well non-tissue culture treated plates (Falcon 351146) and left to adhere overnight in a humidified incubator with 5% CO_2 at 37°C. BMDMs were challenged with live *E. coli* and *L. innocua* at a MOI 25. The plates were centrifugated at 2000 rpm for 5 minutes (Heraeus Multifuge 1 S-R, rotor 75002010, Thermo Fisher) and incubated for 18hrs. The medium was removed and cells were gently washed with PBS 1X. Cells were incubated few minutes with PBS 1X supplemented with 5 mM EDTA (Invitrogen AM9260G) and macrophages were harvested in a falcon tube. Cells were counted (Zeiss Microscope Primovert) and centrifugated at 1500 rpm for 5 minutes (Heraeus Multifuge 1 S-R, rotor 75002010, Thermo Fisher). The cell pellet was resuspended with R10 medium and centrifugated at 1500 rpm for 5 minutes at 4°C (Eppendorf centrifuge 5415R, rotor F45-24-11). The cell pellets were stored at -80°C until use. Mitochondria were isolated as previously described in the section “4.3.1 Isolation of mitochondria from macrophages”.

The immunoprecipitation follows manufacture’s protocol (Abcam 109779). Mitochondria were resuspended in 300 µl of buffer B and 1/10 volume of PBS 1X + 0% lauryl maltoside (Abcam ab109857) was added to the sample. The solution was mixed and incubated on ice for 30 minutes. The sample was then centrifugated at 16000 rpm for 30

minutes at 4°C (Eppendorf centrifuge 5415R, rotor F45-24-11). The supernatant was collected and 30 µl of agarose beads cross-linked to specific monoclonal antibodies were added. The mix was incubated overnight at 4°C, constantly moving on a rotating device. The beads were washed three times with 500 µl PBS 1X + 0.05% lauryl maltoside and the proteins were eluted with 40 µl 2x Laemmli sample buffer (Biorad 1610737).

The proteomic analysis was performed by the proteomic facility located in Bordeaux.

4.14 *In vivo* experiments

For in vivo experiments, female C57BL/6N mice were intraperitoneally injected (i.p.) with 160 mg/kg dimethyl malonate (DMM) [4] and, after 2hrs, mice were i.p. injected with 1x10^9 live *E. coli* or *L. innocua*. 2 hrs later, mice were sacrificed and blood was collected from the venous sinus. Samples were centrifuged for 5 min at 7000 rpm at 4°C (Eppendorf centrifuge 5415R, rotor F45-24-11) and supernatants were stored at -80°C until use. The samples were used to measure the *in vivo* cytokine profile by ELISA (see section 4.11).

4.15 Statistical analysis

The results were expressed as mean ± SEM and analysed using GraphPad Prism 9 software. The unpaired Student's t test was used to compare two independent groups. NS, not significant, *P < 0.05, **P < 0.01, ***P < 0.001.

Results

5.1. Structural and functional analysis of ETS in cultured macrophages

In isolated mitochondria from cultured bone marrow derived macrophages (BMDMs), solubilized with digitonin and analysed by 1D BN-PAGE (for details, see section 4.6.1 in Materials and Methods), it is possible to observe the presence of high molecular weight bands (> 1500 kDa), suggesting the presence of respiratory supercomplexes (SC) (Figure 28a). Using 2D SDS-PAGE followed by Western blot and immunodetection with specific monoclonal antibodies against single subunits of the redox complexes of the respiratory chain. The antibodies were sequentially incubated on the membrane in order to precisely identify the protein of interest. We detected the presence of two vertically aligned spots that reveal the nature of such high molecular weight bands, as indicated in Figure 28.

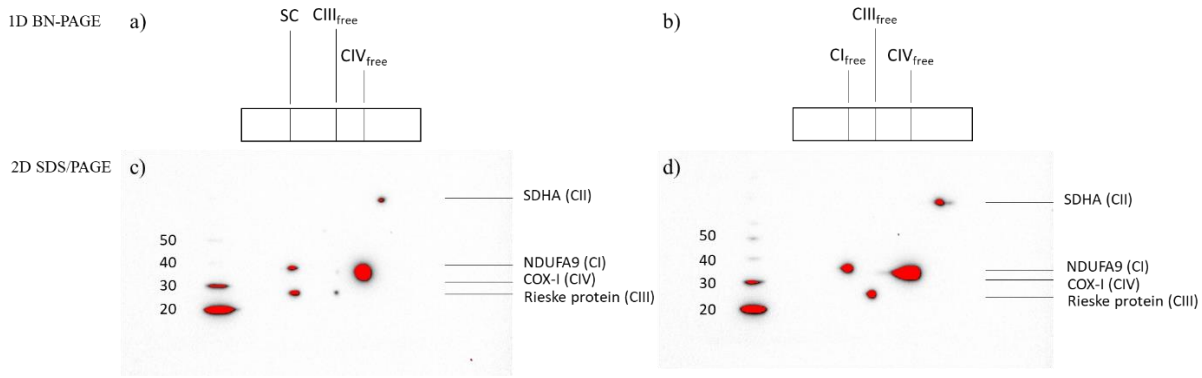

Figure 28. Chemiluminescent immunodetection of respiratory complexes and supercomplexes after 2D BN/SDS–PAGE analysis in C57BL/6N macrophages from control mice treated with a,c) 3,75% digitonin or b,d) 1,7% dodecyl maltoside (DDM). Immunodetection with specific monoclonal antibodies: NDUFA9 of CI (39 kDa), SDHA of CII (70 kDa), Rieske protein of CIII (22 kDa) and COX-I of CIV (37 kDa). One experiment representative of three independent experiments with similar results. Abbreviations: CI-CIV, Complex I-IV, SC, supercomplex.

In particular, the Figure 28a,d shows the vertical alignment of Complex I and Complex III, due to the original assembly of these two complexes forming the SC I_1III_2 in native conditions. In the same image, other isolated spots with lower molecular weight, can be identified as Complex II, Complex III and Complex IV in a free form (i.e. not bound in form of SC, see chapter 2.3.2.7). It was not possible to detect the presence of CIV in form

of high molecular weight assemblies (SC $I_1III_2IV_n$ and the SC III_2IV), consistent with previous work from the laboratory and from others [3].

Conversely, the *in vitro* solubilization of the mitochondrial sample with 10% DDM causes the dissociation of the native SCs into their individual respiratory enzyme components (Figure 28b,d). In fact, in this case, only the subunits of the free complexes CI-CIV are visible, on the right, whereas any spots related to SC disappeared.

5.1.1 Sensing of bacteria affects mitochondrial ETS supramolecular organization

To determine whether the activation of BMDMs affects the organization of the mitochondrial respiratory system, we analysed the ETS in BMDMs stimulated with different strains of bacteria. Mitoplasts were prepared from BMDMs challenged with live *E. coli* (Gram-negative bacteria) and *L. innocua* (Gram-positive bacteria) were solubilized with digitonin and analysed by 1D BN-PAGE (Figure 29).

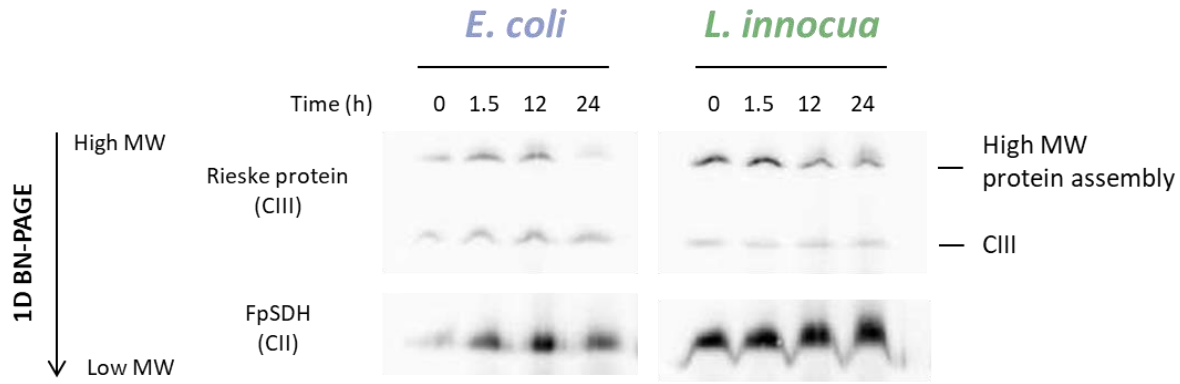

Figure 29. 1D BN–PAGE analysis in mitoplasts isolated from BMDMs untreated (time 0) and treated in culture with Gram- bacteria (*E. coli*) or Gram+ bacteria (*L. innocua*) for different time points (1.5hrs, 12hrs and 24hrs). Immunodetection with specific monoclonal antibodies: SDHA of CII (70 kDa) and Rieske protein of CIII (22 kDa). One experiment representative of two independent experiments with similar results. Abbreviations: CII-CIII, Complex II-III, III_2, free CIII in dimeric form.

We observed the presence of high molecular weight bands suggesting the presence of respiratory supercomplexes, either in *E. coli* (left panel) and *L. innocua* (right panel). A slight increase of the band of SC band is observed in *E. coli*-treated macrophages at 1.5hrs and followed by a progressive decrease during the period of infection. Conversely, in *L. innocua*-treated macrophages there is a continuous mild decrease of intensity of the SC band throughout the duration of the infection (Table 1).

	CIII free (%)	CIII bound (%)
Ctrl	69,8 ± 16,0 [6]	30,2 ± 16,0 [6]
E. coli 1.5h	36,9 ± 1,0 [2]	63,1 ± 1,0 [2]
E. coli 12h	47,7 ± 7,9 [2]	52,3 ± 7,9 [2]
E. coli 24h	70,8 ± 1,3 [2]	29,2 ± 1,3 [2]
L. innocua 1.5h	13,1 ± 4,6 [2]	86,9 ± 4,6 [2]
L. innocua 12h	18,9 ± 13,1 [2]	81,1 ± 13,1 [2]
L. innocua 24h	21,4 ± 7,0 [2]	78,6 ± 7,0 [2]

Table 1. Densitometry analysis of a 1D-BN-PAGE of BMDMs treated with live *E. coli* and *L. innocua* at MOI 25 for different time points (1.5hrs, 12hrs, 24hrs). Values are expressed as percent of CIII free or CIII bound normalized against total CIII in each condition, set as 100%. Values in square brackets indicate the number of independent samples.

Moreover, under any condition, Complex II was not found associated into high molecular weight protein assembly. The different chemiluminescent intensity of the bands throughout the time of infection needs further investigation to ensure it is not a technical problem during the protein extraction.

The 1D BN-PAGE is a technique which allowed us to make comparisons within the same gel and to observe the different organization of the mitochondrial respiratory complexes during bacterial infection. At the same time, this method is controversial as the run of proteins in native form can present problems during the immunodetection phase.

In addition, BMDMs samples treated with live *E. coli* or *L. innocua* were analysed by 2D SDS-PAGE followed by Western blot and immunodetection to identify the respiratory complexes bound in the high molecular weight protein assembly (SCs).

As shown in Figure 30 (a-c) and Figure 31 (d-f), our result indicate that the high molecular weight assembly observed in Figure 29 is composed by Complex I and Complex III. The vertical alignment of the two subunits of CI and the two subunits of CIII confirms the direct involvement of these two redox components in the formation of SC I_1III_2 in native conditions. It is also possible to observe the CI and CIII not assembled into the SC.

As expected, the two spots of CII and CV confirm the presence of these two respiratory enzymes only in a free form. Moreover, it is confirmed the presence of Complex IV not assembled into the SC, so it is not possible to detect high molecular weight assemblies such as SC $I_1III_2IV_n$ and the SC III_2IV.

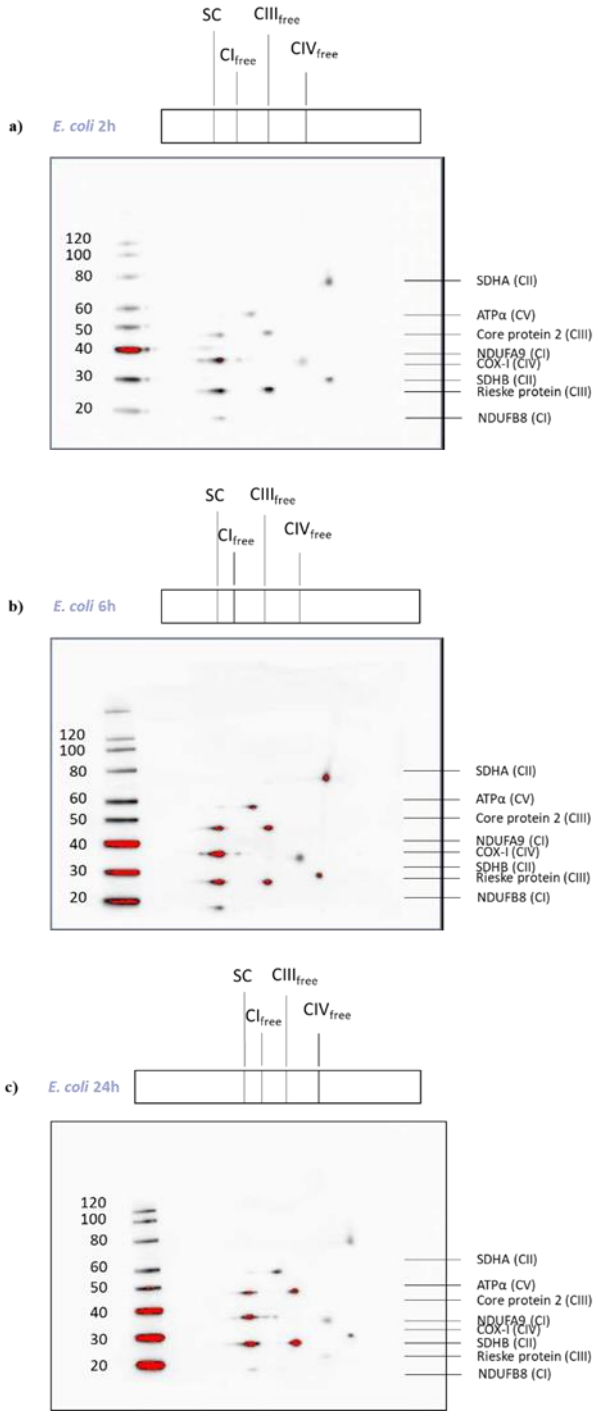

Figure 30. Chemiluminescent immunodetection of respiratory complexes and supercomplexes after 2D BN/SDS–PAGE analysis in BMDMs treated with *E. coli* (a-c) for different time points (2hrs, 6hrs and 24hrs). Protein extracts were solubilised from cells samples by using digitonin at a detergent to protein ratio of 8 (w:w) in order to preserve native supercomplexes. Immunodetection was performed using specific monoclonal antibodies: NDUFA9 of CI (39 kDa), NDUFB8 of CI (17 kDa), SDHA of CII (70 kDa), SDHB of CII (28 kDa) Rieske protein of CIII (22 kDa), Core 2 of CIII (42 kDa), COX-I of CIV (37 kDa) and subunit α of ATP synthase (56 kDa). Data are from one experiment. Abbreviations: CI-CV, Complex I-V, SC, supercomplex.

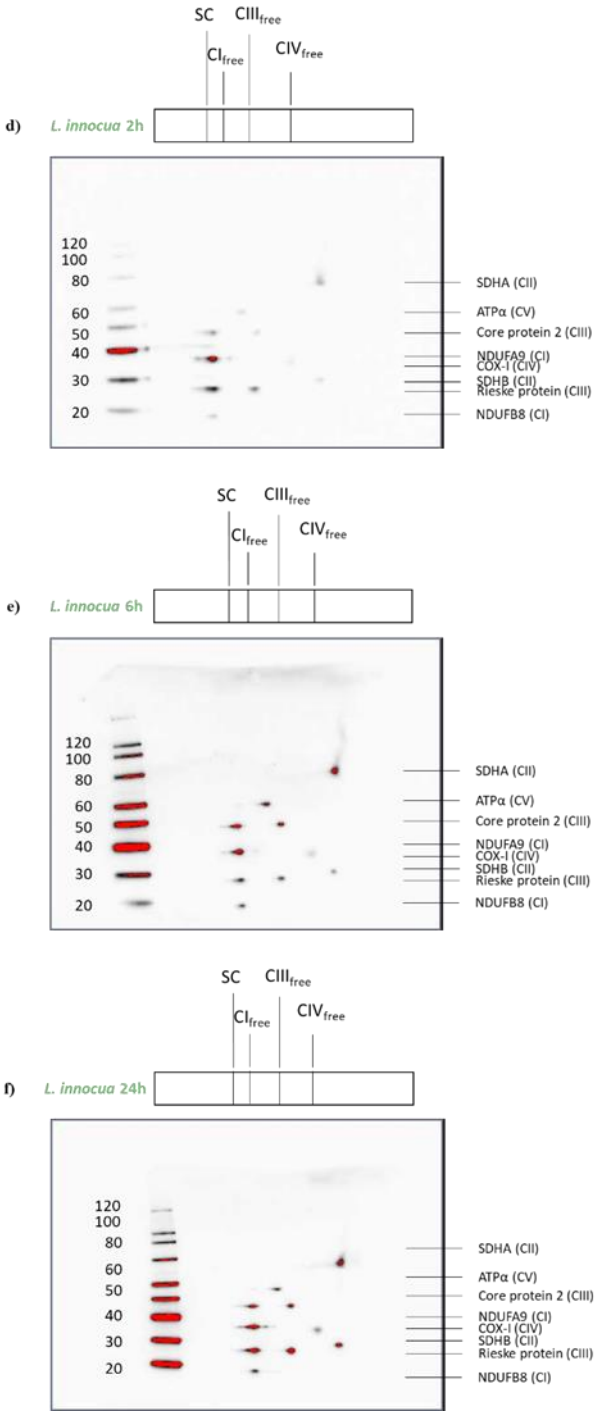

Figure 31. Chemiluminescent immunodetection of respiratory complexes and supercomplexes after 2D BN/SDS–PAGE analysis in BMDMs treated with *L. innocua* (d-f) for different time points (2hrs, 6hrs and 24hrs). Protein extracts were solubilised from cells samples by using digitonin at a detergent to protein ratio of 8 (w:w) in order to preserve native supercomplexes. Immunodetection was performed using specific monoclonal antibodies: NDUFA9 of CI (39 kDa), NDUFB8 of CI (17 kDa), SDHA of CII (70 kDa), SDHB of CII (28 kDa) Rieske protein of CIII (22 kDa), Core 2 of CIII (42 kDa), COX-I of CIV (37 kDa) and subunit α of ATP synthase (56 kDa). Data are from one experiment. Abbreviations: CI-CV, Complex I-V, SC, supercomplex.

This technique does not allow to observe significant differences on the amount of SC in cultured BMDMs stimulated either in *E. coli* or *L. innocua* at the three infection times analysed (2hrs, 6hrs and 24hrs). In fact, here it seems that there are not major variations in the vertical alignment of Complex I and Complex III, forming the SC I_1III_2. The samples were run in separated gels, then the chemiluminescent intensity of the spots are not comparable quantitatively between the gels. However, within each 2D gel, it is possible to compare the chemiluminescent intensity of the free and bound subunits belonging to the same complex and precisely estimate the relative percentage of free and/or bound forms. Moreover, it is possible to demonstrate the different redox components associated in the SCs (vertical alignment of subunits of distinct respiratory complexes) and consequently to accurately detect any alteration in the level of SCs.

5.1.2 Sensing of bacteria affects the mitochondrial ATP production

To assess whether the metabolic reprogramming in macrophages induces a change in ATP production upon bacterial infection, we measured the mitochondrial and glycolytic ATP synthesis in BMDMs stimulated with live *E. coli* and *L. innocua* at a MOI 25 for 24hrs. In particular, to measure the mitochondrial ATP contribution we incubated macrophages stimulated with OXPHOS cocktail inhibitors (antimycin 100 µM, rotenone 0,5 µM and oligomycin 3 µM) for 1h before the ATP dosage.

As shown in Figure 32, an increase of the total ATP is induced by both *E. coli* and *L. innocua*. However, upon infection with Gram-bacteria, activated macrophages increase the glycolytic ATP production while Gram+ bacteria they increase the mitochondrial ATP synthesis.

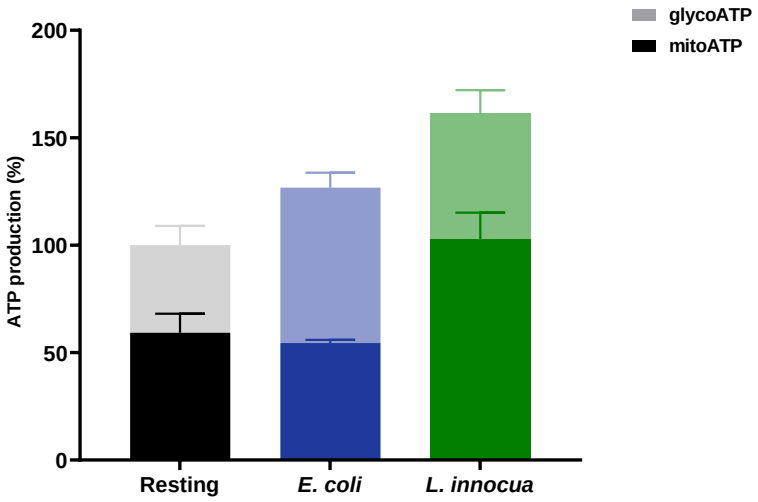

Figure 32. ATP synthesis in BMDMs untreated (Resting, black/grey column) and treated with Gram- bacteria (*E. coli*, blue column) or Gram+ bacteria (*L. innocua*, green column) at MOI 25 for 24hrs. The lower section of the chart bar (dark colours) indicates the mitochondrial ATP levels, whereas the upper section (light colours) indicates the glycolytic ATP. The mitochondrial ATP levels were measured incubating OXPHOS cocktail inhibitors (antimycin 100 µM, rotenone 0,5 µM and oligomycin 3 µM) for 1h before the dosage. Values are expressed as percent of ATP production normalized against total ATP production in Resting condition, set as 100%. Data are from four independent experiments with four technical replicates (mean and s.e.m.).

To exclude that this difference is specifically associated with the two bacterial strains employed, we repeated a similar experiment and measured the ATP levels in BMDMs stimulated with other Gram- (*ΔSpi1/2 S. enterica* and *P. aeruginosa*) and Gram+ bacteria (*ΔLLO/FliC L. monocytogenes* and *S. aureus*). In this case (Figure 33) our preliminary data confirm that all the Gram-negative bacteria increase the amount of glycolytic ATP while all the Gram-positive bacteria increase the mitochondrial ATP.

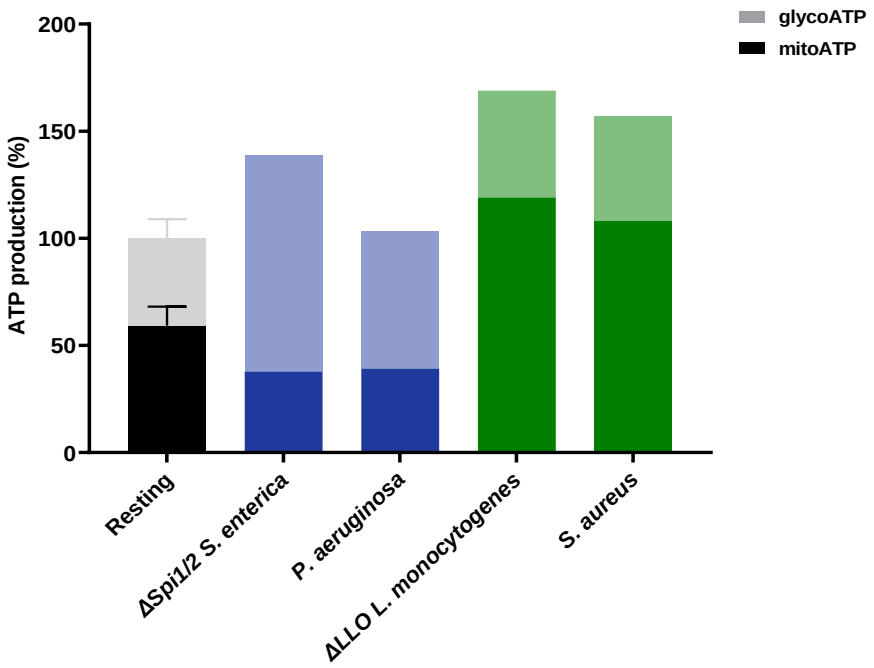

Figure 33. ATP synthesis in BMDMs untreated (Resting, black/grey column) and treated with various live Gram- bacteria (*ΔSpi1/2 S. enterica* and *P. aeruginosa*, blue column) or Gram+ bacteria (*ΔLLO/FliC L. monocytogenes* and *S. aureus*, green column) at MOI 25 for 24hrs. The lower section of the chart bar (dark colours) indicates the mitochondrial ATP levels, whereas the upper section (light colours) indicates the glycolytic ATP. The mitochondrial ATP levels were measured incubating OXPHOS cocktail inhibitors (antimycin 100 µM, rotenone 0,5 µM and oligomycin 3 µM) for 1h before the dosage. Values are expressed as percent of ATP production normalized against total ATP production in Resting condition, set as 100%. Data are from one experiment.

5.1.3 Sensing of bacteria affects the mitochondrial respiration in macrophages

To better understand the increase of ATP production, we have also investigated the mitochondrial respiration in macrophages upon bacterial infection. BMDMs were stimulated with live *E. coli* and *L. innocua* for different time points and the oxygen consumption rate was measured using an Agilent Seahorse XF Analyzer with glucose, pyruvate and glutamine in the respiratory medium (Figure 34).

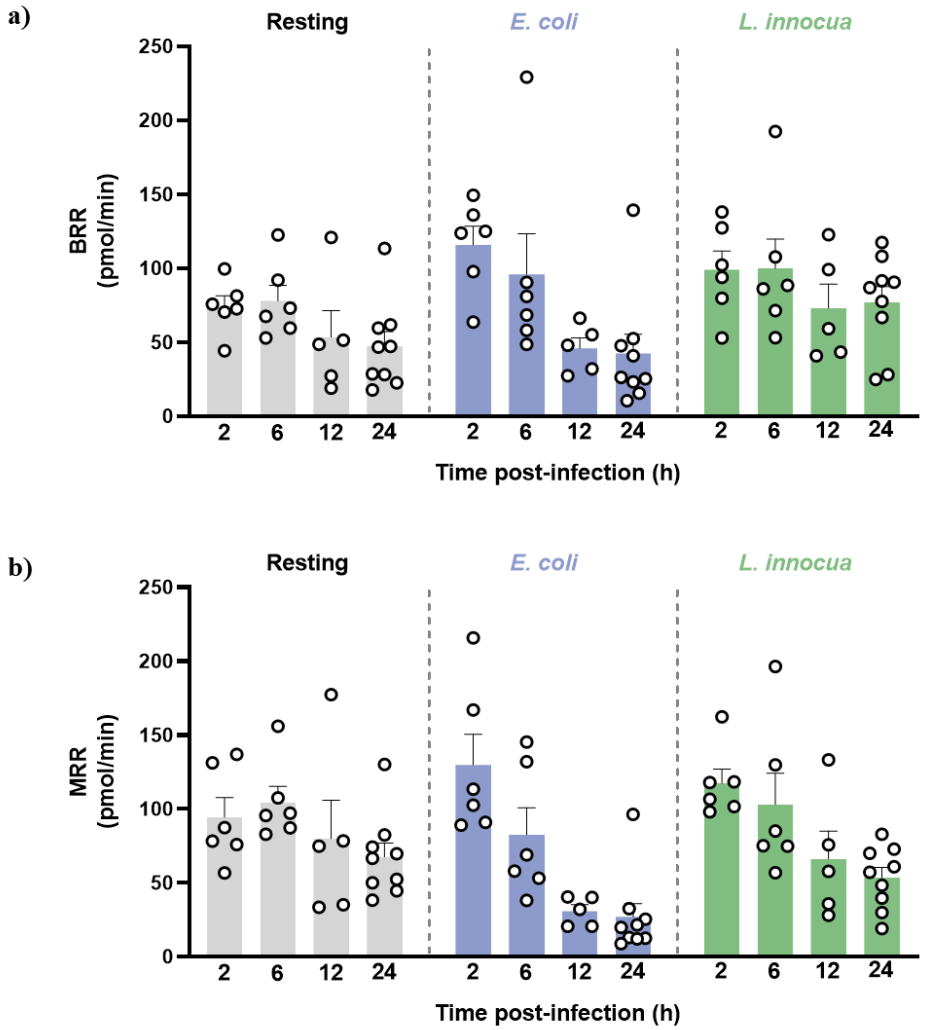

Figure 34. a) Basal respiration rate (BRR) and b) maximal respiration rate (MRR) of 1.5 x 10^5 BMDMs/well untreated (Resting, grey columns) and treated with *E. coli*, (Gram-, blue columns) and *L. innocua* (Gram+, green column) at MOI 25 at different time points (2hrs, 6hrs, 12hrs and 24hrs). Each symbol represents an individual experiment. Data are from two to nine independent experiments with six technical replicates (mean and s.e.m.).

Our data show that the sensing of *E. coli* and *L. innocua* differently modulates mitochondrial oxygen consumption rate throughout the time of infection. In particular, *E. coli* induce a transient (2-6hrs) increase of both the basal and the maximal respiration rate while *L. innocua* progressively increase their mitochondrial respiratory capacity if compared to Resting macrophages at the corresponding time of treatment, while a partial increase is observed in MRR at short treatment times (2-6hrs).

We also checked the sensing of other live Gram- (*ΔSpi1/2 S. enterica*) and Gram+ (*ΔLLO/FliC L. monocytogenes*) bacteria for the same time points of treatment of cultured macrophages. Our data confirm that all Gram- bacteria tested induce only a transient increase of the oxygen consumption rate (both BRR and MRR) while Gram+ bacteria increase their BRR at short time treatment and tend to maintain it up to 24hrs of infection (Figure 35).

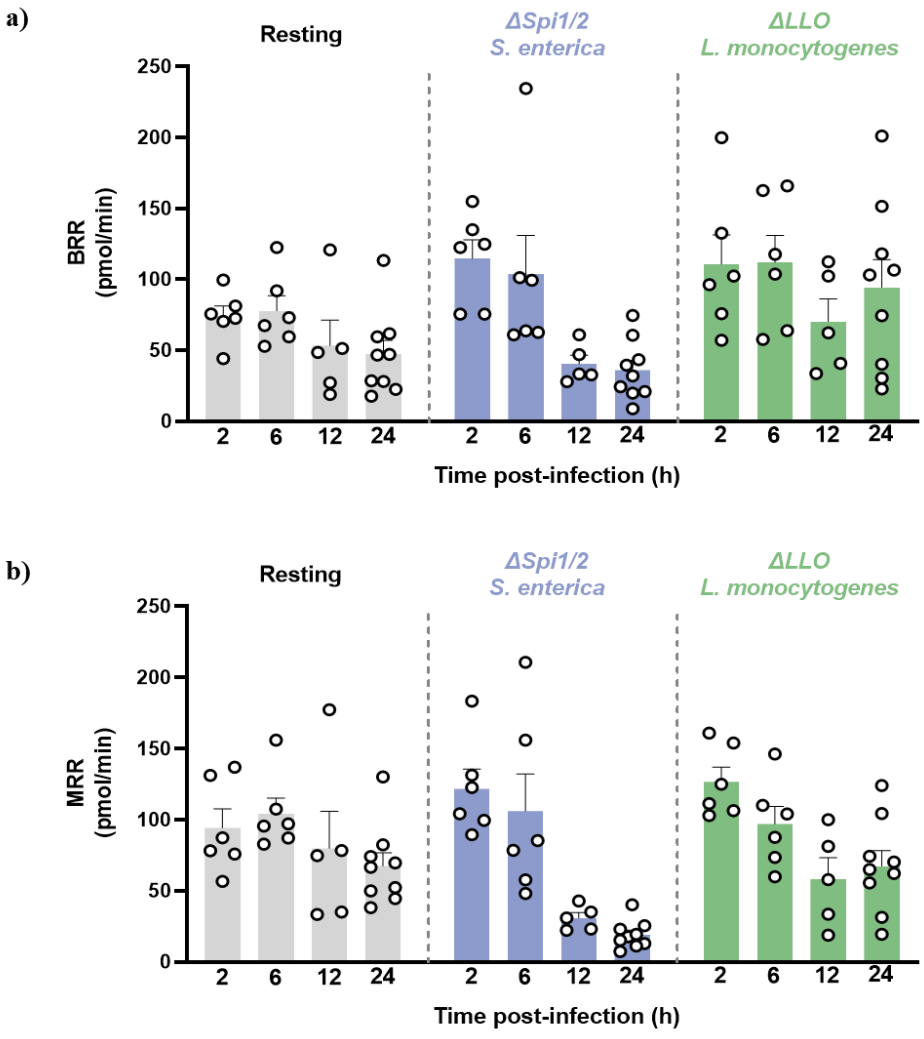

Figure 35. a) Basal respiration rate (BRR) and b) maximal respiration rate (MRR) of 1.5 x 10^5 BMDMs/well untreated (Resting, grey columns) and treated with *ΔSpi1/2 S. enterica*, (Gram-, blue columns) and *ΔLLO/FliC L. monocytogenes* (Gram+, green column) at different time points (2hrs, 6hrs, 12hrs and 24hrs). Each symbol represents an individual experiment. Data are from two to nine independent experiments with six technical replicates (mean and s.e.m.).

5.1.4 Sensing of bacteria differently affect CII activity

Previous results in the literature indicate that CII/SDH enzyme activity is increased in macrophages upon *E. coli* infection [3]. To understand whether the sensing of the different bacteria strains employed in our study may differently alter CII activity, we applied spectrophotometric analysis of succinate dehydrogenase activity by monitoring the reduction of 2,6-Dichlorophenolindophenol (DCPIP) in BMDMs upon Gram- and Gram+ bacterial infection (Figure 36).

BMDMs were treated *in vitro* with *E. coli* (Gram- bacteria) and *L. innocua* (Gram+ bacteria) at a MOI 25 at different time points (2hrs, 6hrs and 18hrs) and we have evaluated spectrophotometrically the specific activity of CII.

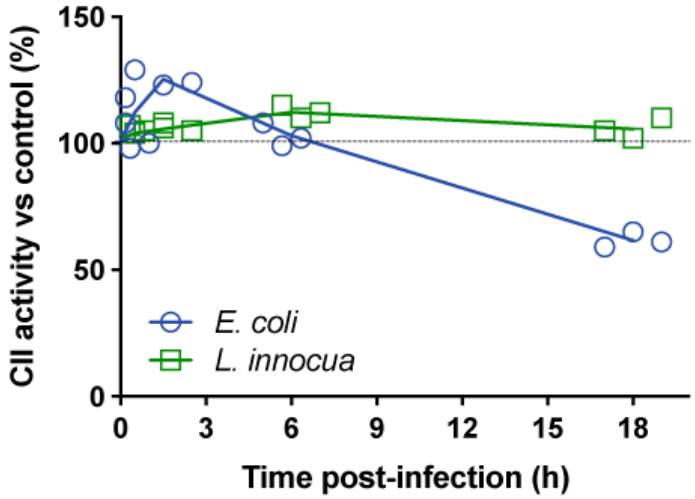

Figure 36. Succinate dehydrogenase activity in BMDMs treated with live *E. coli*, (Gram-, blue line) and *L. innocua* (Gram+, green line) at MOI 25 for different time points. Data are from three independent experiments.

Our preliminary results confirm that CII/SDH activity is transiently increased in activated macrophages after *E. coli* infection. The maximum activity is reached approximately 2 hours after infection and then progressively decreases during the period of infection, reaching values almost halved compared to zero time. Conversely, macrophages treated

with *L. innocua* only slightly increase CII/SDH activity at 6 hours post-infection and then maintain constant this CII activity throughout the duration of the infection.

5.2 Structural and functional analysis of isolated mitochondria from infected tissues

To assess SCs correlation with to macrophage antibacterial responses, we intraperitoneal injected 1x10^9 live *E. coli* in mice, after 72hrs post-infection mice were sacrificed and mitochondria were isolated from spleen, liver and heart (see section 4.3.3 in Materials & Methods).

The 2D BN/SDS-PAGE analysis followed by immunodetection, with specific monoclonal antibodies (Figure 37), indicates the presence of SCs in all the control samples, but also suggests a partial SC dissociation, a different free/bound forms ratio of CI and CIII, in spleen upon bacterial infection.

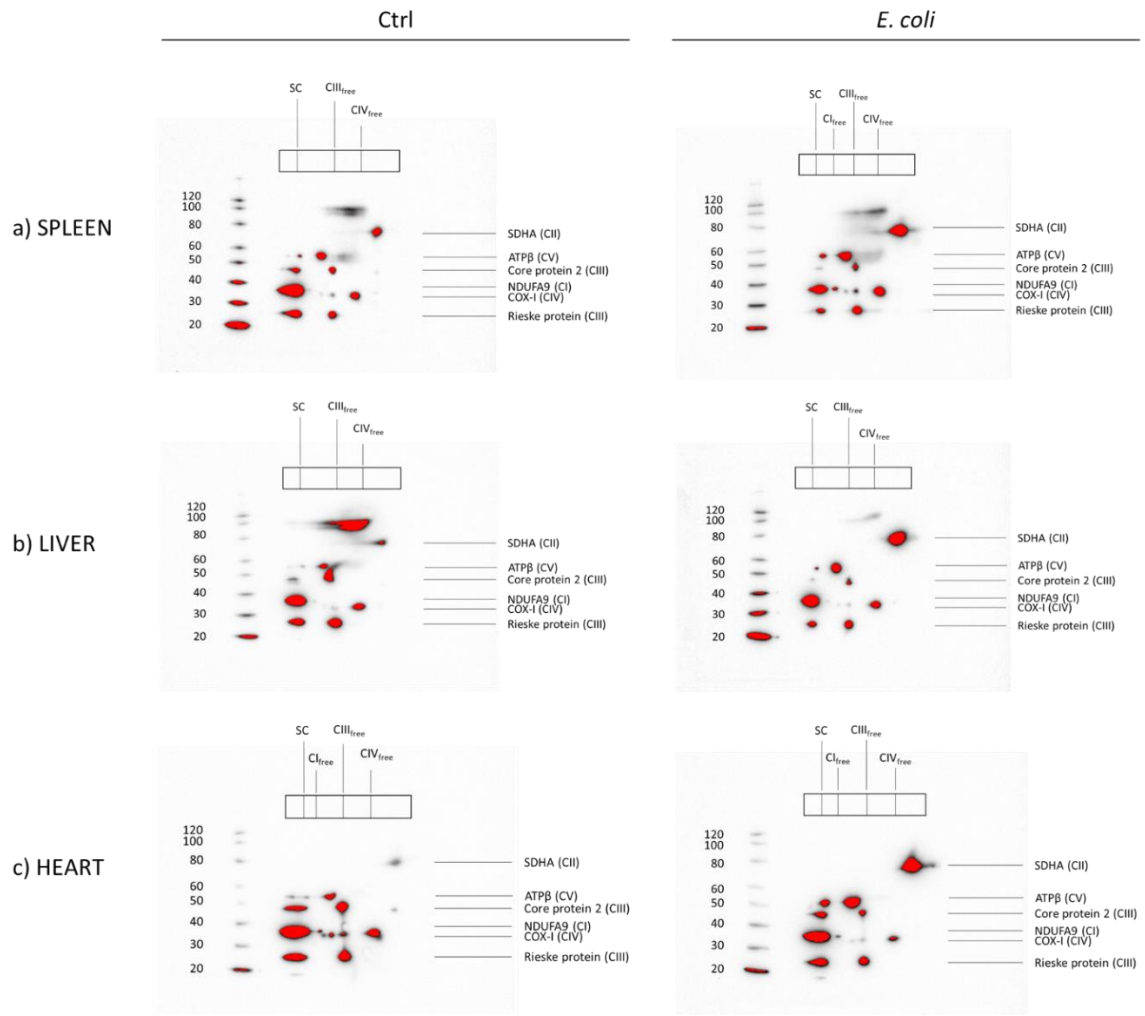

Figure 37. Chemiluminescent immunodetection of respiratory complexes and supercomplexes after 2D BN/SDS–PAGE analysis in a) spleen, b) liver and c) heart mitochondria isolated from control (Ctrl) or *E. coli* infected (*E. coli*) tissues. Protein extracts were solubilised from cells samples by using digitonin at a detergent to protein ratio of 8 (w:w) in order to preserve native supercomplexes. Immunodetection was performed using specific monoclonal antibodies: NDUFA9 of CI (39 kDa), NDUFB8 of CI (17 kDa), SDHA of CII (70 kDa), SDHB of CII (28 kDa) Rieske protein of CIII (22 kDa), Core 2 of CIII (42 kDa), COX-I of CIV (37 kDa) and subunit α of ATP synthase (56 kDa). Data are from one experiment. Abbreviations: CI-CV, Complex I-V, SC, supercomplex.

In fact, these preliminary results show a large amount of SC I_1III_2 and a relatively low amount of CI in free form in the control samples. In particular, in spleen and liver mitochondria the 100% of CI is bound to dimeric CIII, whereas in heart mitochondria SC I_1III_2 is 97% and a small amount of CI in free form is also detectable. Instead, the dimeric CIII in free form increase from 38% in spleen samples to 64% and 52% in liver and heart samples, respectively. Mitochondria isolated from infected mice tissues still have high percentages of CI bound to SC I_1III_2 but the amount of CI bound to CIII decreases to 94% in spleen mitochondria and the CIII in free form increase at 71%. The percentage of CIII bound to CI in infected liver slight increases at 70% while in infected heart mitochondria decreases to 40%.

We have also evaluated the specific activity of CI, the integrated activity by CI and CIII, the succinate-dependent integrated activity by CII and CIII and the overall respiratory activity in the above-mentioned mitochondrial samples (Table 2). As expected from the unchanged amounts of SCs after infection, also the NADH-cytochrome c activity catalysed by CI and CIII was not changed upon infection.

		NADH:oxidase (μmoli NADH/min/mg prot.)	**NADH:ubiquinone oxidoreductase** (μmoli NADH/min/mg prot.)	**NADH:cytochrome c oxidoreductase** (μmoli cyt c/min/mg prot.)	**succinate:cytochrome c oxidoreductase** (μmoli cyt c/min/mg prot.)
SPLEEN	Ct	0.143 [1]	0.126 [1]	0.303 ± 0.018 [2]	0.378 ± 0.002 [2]
	EC	0.153 [1]	0.139 [1]	0.311 ± 0.053 [2]	0.464 ± 0.007 [2]
LIVER	Ct	0.090 ± 0.006 [4]	0.084 ± 0.018 [3]	0.111 ± 0.042 [6]	0.247 ± 0.036 [3]
	EC	0.137 ± 0.004 [2]	0.100 ± 0.007 [2]	0.081 ± 0.021 [3]	0.338 ± 0.002 [2]
HEART	Ct	1.488 ± 0.082 [2]	0.620 ± 0.051 [2]	0.951 ± 0.169 [4]	0.991 ± 0.004 [2]
	EC	1.023 ± 0.040 [2]	0.674 ± 0.077 [2]	0.741 ± 0.094 [4]	0.849 ± 0.062 [2]

Table 2. Enzyme activity values in control tissue mitochondria (Ct) and in mitochondria from tissues of *E. coli*-infected mice (EC). Data are expressed as mean ± s.d. Values in square brackets indicate the number of independent samples.

5.3 Sensing of Gram- and Gram+ bacteria leads to a distinct metabolic reprogramming

It is known from literature [10] that metabolic changes occur during macrophages activation. We wondered if the different nature of the bacteria strains employed in our study may induce a different reprogramming of the main metabolic pathway of BMDMs in our experimental conditions.

Cultured BMDMs were challenged overnight with live Gram- (*E. coli*, *ΔSpi1/2 S. enterica* and *P. aeruginosa*) and Gram+ bacteria (*L. innocua*, *ΔLLO/FliC L. monocytogenes* and *S. aureus*) and the next day cells were collected for the metabolomics analysis was performed in collaboration with the metabolomic facility in Toulouse (MetaToul) (Figure 38).

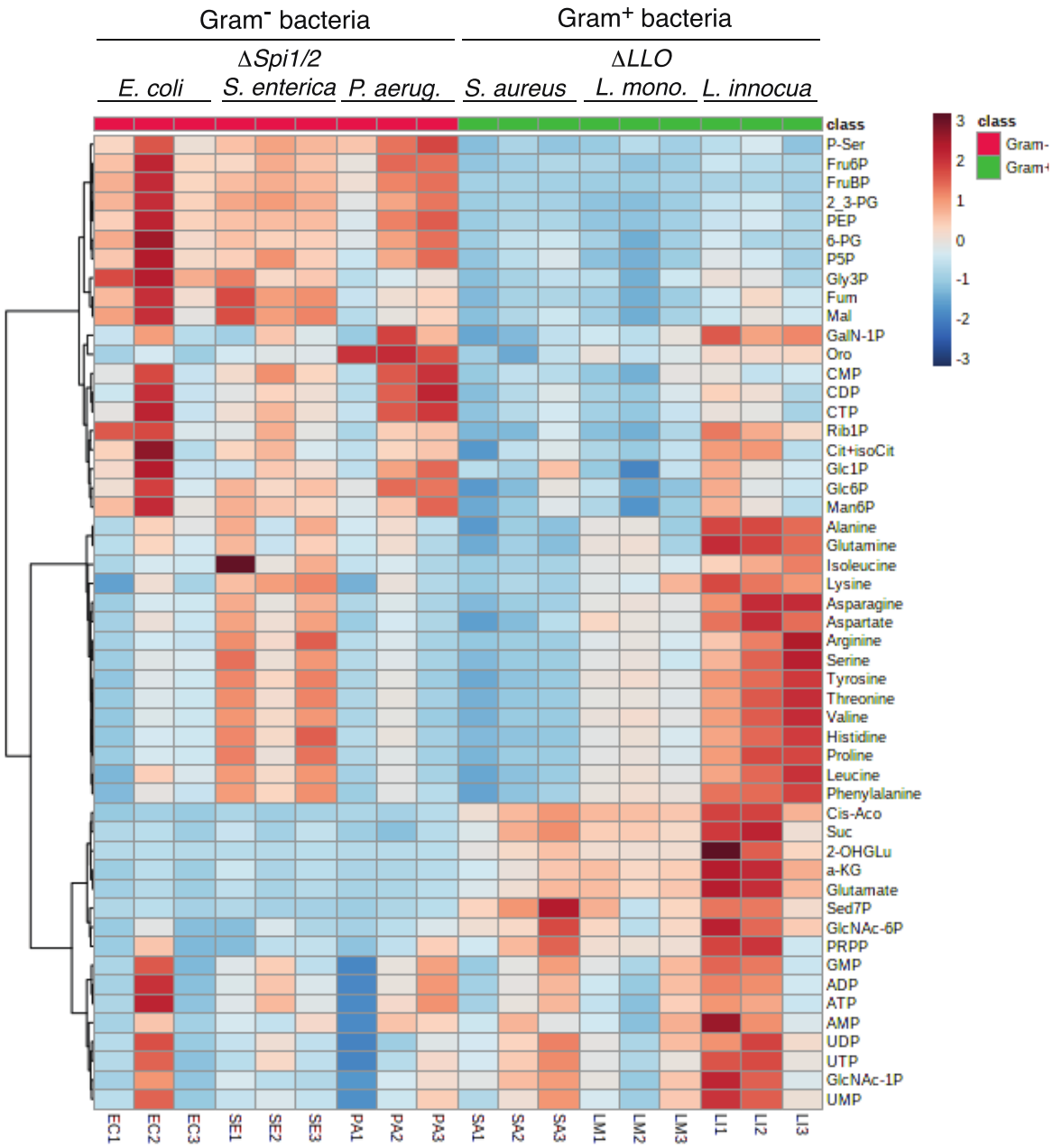

Figure 38. Hierarchical clustering heatmap representing significantly different metabolites identified from BMDMs treated with Gram- bacteria (*E. coli*, *ΔSpi1/2 S. enterica* and *P. aeruginosa*, left panel) and Gram+ bacteria (*L. innocua*, *ΔLLO/FliC L. monocytogenes* and *S. aureus*, right panel). Data are from three independent experiments.

The data listed in the report show that Gram-negative treated macrophages strengthen the abundance of some metabolites of glycolysis and pentose phosphate pathway (e.g. listed items from Fru6P to Gly3P in Figure 38) while Gram-positive treated macrophages generate an increase of metabolites of the TCA cycle and amino acid metabolism (Figure 39).

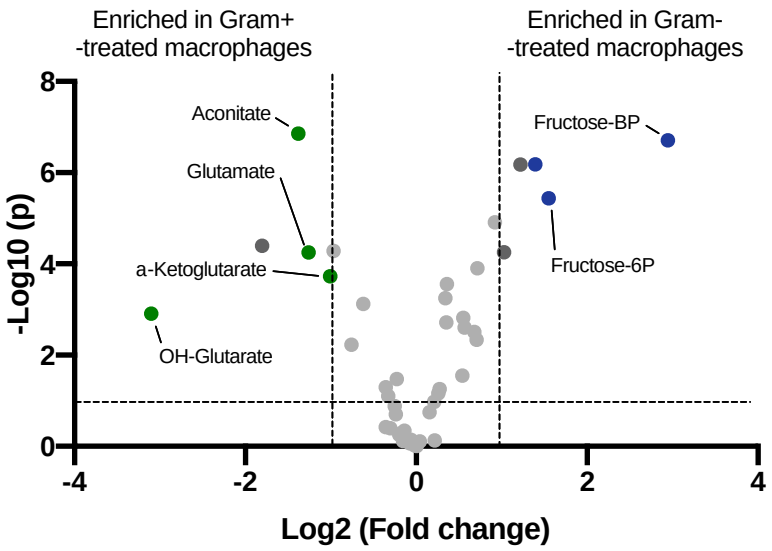

Figure 39. Volcano plot of log_2 fold-change (x axis) versus $-log_{10}$ p-value (y axis, representing the probability that the metabolite is significantly regulated), based on metabolomics data for the comparisons of Gram+ treated macrophages (left) and Gram- treated macrophages (right). Scattered points represent metabolites. Metabolites with log_2FC above 1 are up-regulated, while metabolites with log_2FC below 1 are considered as down regulated.

In particular, we focused on the metabolites of the TCA cycle (Figure 40) since it is well known that some metabolites, such as succinate, fumarate and α-ketoglutarate, contribute to histone- and DNA demethylation of cytokine loci [6].

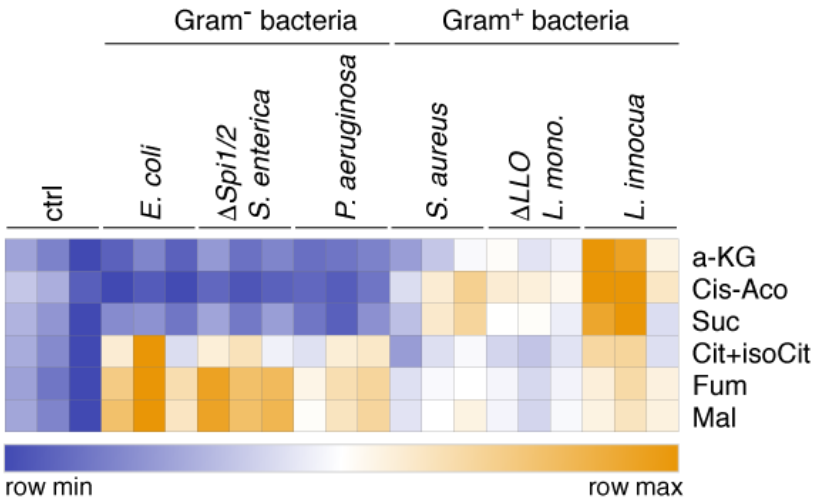

Figure 40. Heatmap representing the significantly different TCA cycle metabolites identified from BMDMs untreated (Ctrl), treated with Gram- bacteria (*E. coli*, *ΔSpi1/2 S. enterica* and *P. aeruginosa*, on the left) and Gram+ bacteria (*L. innocua*, *ΔLLO/FliC L. monocytogenes* and *S. aureus*, on the right). Data are from three independent experiments.

Our metabolomic analysis confirms that sensing of Gram- bacteria by macrophages induces a TCA cycle reprogramming characterized by the accumulation of fumarate while Gram+ bacteria-treated macrophages accumulate α-ketoglutarate. In fact, the tendency of the fumarate/α-ketoglutarate ratio is therefore different between Gram- and Gram+ treated samples (Figure 41).

These results are preliminary data and further epigenetic studies are ongoing to highlight significant different histone- and DNA demethylation of cytokine loci upon macrophage activation by sensing of Gram- and Gram+ bacteria.

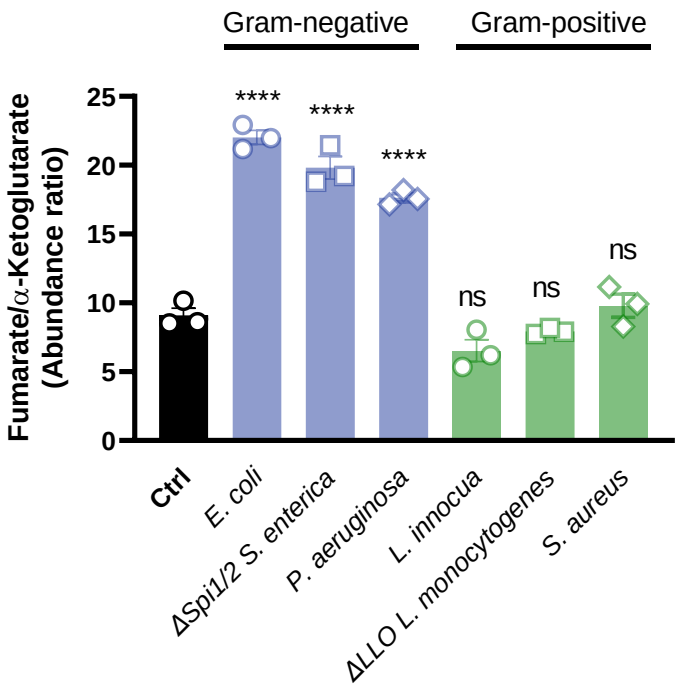

Figure 41. Fumarate/α-ketoglutarate ratio of BMDMs untreated (Ctrl) and treated with Gram- bacteria (*E. coli*, *ΔSpi1/2 S. enterica* and *P. aeruginosa*, blue columns) and Gram+ bacteria (*L. innocua*, *ΔLLO/FliC L. monocytogenes* and *S. aureus*, green columns). NS, not significant; **P* < 0.05; ***P* < 0.01; ****P* < 0.001 (two-tailed unpaired Student's *t*-test). Data (mean and s.e.m.) are from three independent experiments.

5.3.1 Pharmacological manipulation of fumarate/α-ketoglutarate ratio in macrophages

The results regarding the different fumarate/α-ketoglutarate ratio, depending on the nature of the bacteria, led us to wonder if a pharmacological modification of this ratio could affect the production of cytokines.

Cultured BMDMs were treated *in vitro* with 25 and 100 µM of dimethyl-fumarate (DMF) or with 0.1 and 1 mM of α-ketoglutarate (α-KG) for 4h before adding live bacteria as usual in our previous experiments. Then, after 24hrs post-infection, the cytokine levels were measured by ELISA.

In *E. coli*–treated macrophages (Figure 42), the presence of DMF decreases in a dose-dependent mode the IL-10 production and increases the TNFα and IL-1β production. No significant effect on the IL-6 production was observed under our experimental conditions. Conversely, the α-KG reatment does not seem to affect the cytokine production by macrophages challenged with *E. coli*.

In *L. innocua*–treated macrophages (Figure 43), presence of the DMF also decreases in a dose-dependent mode the IL-10 production and increases the TNFα and IL-1β production. Again, no significant effect on the IL-6 production was observed under our experimental conditions. At difference from *E. coli*–treated samples, α-KG increases the IL-6 and IL-10 production in macrophages stimulated with *L. innocua*.

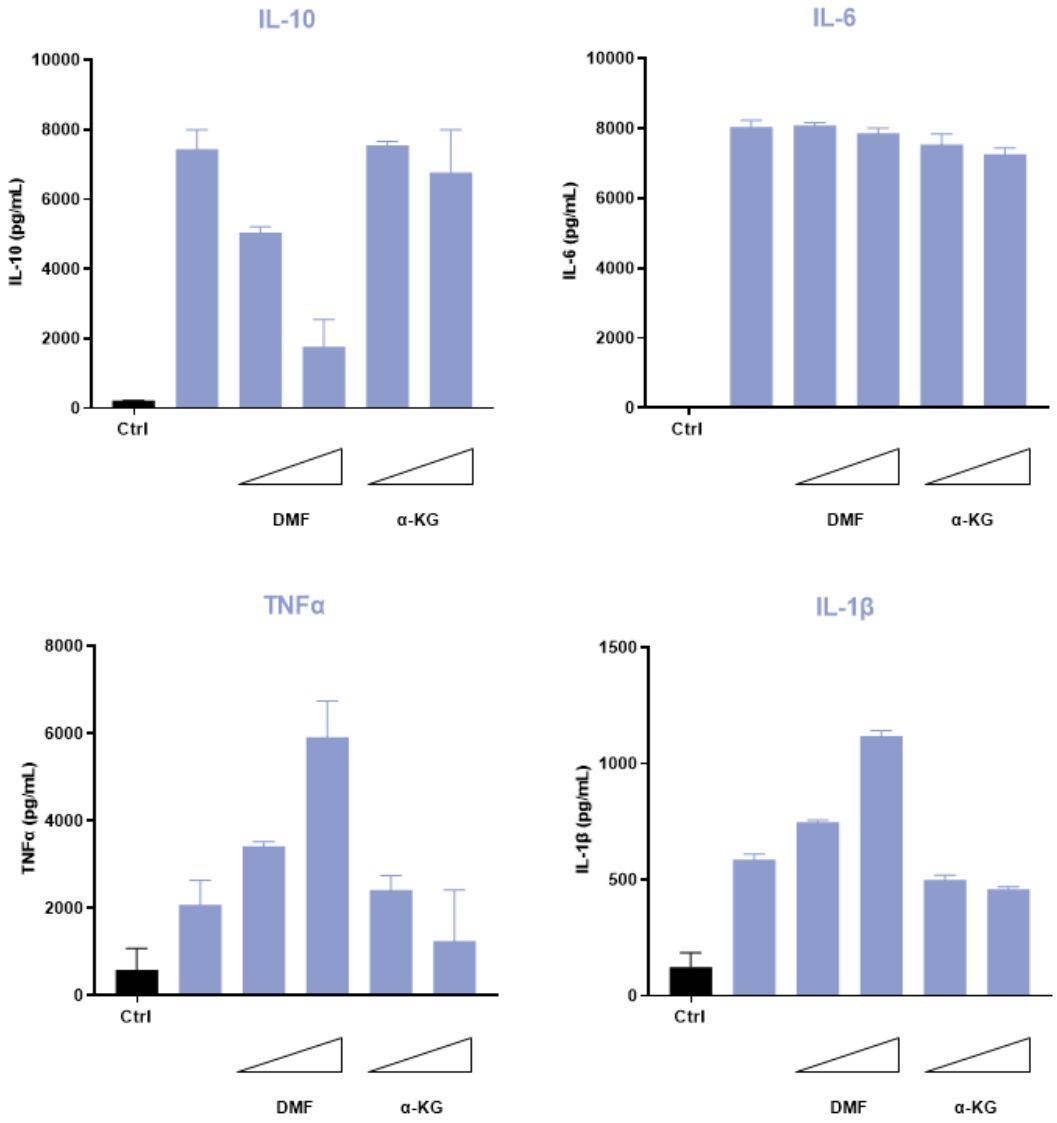

Figure 42. Cytokine production in BMDMs in the absence (first blue column) and in the presence of 25, 100 µM DMF or 0.1, 1 mM α-KG for 4h prior to infection with *E. coli* (Gram- bacteria) at MOI 25 for 24h. IL-10, IL-6, TNFα and IL-1β levels were measured as described in "Materials and Methods". The small triangles below the graphs represent the low-high quantities of the corresponding metabolite added in culture. Data (mean and s.e.m.) are from two independent experiments.

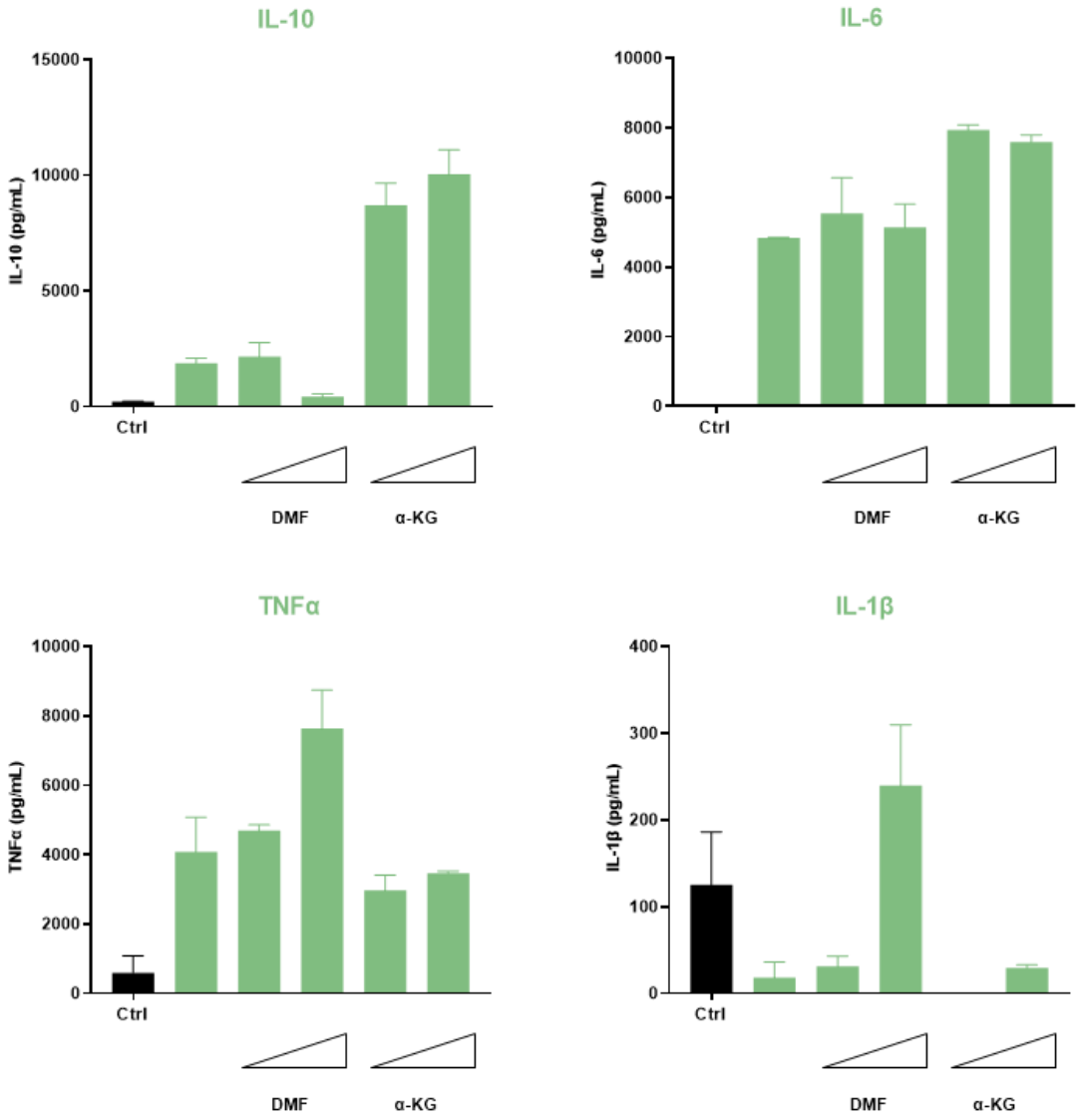

Figure 43. Cytokine production in BMDMs in the absence (first green column) and in the presence of 25, 100 µM DMF or 0.1, 1 mM α-KG for 4h prior to infection with *L. innocua* (Gram+ bacteria) at MOI 25 for 24h. IL-10, IL-6, TNFα and IL-1β levels were measured as described in "Materials and Methods". The small triangles below the graphs represent the low-high quantities of the corresponding metabolite added in culture. Data (mean and s.e.m.) are from two independent experiments.

5.3.2 Identification of CII/SDH post-translational modifications in macrophages upon infection

It is known from the literature [108] that CII activity is regulated by post-translational modifications (PTMs) of SDH subunits, in particular phosphorylation and acetylation. Increased CII activity, in macrophages, requires the phosphorylation of SDHA Tyr604, by the action of Src-family tyrosine kinase Fgr [109]. Moreover, inhibition of TEN-like mi-tochondrial phosphatase-1 (PTPMT1) leads to an increased phosphorylation and CII activity, while a decreased SDH activity results by acetylation of lysines of SDHA.

To further investigate the PTMs on the role of CII/SDH activity, we performed proteomic analysis on macrophages upon Gram- and Gram+ bacterial infection in order to identify specific PTMs.

Cultured BMDMs were treated with live *E. coli* and *L. innocua* for 18hrs. The four subunits of CII/SDH (SDHA, SDHB, SDHC and SDHD) were immunoprecipitated and subsequently analysed by mass-spectrometry analysis to identify PTMs (Figure 44). The proteomic analysis, performed in collaboration with the proteomic facility located in Bordeaux (J.W. Dupuy), reveals some PTMs in different amino acid residues, depending on the nature of bacteria. In *E. coli* – treated macrophages we found the phosphorylation of SDHA Thr262, the succinylation of SDHA Ly95 and Lys538 and the acetylation of SDHA Lys423. Instead, in *L. innocua* – treated macrophages we detected the phosphorylation of SDHA Ser470 and Tyr365 and the phosphorylation of SDHC Ser95.

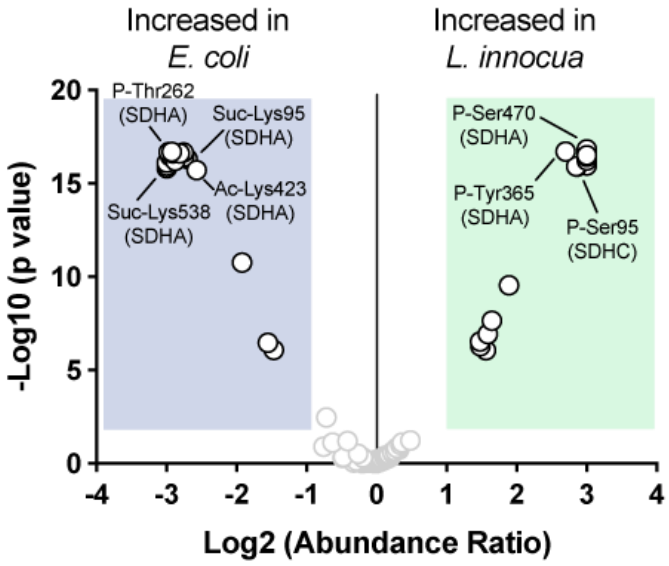

Figure 44. Volcano plot representing some post-translational modifications (PTMs) found in subunits of CII/SDH in BMDMs treated with live *E. coli*, (Gram-, on the left) and *L. innocua* (Gram+, on the right). Abbreviations: SDHA-C, subunit A-C of CII/SDH; P, phosphorylation; Suc, succinylation; Ac, acetylation.

Interestingly, from the analysis was not detected phosphorylation of the SDHA Tyr604, known to be one of the amino acid residues involved in the transient increase in CII activity upon *E. coli* infection [[109]].

5.4 Sensing of bacteria induce different cytokine production

Upon activation, macrophages release cytokines to trigger an immune response, so we investigated whether sensing of different bacteria, and the consequent metabolic alteration that we described in the previous sections, may affect the cytokine production.

Cultured BMDMs were stimulated with Gram-negative (*E. coli*, *ΔSpi1/2 S. enterica* and *P. aeruginosa*) and Gram-positive bacteria (*L. innocua*, *ΔLLO/FliC L. monocytogenes* and *S. aureus*) as in our previous experiments. After 24h, supernatants were collected and the concentrations of IL-1β, IL-10, IL-6 and TNFα were measured by ELISA (Figure 45).

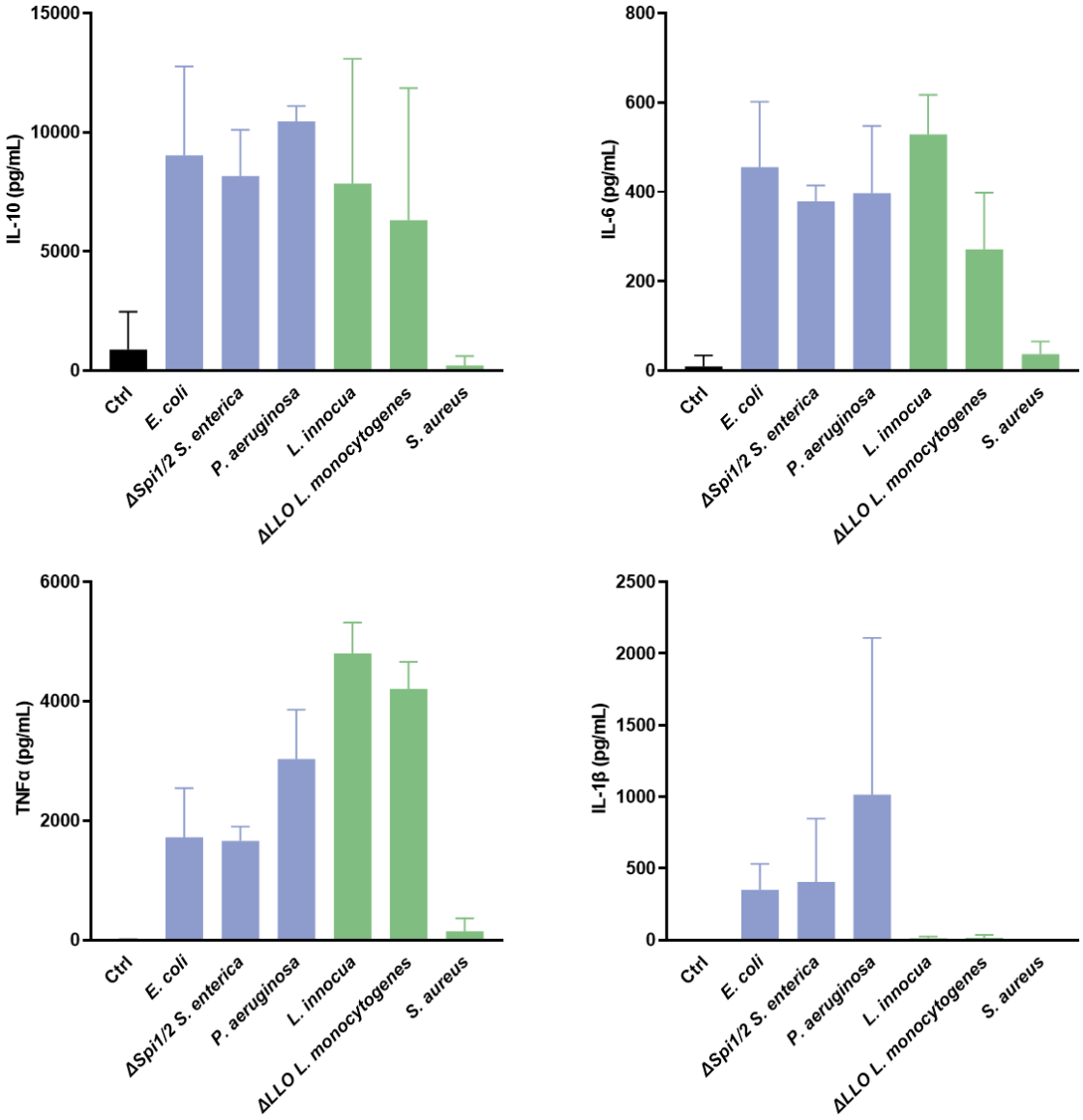

Figure 45. Cytokine production in BMDMs untreated (Ctrl) and treated with Gram- bacteria (*E. coli*, *ΔSpi1/2 S. enterica* and *P. aeruginosa*, blue columns) and Gram+ bacteria (*L. innocua*, *ΔLLO/FliC L. monocytogenes* and *S. aureus*, green columns) at MOI 25 for 24hrs. IL-10, IL-6, TNFα and IL-1β levels were measured as described in "Materials and Methods". Data (mean and s.e.m.) are from two independent experiments.

Our preliminary data show an increase in IL-1β production in Gram- treated macrophages whereas IL-1β is quite completely absent in Gram+ bacteria treated samples. Moreover, a higher TNFα production is observed in Gram+ treated macrophages. No major differences between the two types of bacterial treatment are observed for IL-6 and IL-10 production.

Interestingly, *S. aureus* seems not to respond as the other Gram+ bacteria tested in our study, so further studies are needed to better investigate this behavior.

5.5 Effect of CII inhibitors on the mitochondrial ETS organization and macrophage metabolism

To investigate the role of CII and its possible pathological alterations in macrophage reprogramming upon infection, we cultured *in vitro* BMDMs with CII inhibitors, 3-nitropropionic acid (3-NPA) and dimethyl malonate (DMM).

Mitoplasts were isolated from BMDMs untreated or treated either with 0.5 mM 3NPA for 1h (Figure 46-panel A) or 10 mM DDM for 3 hrs (Figure 46-panel B) prior to challenging the cells with live *E. coli* or *L. innocua* for different time points. Samples were analysed by 1D BN-PAGE followed by immunoblotting.

Our preliminary data do not show major differences in the time dependent mitochondrial respiratory adaptations in infected BMDMs as a consequence of the presence of the CII inhibitors compared to time-dependent adaptations we have already described (see also section 5.1.1) for non-inhibited BMDMs.

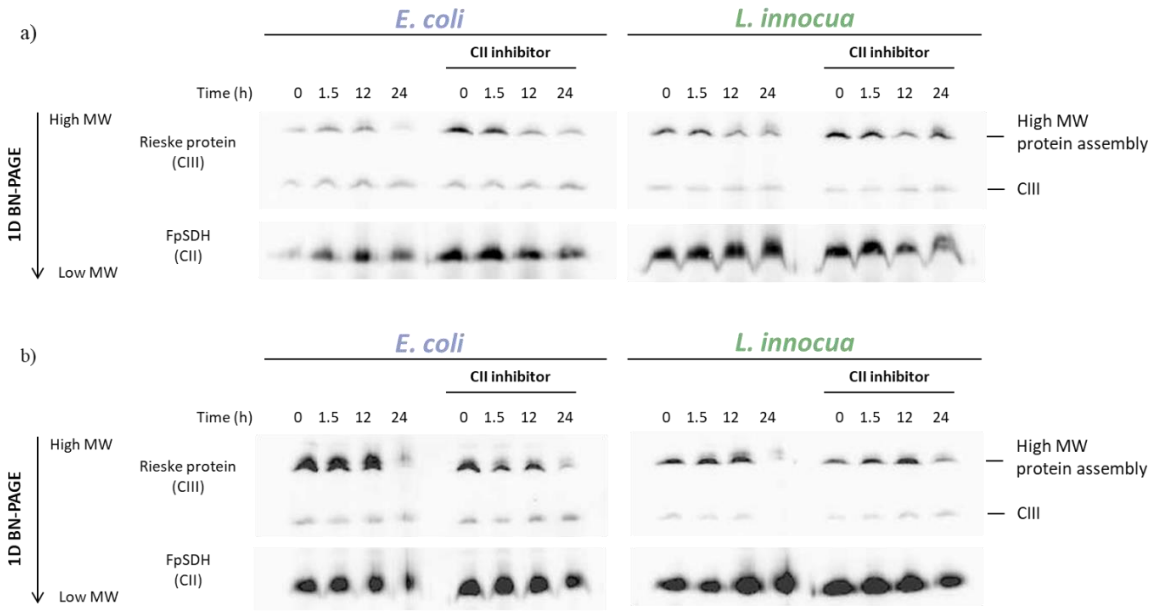

Figure 46. 1D BN-PAGE in mitoplasts isolated from BMDMs untreated (time 0) or treated with a) 0.5 mM 3NPA for 1h or b) 10 mM DMM for 3h before adding bacteria. Cells were challenged with *E. coli* (Gram- bacteria) or *L. innocua* (Gram+ bacteria) for different time points (1.5hrs, 12hrs and 24hrs). Immunodetection with specific monoclonal antibodies: SDHA of CII (70 kDa) and Rieske protein of CIII (22 kDa). One experiment representative of two independent experiments with similar results. Abbreviations: CII-CIII, Complex II-III, III_2, free CIII in dimeric form.

5.5.1 Effect of CII inhibitors on the ATP production

To further investigate possible pathological consequences of CII in inhibition on macrophage metabolism and sensing of bacteria, we measured the ATP levels in cultured BMDMs untreated or treated with 0.5 mM 3NPA for 1h or 10 mM DMM for 3h before adding live *E. coli* and *L. innocua* overnight (Figure 47).

From our preliminary data, the ATP generation from BMDMs (see also section 5.1.2) treated with either one of the two Gram- bacterial strains employed in this study (*E. coli* and *ΔSpi1/2 S. enterica*) or one of the two Gram+ bacteria (*L. innocua* and *ΔLLO/FliC L. monocytogenes*) is unaffected by both CII inhibitors.

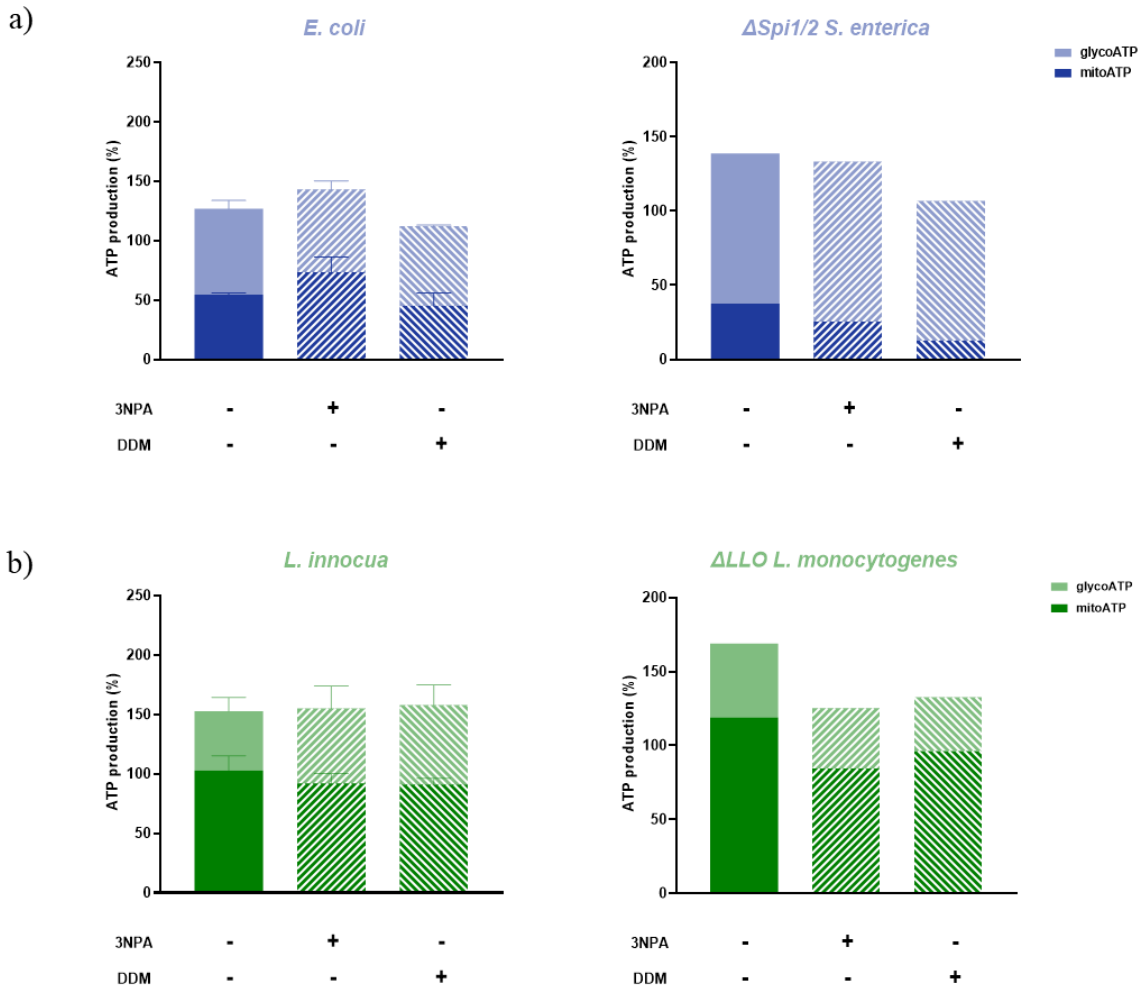

Figure 47. ATP synthesis in cultured macrophages untreated or treated with 0.5 mM 3NPA for 1h or 10 mM DMM for 3h before adding bacteria. Cells were challenged with a) Gram- bacteria (*E. coli* and *ΔSpi1/2 S. enterica*, dark blue/light column) or b) Gram+ bacteria (*L. innocua* and *ΔLLO/FliC L. monocytogenes*, dark green/light column) at MOI 25 for 24h. The mitochondrial ATP levels were measured incubating OXPHOS cocktail inhibitors (antimycin 100 µM, rotenone 0,5 µM and oligomycin 3 µM) for 1h before the dosage. Data are from four independent experiments with four technical replicates (mean and s.e.m.).

5.5.2 Effect of CII inhibitor on the mitochondrial respiration

Although the ATP production was not affected by the effect of CII inhibition (see section 5.5.1), we checked more in detail the effect of the 3NPA CII inhibitor on the mitochondrial respiration.

Cultured BMDMs were treated with 0.5 mM 3NPA for 1h before adding live *E. coli* and *L. innocua* for different time points and the oxygen consumption rate was measured using an Agilent Seahorse XF Analyzer with glucose, pyruvate and glutamine in the respiratory medium.

Our preliminary data show that the basal respiration rate (BRR) in BMDMs treated with Gram- and Gram+ bacteria (see section 5.1.3) seems unaffected by pre-incubation of the cells with the CII inhibitor (Figure 48). On the contrary, the maximal respiratory rate (MRR), which is by definition the rate of oxygen consumption in the presence of uncouplers, is strongly influenced by the presence of specific inhibitor of CII (Figure 49). This indicates that the 3-NPA concentration used in our experiments is actually able of interfering with the catalytic activity of the mitochondrial CII.

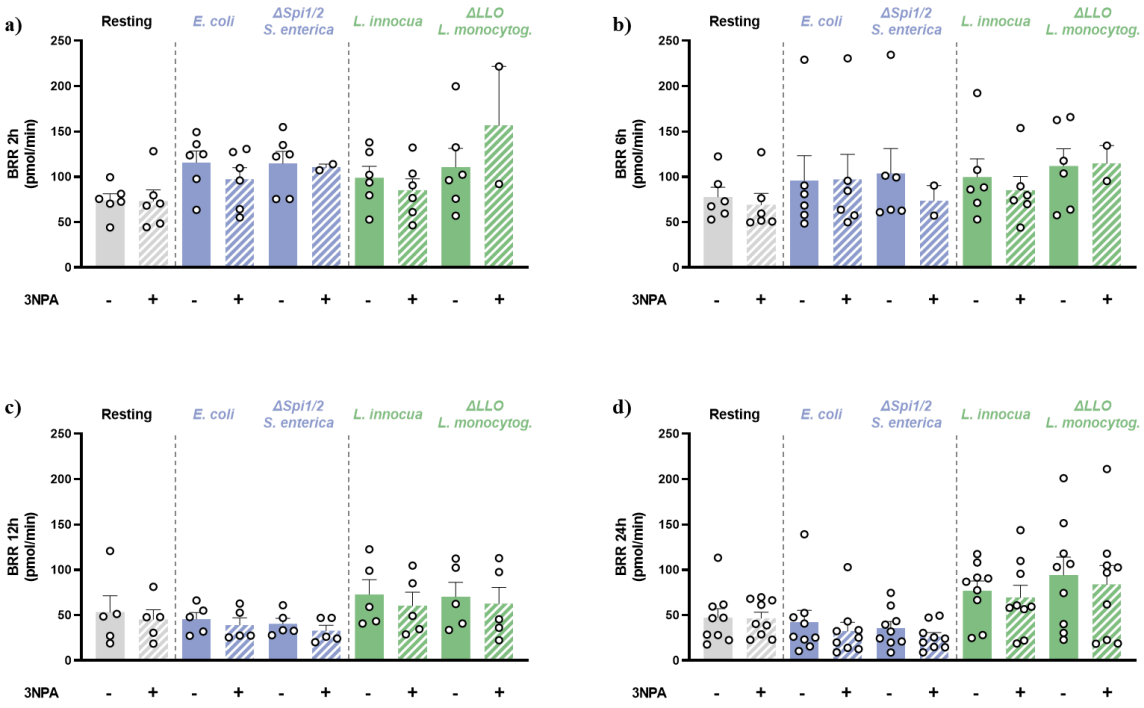

Figure 48. Basal respiration rate (BRR) of 1.5 x 10^5 BMDMs/well cultured with 0.5 mM 3NPA for 1h before adding bacteria. Cells were untreated (Resting, grey columns) or treated with Gram- bacteria (*E. coli* and *ΔSpi1/2 S. enterica*, blue columns) and Gram+ bacteria (*L. innocua* and *ΔLLO/FliC L. monocytogenes*, green columns) at different time points a) 2hrs, b) 6hrs, c) 12hrs and d) 24hrs. Each symbol represents an individual experiment. Data are from two to nine independent experiments with six technical replicates (mean and s.e.m.).

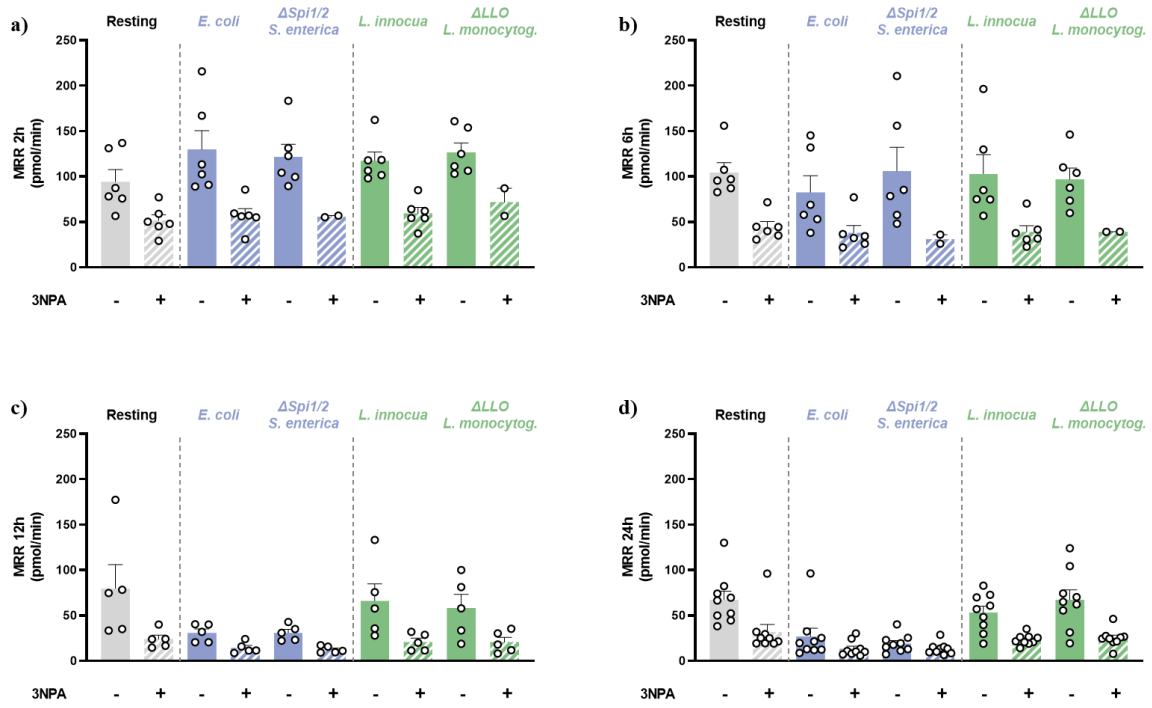

Figure 49. Maximal respiration rate (MRR) of 1.5 x 10^5 BMDMs/well cultured with 0.5 mM 3NPA for 1h before adding bacteria. Cells were untreated (Resting, grey columns) or treated with Gram- bacteria (*E. coli* and *ΔSpi1/2 S. enterica*, blue columns) and Gram+ bacteria (*L. innocua* and *ΔLLO/FliC L. monocytogenes*, green columns) at different time points a) 2hrs, b) 6hrs, c) 12hrs and d) 24hrs. Each symbol represents an individual experiment. Data are from two to nine independent experiments with six technical replicates (mean and s.e.m.).

5.5.3 *In vitro* effect of CII inhibitors on the cytokine production

To elucidate whether a pathological condition of CII, as induced *in vitro* by exogenous inhibitors, could affect the metabolism of cultured BMDMs in term of cytokine production, in addition to the observed impairment of their mitochondrial respiration (see section 5.5.2), we analysed serum concentration of IL-1β, IL-10, IL-6 and TNFα in 3NPA- and DMM-treated samples.

Our preliminary data show a global decrease of cytokine production both in Gram- (Figure 50) and in Gram+ treated macrophages (Figure 51) in the presence of CII inhibitors. However, the original work of this thesis on Gram+ (*L. innocua*) treated macrophages points out that the inhibition of CII affects cytokine production more than in macrophages challenged with Gram- bacteria (*E. coli*).

In particular, in *L. innocua*-treated BMDMs DDM induce IL-10 level decrease of 89% compared to the 73% in *E. coli* -treated macrophages. Moreover, the IL-6 levels strongly diminished of 93% induced by CII inhibition in in *L. innocua*-treated BMDMs, while it is reduced of only 23% upon *E. coli* infection. Finally, DDM induce a reduction of 39% and 46% of TNFα and IL-1β, respectively, in *E. coli* -treated BMDMs, but the effect of CII inhibition is more evident in *L. innocua*-treated BMDMs where the decreases reach the 63% of TNFα level and 100% in IL-1β production (Table 3).

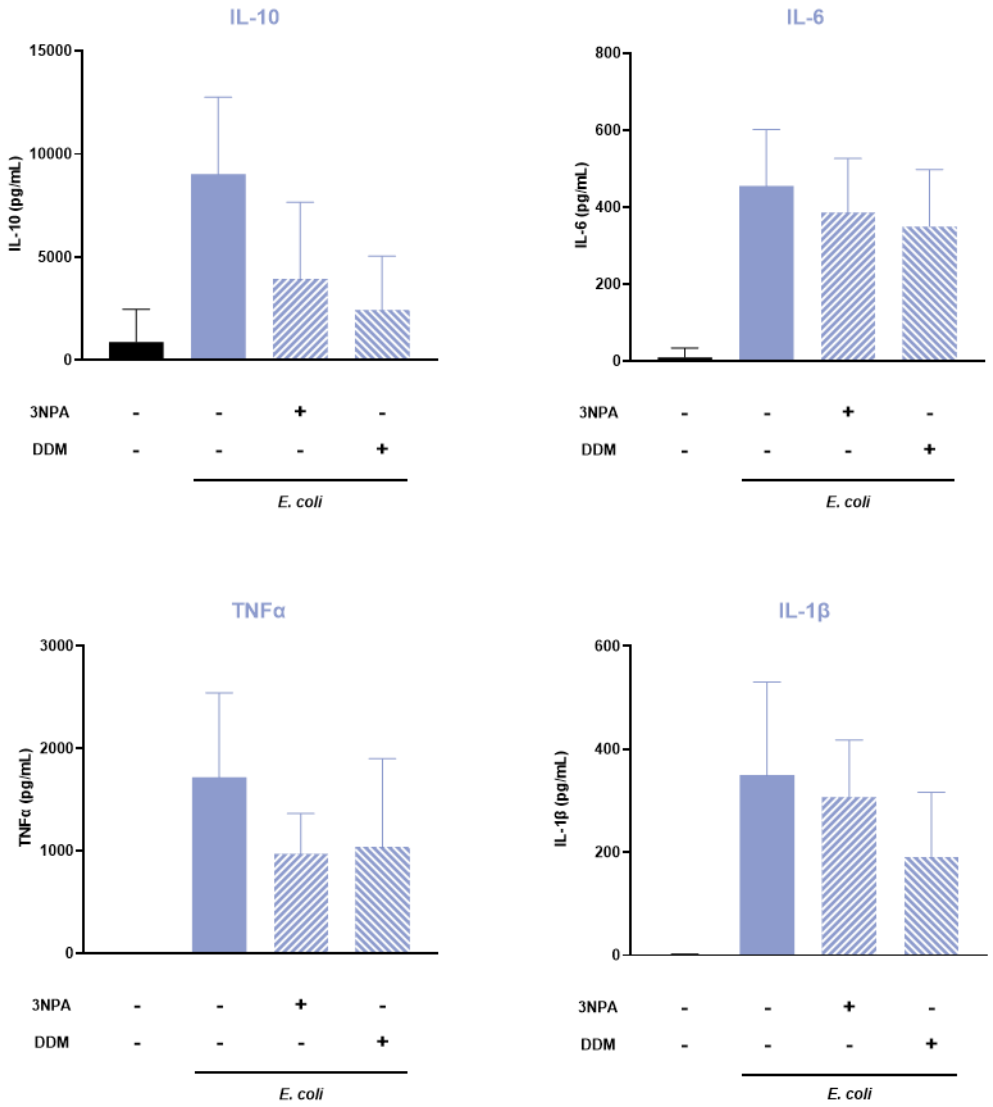

Figure 50. *In vitro* cytokine production in BMDMs untreated (black column) and treated with 0.5 mM 3NPA for 1h or 10 mM DDM for 3h before *E. coli* (Gram- bacteria) infection at MOI 25 for 24hrs. IL-10, IL-6, TNFα and IL-1β levels were measured as described in "Materials and Methods". Data (mean and s.e.m.) are from six independent experiments with three technical replicates.

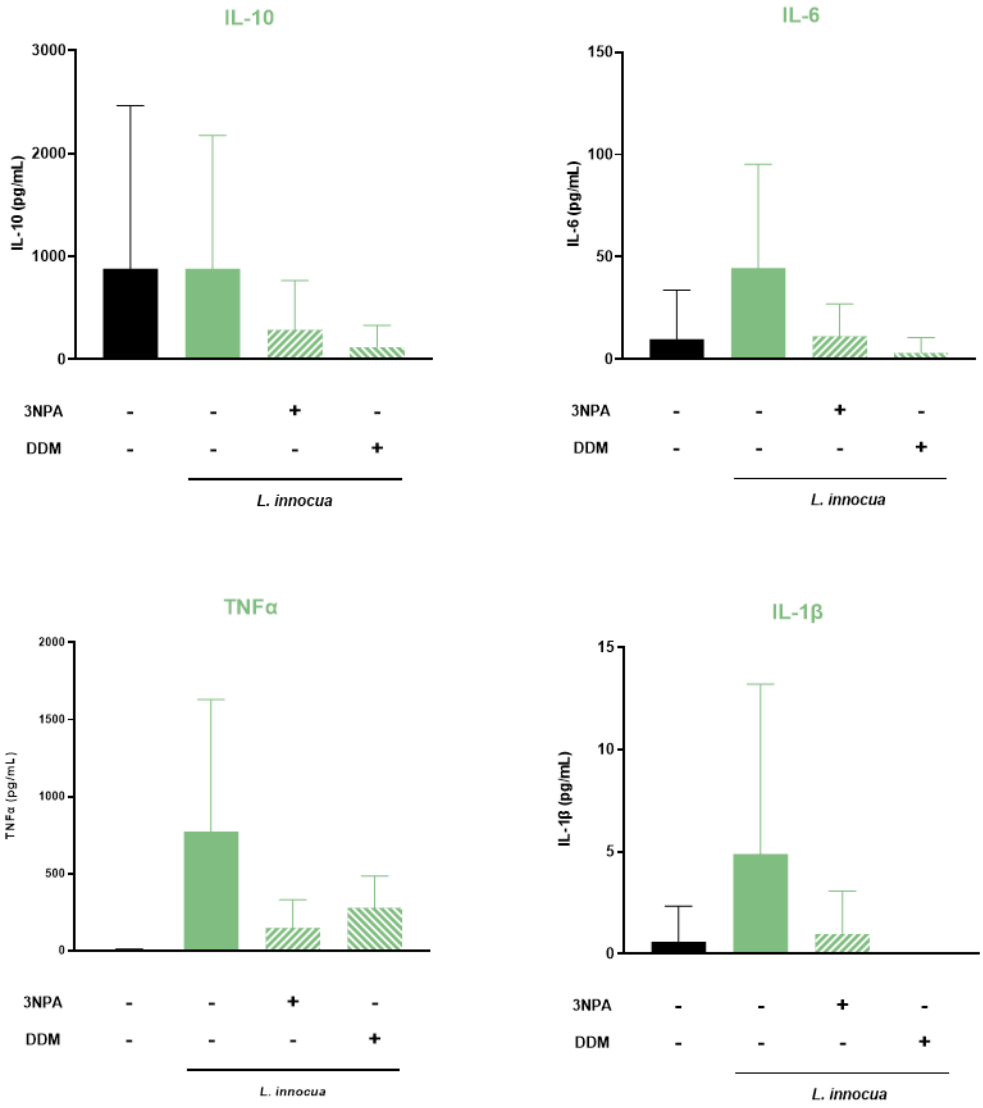

Figure 51. *In vitro* cytokine production in BMDMs untreated (black column) and treated with 0.5 mM 3NPA for 1h or 10 mM DDM for 3h before *L. innocua* (Gram+ bacteria) infection at MOI 25 for 24hrs. IL-10, IL-6, TNFα and IL-1β levels were measured as described in "Materials and Methods". Data (mean and s.e.m.) are from six independent experiments with three technical replicates.

	IL-10 (pg/mL)	IL-6 (pg/mL)	TNFα (pg/mL)	IL-1β (pg/mL)
E. coli	9028,9	455,2	1718,9	350
+ DMM	2440,9 (-73%)	349,7 (-23%)	1040,3 (-39%)	190,4 (-46%)
L. innocua	588,1	44,5	772,9	4,9
+ DMM	60,3 (-89%)	3,1 (-93%)	278,9 (-64%)	0 (-100%)

Table 3. *In vitro* cytokine values (expressed as pg/ml) in BMDMs treated with live *E. coli* and *L. innocua* at MOI 25 for 24hrs. The percentage represent the inhibition of cytokine production induced by dimethyl malonate (DMM) normalized against the corresponding controls without CII inhibitor.

5.5.4 *In vivo* effect of CII inhibitor on the cytokine production

In the attempt to evaluate also the *in vivo* impact of CII on cytokine production we intraperitoneally injected wild-type C57BL/6N mice with non-lethal doses of DMM, a specific CII inhibitor, prior to infection by intraperitoneal injection of live *E. coli* or *L. innocua*. Two hours later, mice were sacrificed, blood was collected from the venous sinus and the cytokine levels were quantified by ELISA.

As shown in Figure 52, DMM seems not to affect the cytokine production in mice infected with Gram- bacteria (*E. coli*). On the contrary, in mice infected with Gram+ bacteria (*L. innocua*), CII inhibition increases the IL-10 production and decreases the TNFα level.

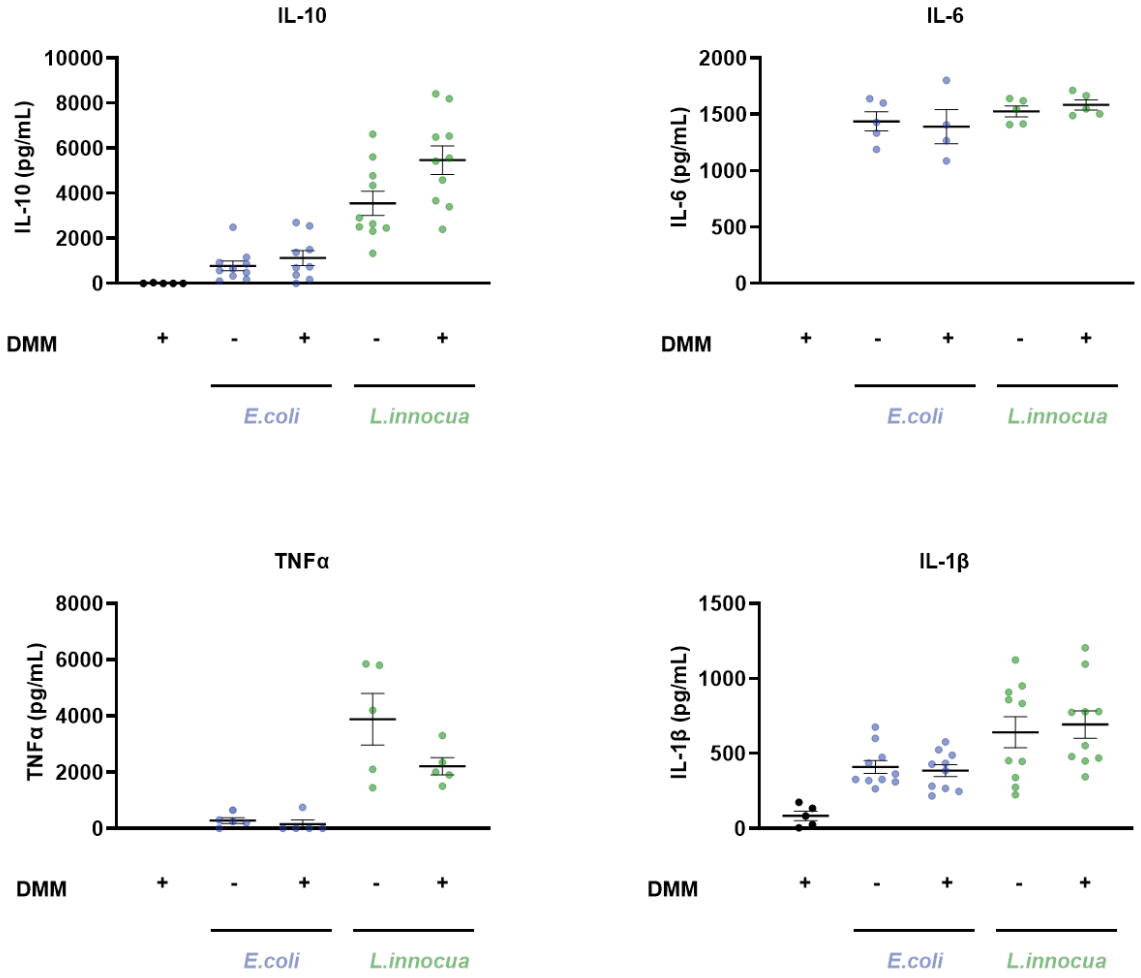

Figure 52. *In vivo* cytokine production in wild-type C57BL/6N mice treated with intraperitoneal injection of dimethyl malonate (DMM, 160 mg per kg body weight) and, after 2hrs, 1x10^9 live *E. coli* (Gram- bacteria, blue dots) or *L. innocua* (Gram+ bacteria, green dots). Two hours later, blood samples were collected and IL-10, IL-6, TNFα and IL- levels were measured as described in "Materials and Methods". Each symbol represents an individual mouse; small horizontal lines indicate mean (± s.e.m.) Data are from two independent experiments with five to ten mice per group.

Surprisingly, these *in vivo* results are not in line with the trend observed *in vitro* on the DMM effect in cultured BMDMs (see section 5.5.3), so further investigations are needed to clarify the different CII effect on macrophages *in vivo* or *in vitro* upon bacterial infection.

Discussion

Metabolic reprogramming has recently appeared as a major feature of innate immune cells following microbial infection. Emerging studies have identified metabolic pathways that, if altered, cause immune dysfunction and disease development [110,111,112]. Macrophages are key cells of immune system that maintain the homeostasis functions into many different tissues but also play an important role in inflammatory response. The activation of macrophages upon bacterial infection drives the conversion of immune cells from metabolically quiescent stage to a highly active metabolic state [113]. Metabolic transitions require the distribution of nutrients into different pathways and therefore there is a growing interest in how metabolic pathways are regulated to support or to guide functional changes. ATP production is crucial to provide energy for cellular functions both in the quiescent state and during macrophage activation. The main energy metabolism organelles present in the cell are mitochondria, thus they are at the core of the metabolic reprogramming. The mitochondrial tricarboxylic acid (TCA) cycle generates the reducing equivalents nicotinamide adenine dinucleotide (NADH) and succinate, which donate electrons to the mitochondrial electron transport system (ETS) complexes of the IMM to fuel oxidative phosphorylation (OXPHOS). The respiratory complexes, except Complex II, are organized into supercomplexes (SCs), supramolecular assemblies, which have been proposed to confer functional advantages to the cells, such as regulate electron flux via substrate channelling [49,114], to decrease the reactive oxygen species production [85], to stabilize individual complexes, etc. To our knowledge, despite the numerous studies that have demonstrated changes in SC content under physiological and pathological conditions [115,116], the role of SCs in metabolic adaptations in immune host defence has not fully understood. The understanding of mitochondrial reprogramming upon infection can help design new vaccines not yet available or enhance existing ones, or help in understanding inflammatory and infectious diseases, or develop targeted therapies.

As has been pointed out in the aim of this thesis, there is interest in fully understanding the precise characterization of adaptations of the mitochondrial respiratory chain and in elucidating the role of the respiratory CII/SDH in cultured BMDMs upon bacterial infection.

In resting condition, we confirmed the physiological presence of supercomplex I_1III_2 (SC I_1III_2) in bone marrow-derived macrophages (Figure 28). Upon bacterial infection, it is

possible to observe an alteration of the organization of the respiratory complexes in response to the detection of viable Gram-negative and Gram-positive bacteria in cultured macrophages (Figure 29). Upon Gram-negative bacterial infection, the abundance of respiratory SCs is transiently decreased, while the CII activity briefly increased (Figure 36). In contrast, Gram-positive bacteria maintain stable the amount of SCs and the CII activity during the time of the infection. These preliminary results suggest that CII activity and SCs architecture are connected to the mitochondrial metabolism reprogramming in macrophages which is dependent on the nature of the bacteria encountered. The decrease of the SCs can have multiple consequences, for example Complex I, one of the two components of the SC, is a large enzyme particularly unstable and its stability is influenced by several factor, or an over reduction of the Q pool which induce a reverse electron transfer toward CI.

Interconnections between structural and functional aspects of the respiratory chain are notoriously complex. In fact, our samples, culture macrophages challenged with bacteria (Figures 30 and 31) and mitochondria from tissues infected (Figure 37), do not reveal significant differences. All the experiments should be repeated since most of them are single experiment and it is difficult to establish a difference between Gram-negative and Gram-positive bacterial infection.

The challenge of macrophages by bacteria distinct in nature differentially modulate ATP production by phagocyting cells. Macrophages increase their ATP production in response to the recognition of pathogens. Interestingly the source of ATP differs when macrophages are challenged with Gram-negative bacteria or Gram-positive bacteria (Figures 32 and 33). The increase of ATP production from glycolysis induced by Gram-negative bacteria compared to the increase mitochondrial ATP production induced by Gram-positive bacteria is consistent with the transient increase of the basal and maximal respiratory rate in Gram-negative treated macrophages opposite to the high mitochondrial respiration maintained in macrophages during all the time of the Gram-positive bacterial infection (Figures 34 and 35). These observations suggest that, in Gram-positive bacterial infection, macrophages need to preserve an intact TCA cycle while in Gram-negative bacteria-treated macrophages the TCA cycle is discontinued. Moreover, the CII activity and the mitochondrial respiration show the same dynamic throughout the bacterial

infection, so this is confirming the involvement of the CII in the mitochondrial metabolism.

The ATP production induced by the different nature of the bacteria encountered is also in line with the observed accumulation of intermediates from glycolysis and pentose phosphate pathway in the presence of Gram-negative pathogens and accumulation of metabolites of the TCA cycle and amino acid metabolism by Gram-positive bacteria [117]. We were particularly interested to see that accumulation of TCA intermediates cultured macrophages upon bacterial infection since it is known that these metabolites might contribute to macrophage antimicrobial functions [6]. Recent studies [118] demonstrated that the TCA cycle of macrophages stimulated by the Toll-like receptor 4 (TLR4) ligand lipopolysaccharides (LPS) shows two breakpoints at the isocitrate dehydrogenase (IDH) and at the succinate dehydrogenase (SDH or Complex II, CII). Consistent with those studies, we observed that Gram-negative treated macrophages an accumulation of fumarate, suggesting that TCA cycle is broken at the level of the SDH (Figures 38, 39 and 40). On the contrary, Gram-positive bacteria induce an increase of all TCA cycle intermediates, which together with the increased mitochondrial ATP production suggests that macrophages preserve the metabolism of mitochondria upon Gram-positive bacterial infection. Given the close connection between central metabolism and inflammatory responses and cytokine production, our data suggest that metabolite-driven epigenetics can drive bacterial-induced macrophage differentiation to trigger the immune response.

Interestingly, Gram-negative treated macrophages show an increased fumarate/α-ketoglutarate ratio, while Gram-positive bacteria do not seem to influence the balance (Figure 41). We wondered whether the different fumarate/α-ketoglutarate ratio could act as a biomarker of the type of bacteria that macrophages recognize. Indeed, given the importance of environmental factors, immune cell metabolism in laboratory cell culture is obviously different than *in vivo*. To expand our knowledge of the problem, we had the opportunity to start a collaboration with Delneste's research group of the Center de Recherche en Cancérologie et Immunologie Nantes-Angers (France), who provided plasma samples from patients suffering sepsis with Gram-negative and Gram-positive bacterial infections (Figure 53). Sepsis, defined as "life-threatening organ dysfunction caused by a dysregulated host response to infection" [119], is a major health problem since it is a leading cause of death in intensive care units [120]. The cohort was composed by

110 patients and 29 patients presented a Gram-negative bacterial infection (Gram negative rods) while 24 patients showed a Gram-positive bacterial infection (Streptococcus and Staphylococcus).

	All patients n=110
Baseline characteristics	
Sex (M/F)	76/34
Age (years)	66.2 ± 13.8 [20-88]
Weight (kg)	78.0 ± 18.9 [44-140]
SOFA	9.0 ± 3.7 [1-19]
SAPSII	49.8 ± 18.3 [14-123]
Organ Support at ICU admission, n (%)	
Mechanical ventilation	64 (58.2)
PaO_2/FiO_2	214.2 ± 137 [28-757]
Invasive/non invasive ventilation	54/10
Renal replacement therapy	16 (14.5)
Use of vasopressors	84 (76.4)
Laboratory values at admission	
Serum creatinine (µmol/L)	180.3 ± 171 [26-1311]
Hemoglobin (g/dL)	11.0 ± 2.1 [5.3-16.4]
White blood cells (G/L)	14.7 ± 9.4 [0.3-41.4]
Blood neutrophils (G/L)	13.2 ± 9.4 [0.0-37.7]
Platelets (G/L)	200.0 ± 158 [14.0-999.0]
Blood lactate (mmol/L)	2.65 ± 3.1 [0.3-25.0]
Prothrombin time (%)	57.4 ± 20 [10-96]
Serum fibrinogen (g/L)	5.32 ± 2.1 [1.2-10.3]
Microbiological analysis; n (%)	
Positive blood cultures	38 (34.5)
Beta-hemolytic *Streptococcus*	13 (11.8)
Staphylococcus	11 (10.0)
Gram negative rods	29 (26.4)
Polymicrobial	7 (6.4)
Other	1 (0.9)
Organ support at any time of ICU stay; n (%)	
Mechanical ventilation	65 (59.1)
Renal replacement therapy	22 (20.0)
Use of vasopressors	86 (78.2)
ICU length of stay; days	11.2 ± 14.7 [1-90]
ICU mortality; n (%)	19 (17.3)

Figure 53. Baseline characteristics of patients with sepsis at the time of admission to intensive care unit. Collaboration: JY, Delneste (CRCINA, Angers, France) and JF. Augusto (CHRU, Angers, France).

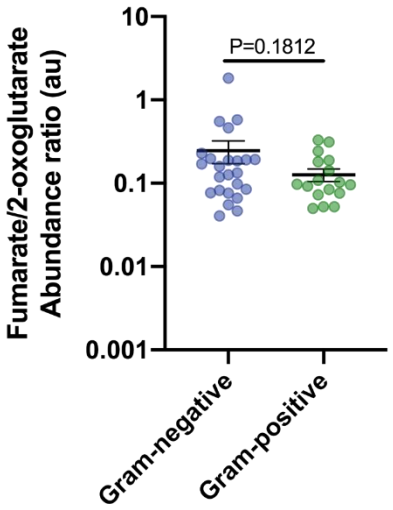

Figure 54. Fumarate/α-ketoglutarate ratio of plasma samples from patients suffering sepsis with Gram-negative (on the left, blue dots) and Gram-positive (on the right, green dots) bacterial infections. NS, not significant; *$P < 0.05$; **$P < 0.01$; ***$P < 0.001$ (two-tailed unpaired Student's *t*-test).

The fumarate/α-ketoglutarate ratio in those samples (Figure 54) does not show statistical difference between fumarate/α-ketoglutarate ratio in patients with Gram-negative and with Gram-positive bacterial infection. The metabolomics analysis on Delneste's samples was performed on plasma samples, so it is possible that the metabolites detected come from all the immune cells inside the plasma and from bacteria present in the bloodstream and all surrounding tissues (i.e. epithelial cells) [121]. A further analysis is needed to evaluate the abundance of the metabolites only in white blood cells isolated from the whole plasma samples.

Since the mitochondrial metabolism is strongly linked to the cytokine production [3], we pharmacologically manipulated TCA metabolites in macrophages in order to induce different inflammatory responses (Figures 42 and 43). In activated macrophages by Gram-negative and Gram-positive bacteria, dimethyl-fumarate decreases IL-10 production and increases TNFα and IL-1β production, which is in contrast with the literature because dimethyl-fumarate is known to be anti-inflammatory treatment in auto-immune diseases (i.e. arteriosclerosis) [122]. Sensing of bacteria induces an accumulation of fumarate and by providing dimethyl fumarate we have further improved pathogen-induced inflammation, probably enhancing bacterial detection, which leads to increased production of pro-inflammatory cytokines. Interestingly, by manipulating the fumarate

levels we induced an IL-1β response in Gram-positive treated macrophages, a condition where normally there is no IL-1β production (Figure 45). Further studies are necessary to better understand how dimethyl fumarate induce IL-1β response in the context of Gram-positive bacterial infection, inducing assessing NLRP3 inflammasome activation or by modifying the expression of IL-1β. Instead of testing dimethyl fumarate, could be interesting to analyse the effect of fumarate, preserving the electrophilic capacity with the natural metabolite. Moreover, while α-ketoglutarate does not affect the cytokine profile in response to Gram-negative bacteria, in Gram-positive treated macrophages α-ketoglutarate boosts the IL-10 production. By manipulating the dimethyl-fumarate and α-ketoglutarate pathway, it is possible to act on the epigenetics means and modulate cytokine production in response to bacterial infection.

From the literature [3], it is known that SDH/CII activity is transiently increased in *E. coli*-treated macrophages and then progressively decreased during the infection. Opposite to the CII activity dynamic observed in *E. coli*-treated macrophages, Gram-positive bacteria maintain CII activity without decreasing it during macrophage differentiation. Moreover, it was also demonstrated that the transient increase in CII activity in macrophages by sensing *E. coli*, requires the involvement of post-translational modifications (PTMs). It is well known CII is regulated [108] and the identification of different PTMs in *E. coli*- and *L. innocua*- treated macrophages suggest that the mitochondrial metabolism reprogramming dependent on the nature of the pathogens, with activation of distinct signalling pathways that regulate CII/SDH activity in macrophages (Figure 44). Treatment with CII inhibitors in macrophages challenged with *E. coli* and *L. innocua* does not affect the SCs organization and the ATP production (Figures 46 and 47). The inhibition of CII does not influence the basal respiration in cultured macrophages while it diminished the maximal respiration rate (MRR) (Figures 48 and 49). Moreover, CII inhibition decreases all the cytokine production regardless of the nature of bacteria (Figures 50 and 51), so CII is important for innate immune receptors mediated macrophage activation. Our data suggest the idea that by inhibiting CII, the cytokine production is reduced and the capacity of macrophages to differentiate and activate is prevented.

In vivo treatment with CII inhibitor shows a different modulation of the cytokine profile compared to cultured macrophages (Figure 52). Although dimethyl malonate *in vitro*

decreases all the cytokine production, *in vivo* it seems to boost the anti-inflammatory response to *L. innocua* bacterial infection. Data suggest that inhibiting CII *in vitro* decrease the capacity of macrophage to get activate, *in vivo* it is possible to manipulate the nature of the immune response by modulating the CII activity. During *L. innocua* infection *in vivo*, it is possible to increase the anti-inflammatory response and decrease the inflammatory response. Further experiments are necessary to clarify this discrepancy, for example trying to isolate macrophages and monocytes in order to better understand where the cytokines production originate. Moreover, another tools to study the CII contribution to anti-microbial responses and to phagocyte differentiation is the use of SDHB KO mice.

References

[1] Sander LE, Garaude J. (2018) The mitochondrial respiratory chain: A metabolic rheostat of innate immune cell-mediated antibacterial responses. *Mitochondrion.* 41:28-36.

[2] Genova ML and Lenaz G. (2014) Functional role of mitochondrial respiratory supercomplexes. *Biochim Biophys Acta.* 1837(4):427-43.

[3] Garaude J, Acín-Pérez R, Martínez-Cano S, Enamorado M, Ugolini M, Nistal-Villán E, Hervás-Stubbs S, Pelegrín P, Sander LE, Enríquez JA, Sancho D. (2016) Mitochondrial respiratory-chain adaptations in macrophages contribute to antibacterial host defense. *Nat Immunol.* 17(9):1037-1045.

[4] Mills EL, Kelly B, Logan A, Costa ASH, Varma M, Bryant CE, Tourlomousis P, Däbritz JHM, Gottlieb E, Latorre I, Corr SC, McManus G, Ryan D, Jacobs HT, Szibor M, Xavier RJ, Braun T, Frezza C, Murphy MP, O'Neill LA. (2016) Succinate dehydrogenase supports metabolic repurposing of mitochondria to drive inflammatory macrophages. *Cell.* 167, 457–470.e13.

[5] Ryan DG and O'Neill LA. (2020) Krebs Cycle Reborn in Macrophage Immunometabolism. *Annual Review of Immunology.* 38:289-313.

[6] Martínez-Reyes & Chandel. (2020) Mitochondrial TCA cycle metabolites control physiology and disease. *Nature Communications.* 11(1):102.

[7] Kotas ME, Medzhitov R. (2015) Homeostasis, inflammation, and disease susceptibility. *Cell.* 160(5):816-827.

[8] Iwasaki A, Medzhitov R. (2015) Control of adaptive immunity by the innate immune system. *Nat Immunol.* 16(4):343-53.

[9] Borst, J., Ahrends, T., Bąbała, N. *et al.* (2018) $CD4^+$ T cell help in cancer immunology and immunotherapy. *Nat Rev Immunol* 18, 635–647.

[10] Locati M, Curtale G, Mantovani A. (2020) Diversity, Mechanisms, and Significance of Macrophage Plasticity. *Annu Rev Pathol.* 15:123-147.

[11] Shapouri-Moghaddam A, Mohammadian S, Vazini H, Taghadosi M, Esmaeili SA, Mardani F, Seifi B, Mohammadi A, Afshari JT, Sahebkar A. (2018) Macrophage plasticity, polarization, and function in health and disease. *J Cell Physiol.* 233(9):6425-6440.

[12] Mantovani A, Sica A, Sozzani S, Allavena P, Vecchi A, Locati M. (2004) The chemokine system in diverse forms of macrophage activation and polarization. *Trends Immunol.* 25(12):677-86.

[13] Russell DG, Huang L, VanderVen BC. (2019) Immunometabolism at the interface between macrophages and pathogens. *Nat Rev Immunol.* 19(5):291-304.

[14] Benmoussa K, Garaude J, Acín-Pérez R. (2018) How Mitochondrial Metabolism Contributes to Macrophage Phenotype and Functions. *J Mol Biol.* 430(21):3906-3921.

[15] Medzhitov R, Janeway C Jr. (1998) Innate immune recognition and control of adaptive immune responses. *Semin Immunol.* 10(5):351-3.

[16] Medzhitov R, Janeway C Jr. (2000) Innate immune recognition: mechanisms and pathways. *Immunol Rev.* 173:89-97.

[17] Mogensen TH. (2009) Pathogen recognition and inflammatory signaling in innate immune defenses. *Clin Microbiol Rev.* 22(2):240-73.

[18] Kumar H , Kawai T, Akira S. (2011) Pathogen recognition by the innate immune system. *Int Rev Immunol.* 30(1):16-34.

[19] Kumar S, Ingle H, Prasad DV, Kumar H. (2013) Recognition of bacterial infection by innate immune sensors. *Crit Rev Microbiol.* 39(3):229-46.

[20] O'Neill LA, Golenbock D, Bowie AG. (2013) The history of Toll-like receptors - redefining innate immunity. *Nat Rev Immunol.* 13(6):453-60.

[21] Drouin M, Saenz J, Chiffoleau E. (2020) C-Type Lectin-Like Receptors: Head or Tail in Cell Death Immunity. *Front Immunol.* 11:251.

[22] Brown, G.D., Willment, J.A. & Whitehead, L. (2018) C-type lectins in immunity and homeostasis. *Nat Rev Immunol.* 18, 374–389.

[23] Mnich, M. E., van Dalen, R., & van Sorge, N. M. (2020) C-Type Lectin Receptors in Host Defense Against Bacterial Pathogens. *Frontiers in cellular and infection microbiology*. *10*,309.

[24] Loo, Y. M., & Gale, M., Jr. (2011) Immune signaling by RIG-I-like receptors. *Immunity*, *34*(5), 680–692.

[25] Rehwinkel J, Gack MU. (2020) RIG-I-like receptors: their regulation and roles in RNA sensing. *Nat Rev Immunol.* 20(9):537-551.

[26] Meunier E, Broz P. (2017) Evolutionary Convergence and Divergence in NLR Function and Structure. *Trends Immunol.* 38(10):744-757.

[27] Geddes K, Magalhães JG, Girardin SE. (2009) Unleashing the therapeutic potential of NOD-like receptors. *Nat Rev Drug Discov.* 8(6):465-79.

[28] Christgen, S., Place, D.E. & Kanneganti, TD. (2020) Toward targeting inflammasomes: insights into their regulation and activation. *Cell Res* 30, 315–327.

[29] Sharma BR, Karki R, Kanneganti TD. (2019) Role of AIM2 inflammasome in inflammatory diseases, cancer and infection. *Eur J Immunol*. 49(11):1998-2011.

[30] Gong, T., Liu, L., Jiang, W. *et al.* (2020) DAMP-sensing receptors in sterile inflammation and inflammatory diseases. *Nat Rev Immunol.* 20, 95–112.

[31] Gram C. (1884) Über die isolierte Färbung der Schizomyceten in Schnittund Trockenpräparaten. *Fortschr Med.* 2:185–189.

[32] Brown L, Wolf JM, Prados-Rosales R, Casadevall A. (2015) Through the wall: extracellular vesicles in Gram-positive bacteria, mycobacteria and fungi. *Nat Rev Microbiol.* 13(10):620-30.

[33] Sperandeo P, Martorana AM, Polissi A. (2019) Lipopolysaccharide Biosynthesis and Transport to the Outer Membrane of Gram-Negative Bacteria. *Subcell Biochem.* 92:9-37.

[34] Lin TL, Shu CC, Chen YM, Lu JJ, Wu TS, Lai WF, Tzeng CM, Lai HC, Lu CC. (2020) Like Cures Like: Pharmacological Activity of Anti-Inflammatory Lipopolysaccharides From Gut Microbiome. *Front Pharmacol*. 11:554.

[35] Mogensen TH. (2009) Pathogen recognition and inflammatory signaling in innate immune defenses. *Clin Microbiol Rev.* 22(2):240-73

[36] Siekevitz P. (1957) Powerhouse of the cells. *Scientific American.* Vol. 97 pp.131-144

[37] Iovine JC, Claypool SM, Alder NN. (2021) Mitochondrial compartmentalization: emerging themes in structure and function. *Trends Biochem Sci.* S0968-0004(21)00121-3.

[38] Choi I, Son H, Baek JH. (2021) Tricarboxylic Acid (TCA) Cycle Intermediates: Regulators of Immune Responses. *Life (Basel).* 11(1):69.

[39] Nelson DL and Cox MM – Lehninger. Principles of biochemistry 7th edition

[40] Lenaz G, Genova ML. (2010) Structure and organization of mitochondrial respiratory complexes: a new understanding of an old subject. *Antioxid Redox Signal.* 12(8):961-1008.

[41] Saada A. (2019) Sea squirt alternative oxidase bypasses fatal mitochondrial heart disease. *EMBO Mol Med.* 11(1):e9962.

[42] Gnaiger E (2020) Mitochondrial pathways and respiratory control. An introduction to OXPHOS analysis. 5th ed.

[43] Parey K, Wirth C, Vonck J, Zickermann V. (2020) Respiratory complex I - structure, mechanism and evolution. *Curr Opin Struct Biol.* 63:1-9.

[44] Kahlhöfer F, Gansen M, Zickermann V. (2021) Accessory Subunits of the Matrix Arm of Mitochondrial Complex I with a Focus on Subunit NDUFS4 and Its Role in Complex I Function and Assembly. *Life (Basel).* 11(5):455.

[45] Chomyn A, Mariottini P, Cleeter MW, Ragan CI, Matsuno-Yagi A, Hatefi Y, Doolittle RF, Attardi G. (1985) Six unidentified reading frames of human mitochondrial DNA encode components of the respiratory-chain NADH dehydrogenase. *Nature.* 314(6012):592–597.

[46] Hirst J, Carroll J, Fearnley IM, Shannon RJ, Walker JE. (2003) The nuclear encoded subunits of complex I from bovine heart mitochondria. *Biochim Biophys Acta.* 1604(3):135–150.

[47] Cabrera-Orefice A, Yoga EG, Wirth C, Siegmund K, Zwicker K, Guerrero-Castillo S, Zickermann V, Hunte C, Brandt U. (2018) Locking loop movement in the ubiquinone pocket of complex I disengages the proton pumps. *Nat Commun.* 9(1):4500.

[48] Galemou Yoga E, Schiller J, Zickermann V. (2021) Ubiquinone Binding and Reduction by Complex I-Open Questions and Mechanistic Implications. *Front Chem.* 9:672851.

[49] Lenaz G, Tioli G, Falasca AI, Genova ML. (2016) Complex I function in mitochondrial supercomplexes. *Biochim Biophys Acta.* 1857(7):991-1000.

[50] Hederstedt L. (2003) Structural biology. Complex II is complex too. *Science.* Vol. 299, pp. 671-672.

[51] Van Vranken JG, Na U, Winge DR, Rutter J. (2015) Protein-mediated assembly of succinate dehydrogenase and its cofactors. *Crit Rev Biochem Mol Biol.* 50(2):168-80.

[52] Sharma P, Maklashina E, Cecchini G, Iverson TM. (2019) Maturation of the respiratory complex II flavoprotein. *Curr Opin Struct Biol.* 59:38-46.

[53] Moog S, Lussey-Lepoutre C, Favier J. (2020) Epigenetic and metabolic reprogramming of SDH-deficient paragangliomas. *Endocr Relat Cancer.* 27(12):R451-R463.

[54] Burnichon N, Brière JJ, Libé R, Vescovo L, Rivière J, Tissier F, Jouanno E, Jeunemaitre X, Bénit P, Tzagoloff A, Rustin P, Bertherat J, Favier J, Gimenez-Roqueplo AP. (2010) SDHA is a tumor suppressor gene causing paraganglioma. *Hum Mol Genet.* 19(15):3011-20.

[55] Moreno-Sánchez R, Hernández-Esquivel L, Rivero-Segura NA, Marín-Hernández A, Neuzil J, Ralph SJ, Rodríguez-Enríquez S. (2013) Reactive oxygen species are generated by the respiratory complex II-evidence for lack of contribution of the reverse electron flow in complex I. *FEBS J.* 280(3):927-38.

[56] Hadrava Vanova K, Kraus M, Neuzil J, Rohlena J. (2020) Mitochondrial complex II and reactive oxygen species in disease and therapy. *Redox Rep.* 25(1):26-32.

[57] Ndi M, Marin-Buera L, Salvatori R, Singh AP, Ott M. (2018) Biogenesis of the bc_1 Complex of the Mitochondrial Respiratory Chain. *J Mol Biol.* 430(21):3892-3905.

[58] Mitchell P. (1975) The protonmotive Q cycle: a general formulation. *FEBS Lett.* 59(2):137-9.

[59] Wu M, Gu J, Zong S, Guo R, Liu T, Yang M. (2020) Research journey of respirasome. *Protein Cell.* 11(5):318-338.

[60] Hernansanz-Agustín P, Enríquez JA. (2021) Functional segmentation of CoQ and cyt c pools by respiratory complex superassembly. *Free Radic Biol Med.* 167:232-242.

[61] Covian R, Zwicker K, Rotsaert FA, Trumpower BL. (2007) Asymmetric and redox-specific binding of quinone and quinol at center N of the dimeric yeast cytochrome bc1 complex. Consequences for semiquinone stabilization. *J Biol Chem.* 282(33):24198-208.

[62] Pagacz J, Broniec A, Wolska M, Osyczka A, Borek A. (2021) ROS signaling capacity of cytochrome bc_1: Opposing effects of adaptive and pathogenic mitochondrial mutations. *Free Radic Biol Med.* 163:243-254.

[63] Guillaud F, Dröse S, Kowald A, Brandt U, Klipp E. (2014) Superoxide production by cytochrome bc1 complex: a mathematical model. *Biochim Biophys Acta.* 1837(10):1643-52.

[64] Zong S, Wu M, Gu J, Liu T, Guo R, Yang M (2018) Structure of the intact 14-subunit human cytochrome c oxidase. *Cell Research.* 28, 1026–1034.

[65] Brischigliaro M and Zeviani M. (2021) Cytochrome *c* oxidase deficiency. *Biochim Biophys Acta Bioenerg.* 1862(1):148335.

[66] Wikström M, Sharma V. (2018) Proton pumping by cytochrome c oxidase - A 40 year anniversary. *Biochim Biophys Acta Bioenerg.* 1859(9):692-698.

[67] Pinke G, Zhou L, Sazanov LA. (2020) Cryo-EM structure of the entire mammalian F-type ATP synthase. *Nat Struct Mol Biol.* 27(11):1077-1085.

[68] Walker JE. (2013) The ATP synthase: the understood, the uncertain and the unknown. *Biochem Soc Trans.* 41(1):1-16.

[69] Kühlbrandt W. (2019) Structure and Mechanisms of F-Type ATP Synthases. *Annu Rev Biochem.* 88:515-549.

[70] Antoniel M, Giorgio V, Fogolari F, Glick GD, Bernardi P, Lippe G. (2014) The oligomycin-sensitivity conferring protein of mitochondrial ATP synthase: emerging new roles in mitochondrial pathophysiology. *Int J Mol Sci.* 15(5):7513-36.

[71] Spikes TE, Montgomery MG, Walker JE. (2020) Structure of the dimeric ATP synthase from bovine mitochondria. *Proc Natl Acad Sci U S A.* 117(38):23519-23526.

[72] Chance B, Williams GR. (1956) The respiratory chain and oxidative phosphorylation. *Adv Enzymol Relat Subj Biochem.* 17:65-134.

[73] Green DE, Tzagoloff A. (1966) The mitochondrial electron transfer chain. *Arch Biochem Biophys.* 116(1):293-304.

[74] Hackenbrock CR, Chazotte B, Gupte SS. (1986) The random collision model and a critical assessment of diffusion and collision in mitochondrial electron transport. *J Bioenerg Biomembr.* 18(5):331-68.

[75] Schägger H, Pfeiffer K. (2000) Supercomplexes in the respiratory chains of yeast and mammalian mitochondria. *EMBO J.* 19(8):1777-83.

[76] Acín-Pérez R, Enriquez JA. (2014) The function of the respiratory supercomplexes: the plasticity model. *Biochim Biophys Acta.* 1837(4):444-50.

[77] Dudkina NV, Eubel H, Keegstra W, Boekema EJ, Braun HP. (2005) Structure of a mitochondrial supercomplex formed by respiratory-chain complexes I and III. *Proc Natl Acad Sci U S A.* 102(9):3225-9.

[78] Dudkina NV, Kudryashev M, Stahlberg H, Boekema EJ. (2011) Interaction of complexes I, III, and IV within the bovine respirasome by single particle cryoelectron tomography. *Proc Natl Acad Sci U S A.* 108(37):15196-200.

[79] Letts JA, Sazanov LA. (2017) Clarifying the supercomplex: the higher-order organization of the mitochondrial electron transport chain. *Nat Struct Mol Biol.* 24(10):800-808.

[80] Mileykovskaya E, Dowhan W. (2014) Cardiolipin-dependent formation of mitochondrial respiratory supercomplexes. *Chem Phys Lipids.* 179:42-8.

[81] Althoff T, Mills DJ, Popot JL, Kühlbrandt W. (2011) Arrangement of electron transport chain components in bovine mitochondrial supercomplex I1III2IV1. *EMBO J.* 30(22):4652-64.

[82] Basu Ball W, Neff JK, Gohil VM. (2018) The role of nonbilayer phospholipids in mitochondrial structure and function. *FEBS Lett.* 592(8):1273-1290.

[83] Novack GV, Galeano P, Castaño EM, Morelli L. (2020) Mitochondrial Supercomplexes: Physiological Organization and Dysregulation in Age-Related Neurodegenerative Disorders. *Front Endocrinol (Lausanne).* 11:600.

[84] Lu YW, Claypool SM. (2015) Disorders of phospholipid metabolism: an emerging class of mitochondrial disease due to defects in nuclear genes. *Front Genet.* 6:3.

[85] Maranzana E, Barbero G, Falasca AI, Lenaz G, Genova ML. (2013) Mitochondrial respiratory supercomplex association limits production of reactive oxygen species from complex I. Antioxid *Redox Signal.* 19(13):1469-80.

[86] Hernansanz-Agustín P, Enríquez JA. (2021) Generation of Reactive Oxygen Species by Mitochondria. *Antioxidants (Basel).* 10(3):415.

[87] West AP, Shadel GS, Ghosh S. (2011) Mitochondria in innate immune responses. *Nat Rev Immunol.* 11(6):389-402.

[88] Vogel RO, Janssen RJ, van den Brand MA, Dieteren CE, Verkaart S, Koopman WJ, Willems PH, Pluk W, van den Heuvel LP, Smeitink JA, Nijtmans LG. (2007) Cytosolic signaling protein Ecsit also localizes to mitochondria where it interacts with chaperone NDUFAF1 and functions in complex I assembly. *Genes Dev.* 21(5):615-24.

[89] West AP, Brodsky IE, Rahner C, Woo DK, Erdjument-Bromage H, Tempst P, Walsh MC, Choi Y, Shadel GS, Ghosh S. (2011) TLR signalling augments macrophage bactericidal activity through mitochondrial ROS. *Nature.* 472(7344):476-80.

[90] Ryan DG, Frezza C, O'Neill LA. (2021) TCA cycle signalling and the evolution of eukaryotes. *Curr Opin Biotechnol.* 68:72-88.

[91] O'Neill LA. (2015) A broken Krebs cycle in macrophages. *Immunity.* 42(3):393-4.

[92] Lampropoulou V, Sergushichev A, Bambouskova M, Nair S, Vincent EE, Loginicheva E, Cervantes-Barragan L, Ma X, Huang SC, Griss T, Weinheimer CJ, Khader S, Randolph GJ, Pearce EJ, Jones RG, Diwan A, Diamond MS, Artyomov MN. (2016) Itaconate Links Inhibition of Succinate Dehydrogenase with Macrophage Metabolic Remodeling and Regulation of Inflammation. *Cell Metab.* 24(1):158-66.

[93] Mills EL, Ryan DG, Prag HA, Dikovskaya D, Menon D, Zaslona Z, Jedrychowski MP, Costa ASH, Higgins M, Hams E, Szpyt J, Runtsch MC, King MS, McGouran JF, Fischer R, Kessler BM, McGettrick AF, Hughes MM, Carroll RG, Booty LM, Knatko EV, Meakin PJ, Ashford MLJ, Modis LK, Brunori G, Sévin DC, Fallon PG, Caldwell ST, Kunji ERS, Chouchani ET, Frezza C, Dinkova-Kostova AT, Hartley RC, Murphy MP, O'Neill LA. (2018) Itaconate is an anti-inflammatory metabolite that activates Nrf2 via alkylation of KEAP1. *Nature.* 556(7699):113-117.

[94] Bambouskova M, Gorvel L, Lampropoulou V, Sergushichev A, Loginicheva E, Johnson K, Korenfeld D, Mathyer ME, Kim H, Huang LH, Duncan D, Bregman H, Keskin A, Santeford A, Apte RS, Sehgal R, Johnson B, Amarasinghe GK, Soares MP, Satoh T, Akira S, Hai T, de Guzman Strong C, Auclair K, Roddy TP, Biller SA, Jovanovic M, Klechevsky E, Stewart KM, Randolph GJ, Artyomov MN. (2018) Electrophilic properties of itaconate and derivatives regulate the IκBζ-ATF3 inflammatory axis. *Nature.* 556(7702):501-504.

[95] Garaude J. (2019) Reprogramming of mitochondrial metabolism by innate immunity. *Curr Opin Immunol.* 56:17-23.

[96] Ryan DG, Murphy MP, Frezza C, Prag HA, Chouchani ET, O'Neill LA, Mills EL. (2019) Coupling Krebs cycle metabolites to signalling in immunity and cancer. *Nat Metab.* 1:16-33.

[97] Zasłona Z, O'Neill LAJ. (2020) Cytokine-like Roles for Metabolites in Immunity. *Mol Cell.* 78(5):814-823.

[98] Afzal R, Dowling JK, McCoy CE. (2020) Impact of Exercise on Immunometabolism in Multiple Sclerosis. *J Clin Med.* 9(9):3038.

[99] Kieler M, Hofmann M, Schabbauer G. (2021) More than just protein building blocks: how amino acids and related metabolic pathways fuel macrophage polarization. FEBS J. 288(12):3694-3714.

[100] Liu Y, Xu R, Gu H, Zhang E, Qu J, Cao W, Huang X, Yan H, He J, Cai Z. (2021) Metabolic reprogramming in macrophage responses. *Biomark Res.* 9(1):1.

[101] Lee JV, Carrer A, Shah S, Snyder NW, Wei S, Venneti S, Worth AJ, Yuan ZF, Lim HW, Liu S, Jackson E, Aiello NM, Haas NB, Rebbeck TR, Judkins A, Won KJ, Chodosh LA, Garcia BA, Stanger BZ, Feldman MD, Blair IA, Wellen KE. (2014) Akt-dependent metabolic reprogramming regulates tumor cell histone acetylation. *Cell Metab.* 20(2):306-319

[102] Liu PS, Wang H, Li X, Chao T, Teav T, Christen S, Di Conza G, Cheng WC, Chou CH, Vavakova M, Muret C, Debackere K, Mazzone M, Huang HD, Fendt SM, Ivanisevic J, Ho PC. (2017) α-ketoglutarate orchestrates macrophage activation through metabolic and epigenetic reprogramming. *Nat Immunol.* 18(9):985-994.

[103] Buffet A, Burnichon N, Favier J, Gimenez-Roqueplo AP. (2020) An overview of 20 years of genetic studies in pheochromocytoma and paraganglioma. *Best Pract Res Clin Endocrinol Metab.* 34(2):101416.

[104] Xiao M, Yang H, Xu W, Ma S, Lin H, Zhu H, Liu L, Liu Y, Yang C, Xu Y, Zhao S, Ye D, Xiong Y, Guan KL. (2012) Inhibition of α-KG-dependent histone and DNA demethylases by fumarate and succinate that are accumulated in mutations of FH and SDH tumor suppressors. *Genes Dev.* 26(12):1326-38.

[105] Arts RJ, Novakovic B, Ter Horst R, Carvalho A, Bekkering S, Lachmandas E, Rodrigues F, Silvestre R, Cheng SC, Wang SY, Habibi E, Gonçalves LG, Mesquita I,

Cunha C, van Laarhoven A, van de Veerdonk FL, Williams DL, van der Meer JW, Logie C, O'Neill LA, Dinarello CA, Riksen NP, van Crevel R, Clish C, Notebaart RA, Joosten LA, Stunnenberg HG, Xavier RJ, Netea MG. (2016) Glutaminolysis and Fumarate Accumulation Integrate Immunometabolic and Epigenetic Programs in Trained Immunity. *Cell Metab.* 24(6):807-819.

[106] Lowry OH, Rosebrough NJ, Farr L, Randall RJ. (1951) Protein measurement with the Folin phenol reagent. *J Biol Chem.* 193(1):265-75.

[107] Smith PK, Krohn RI, Hermanson GT, Mallia AK, Gartner FH, Provenzano MD, Fujimoto EK, Goeke NM, Olson BJ, Klenk DC. (1985) Measurement of protein using bicinchoninic acid. *Anal Biochem* 150:76-85.

[108] Moosavi B, Zhu XL, Yang WC, Yang GF. (2020) Genetic, epigenetic and biochemical regulation of succinate dehydrogenase function. *Biol Chem.* 401(3):319-330.

[109] Acín-Pérez R, Carrascoso I, Baixauli F, Roche-Molina M, Latorre-Pellicer A, Fernández-Silva P, Mittelbrunn M, Sanchez-Madrid F, Pérez-Martos A, Lowell CA, Manfredi G, Enríquez JA. (2014) ROS-triggered phosphorylation of complex II by Fgr kinase regulates cellular adaptation to fuel use. *Cell Metab.* 19(6):1020-33.

[110] O'Neill, L., Kishton, R. & Rathmell, J. (2016) A guide to immunometabolism for immunologists. *Nat Rev Immunol* 16, 553–565.

[111] Makowski L, Chaib M, Rathmell JC. (2020) Immunometabolism: From basic mechanisms to translation. *Immunol Rev.* 295(1):5-14.

[112] Ayres JS. (2020) Immunometabolism of infections. *Nat Rev Immunol.* 20(2):79-80.

[113] Pearce EL, Pearce EJ. (2013) Metabolic pathways in immune cell activation and quiescence. *Immunity.* 38(4):633-43.

[114] Hernansanz-Agustín P, Enríquez JA. (2021) Functional segmentation of CoQ and cyt c pools by respiratory complex superassembly. *Free Radic Biol Med.* 167:232-242.

[115] Genova ML, Lenaz G. (2014) Functional role of mitochondrial respiratory supercomplexes. *Biochim Biophys Acta.* 1837(4):427-43.

[116] Genova ML, Lenaz G. (2015) The Interplay Between Respiratory Supercomplexes and ROS in Aging. *Antioxid Redox Signal.* 23(3):208-38.

[117] Viola A, Munari F, Sánchez-Rodríguez R, Scolaro T, Castegna A. (2019) The Metabolic Signature of Macrophage Responses. *Front Immunol.* 10:1462.

[118] Jha AK, Huang SC-C, Sergushichev A, Lampropoulou V, Ivanova Y, Loginicheva E, et al. (2015) Network integration of parallel metabolic and transcriptional data reveals metabolic modules that regulate macrophage polarization. *Immunity.* 42:419–30.

[119] Singer M, Deutschman CS, Seymour CW, Shankar-Hari M, Annane D, Bauer M, Bellomo R, Bernard GR, Chiche JD, Coopersmith CM, Hotchkiss RS, Levy MM, Marshall JC, Martin GS, Opal SM, Rubenfeld GD, van der Poll T, Vincent JL, Angus DC. (2016) The Third International Consensus Definitions for Sepsis and Septic Shock (Sepsis-3). *JAMA.* 315(8):801-10.

[120] Cavaillon JM, Singer M, Skirecki T. (2020) Sepsis therapies: learning from 30 years of failure of translational research to propose new leads. *EMBO Mol Med*. 12(4):e10128.

[121] Beloborodova N, Pautova A, Sergeev A, Fedotcheva N. (2019) Serum Levels of Mitochondrial and Microbial Metabolites Reflect Mitochondrial Dysfunction in Different Stages of Sepsis. *Metabolites*. 9(10):196.

[122] Koelwyn GJ, Corr EM, Erbay E, Moore KJ. (2018) Regulation of macrophage immunometabolism in atherosclerosis. *Nat Immunol.* 19(6):526-537.